

Nadja Noormofidi

**Amino-Functionalised Poly(norbornene)s Prepared
by Ring Opening Metathesis Polymerisation**

PhD Thesis

Dissertation

zur Erlangung des akademischen Grades einer Doktorin der
technischen Wissenschaften

erreicht an der

Technischen Universität Graz

Betreuer: Univ.-Doz. Dipl. Ing. Dr. techn. Christian Slugovc
Institut für chemische Technologie von Materialien
Technische Universität Graz

Mai 2010

Statutory Declaration

I declare that I have authored this thesis independently, that I have not used other than the declared sources / resources, and that I have explicitly marked all material which has been quoted either literally or by content from the used sources.

.....
date

.....
(signature)

Dedicated to
my family and friends

Nichts ohne Ende
Martin Kippenberger

Thanks to

Natascha Alexakis, Kathrin Bohnemann, **Eva Bradacs**, Daniel Burtscher, Hubert Fasl, Ulrike Fluch, Edgar Gander, Lucas Hauser, Liane Hochgatterer, Josefine Hobisch, Lisa Horvath, Philipp Hütter, Stefan Kappaun, Petra Kaschnitz, KeKelit, **Julia Kienberger**, Astrid Knall, Martin Kniendl, Wolfgang Koller, **Christian Konrad**, **Elisabeth Kreuzwiesner**, Anita Leitgeb, Alexandra Lex-Balducci, Christina Lexer, Eugen Maier, **Wilfried Mörtl**, Fabian Niedermair, Donja Noormofidi, Gerda Noormofidi, Taghi Noormofidi, Andreas Pein, Gerald Pichler, Thomas Rath, Volker Ribitsch, Andreas Ruplitsch, Martina Sandholzer, Robert Saf, Richard Schmid, **Christian Slugovc**, **Franz Stelzer**, Rene Stix, Martin Strobl, Kurt Stubenrauch, Barbara Thallinger, **Magdalena Tendl**, Renate Trebizan, Martin Tscherner, Gregor Trimmel, Hansjörg Weber, Michaela Zirngast and all my friends and colleagues

for apple diving, coffee and cigarettes, discussions, measurements, scientific and non-scientific ‚Seidels‘, tabletop football tournaments, for your friendship, love, patience and support.

Abstract

The prevention of microbial contamination and biofilm formation is a topic of great interest for many different fields of application. In recent years, polymeric antimicrobial materials have been intensively explored as an attractive alternative to low molecular weight agents. These small molecules exhibit severe drawbacks such as human toxicity, the tendency to develop bacterial resistance and to get accumulated in the soil. Such disadvantages could be resolved by the development of novel polymeric contact bactericides.

Herein the synthesis and characterisation of amino-functionalised poly(norbornene)s is presented. The polymers were synthesised using ring opening metathesis polymerisation (ROMP). In addition, the polymerisation behaviour of the amine-bearing monomers and the feasibility of designing block-*c*opolymers were investigated. Subsequently, the antimicrobial activity of both the pure polymers and compound materials with poly(ethylene) was examined.

Furthermore, poly(norbornene)s bearing pendant luminescent 6*d* ruthenium(II) complexes were prepared. Photophysical properties of the monomers and the resultant polymers were investigated and the oxygen sensitive luminescence lifetime of the polymers was tested. The long-term objective is to develop antimicrobial copolymers and simultaneously monitor the presence of aerobic bacteria as a function of luminescence lifetime of the ruthenium moiety.

Zusammenfassung

Die Prävention von mikrobiellen Kontaminationen und Biofilmbildung ist von großem Interesse für viele verschiedene Anwendungsgebiete. In den letzten Jahren konnten sich antimikrobielle Polymere als attraktive Alternative zu niedermolekularen Bioziden vermehrt etablieren. Gründe dafür sind schwerwiegende Nachteile der niedermolekularen Verbindungen wie z.B. deren Toxizität, deren Akkumulation im Erdboden und eine zunehmende Resistenzbildung vieler Keime. Mit der Entwicklung neuartiger Kontaktbiozide sollen diese Probleme umgangen werden.

Im Zuge der vorliegenden Dissertation wurden amino-funktionalisierte Poly(norbornen)e mittels Ring Öffnender Metathese Polymerisation (ROMP) synthetisiert und charakterisiert. Das Polymerisationsverhalten der Monomere und die Möglichkeit Block-copolymeren herzustellen wurde untersucht. Anschließend wurde die antimikrobielle Wirksamkeit der reinen Polymere sowie die Aktivität der Polymere im Verbund mit Poly(ethylen) getestet.

Darüber hinaus wurden Poly(norbornen)e hergestellt, die 6d Ruthenium(II)-Komplexe in der Seitenkette enthalten. Die photophysikalischen Eigenschaften der Übergangsmetall-Komplexe sowie der resultierenden Polymere wurde untersucht und die sauerstoffsensitive Lumineszenz-Lebenszeit der Polymere getestet. Das langfristige Ziel dieser Untersuchungen ist es, antimikrobielle Copolymere herzustellen und gleichzeitig das Vorhandensein aerober Bakterien als Funktion der Lumineszenz-Lebenszeit der Ruthenium-Komplexe nachzuweisen.

Table of content

1	Introduction	1
2	General Background	3
2.1	Influences on the Antimicrobial Activity	3
2.1.1	Species of Microorganisms.....	3
2.1.1.1	Bacteria	3
2.1.1.2	Biofilm, Biofouling Formation and Growth	6
2.1.2	Charge Effects	7
2.1.2.1	Electrostatic Interaction	7
2.1.2.2	Effect of Counterions	7
2.1.2.3	Biocide Mechanisms	7
2.1.3	Polymer Architecture ¹²	10
2.1.3.1	Spacer Length and Hydrophilic-Hydrophobic Balance	10
2.1.3.2	Molecular Weight	11
2.2	Metathesis	12
2.2.1	Mechanism.....	12
2.2.2	Ring Opening Metathesis Polymerisation (ROMP)	13
2.2.2.1	Initiators	14
2.2.2.2	Termination	16
2.3	Luminescence	17
2.3.1	General information.....	17
2.3.1.1	Luminescence Lifetime and Quantum Yield	18
2.3.1.2	Luminescence Quenching	19
2.3.2	Ruthenium-based Metal-Ligand Complexes ³⁶	21
2.3.2.1	Applications of Transition Metal Complexes and Resulting Polymers.....	23
3	Results and Discussion	24
3.1	Amino-Functionalised, Random ROM Polymers	24
3.1.1	Introduction.....	24
3.1.2	Optimisation of Polymerisation Conditions	27
3.1.2.1	Choice of Initiator	27
3.1.2.2	Kinetics	28
3.1.2.3	Effect of Polymerisation Time and Temperature	29
3.1.3	Antimicrobial Activity.....	30
3.1.4	Cytotoxicity Test	33

3.2	Antimicrobial Compound Materials.....	34
3.2.1	Concept	34
3.2.2	Compound Fabrication	34
3.2.3	Antimicrobial Activity of the Compounds	36
3.2.4	Leaching Tests.....	36
3.2.5	Conclusions Drawn on Antimicrobial Compounds	38
3.3	Development of Block-<i>co</i>-polymers	39
3.3.1	Motivation.....	39
3.3.2	Synthesis of Block- <i>co</i> -polymers	40
3.3.3	Determination of Distribution of the Block- <i>co</i> -Polymer in the Matrix.....	45
3.3.3.1	Contact Angle Measurements.....	45
3.3.3.2	Transmission Electron Microscopy Measurements.....	46
3.4	Luminescent Ruthenium Complexes	48
3.4.1	Motivation.....	48
3.4.1.1	Ligand synthesis.....	48
3.4.2	Preparation of the Complexes	50
3.4.3	Polymerisation of the TMCs.....	52
3.4.4	Photophysical Measurements.....	53
3.4.4.1	Optical Properties of the Imidazophenanthroline Ligand 11	53
3.4.4.2	Optical Properties of the Transition Metal Complexes.....	54
3.4.4.3	Effect of Protonation on the Optical Properties of 14	58
3.4.4.4	Optical Properties of the Polymeric Transition Metal Complexes	59
3.4.4.5	Effect of Counter Ion on the Optical Properties	62
3.4.5	Lifetime Measurements.....	64
3.4.5.1	Outlook and Future Work on Polymeric TMCs	65
4	Conclusion & Outlook	66
4.1	Conclusion on the Biocide Polymers	66
4.2	Conclusion on the Luminescent, Polymerisable Ruthenium Complexes.....	67
5	Experimental	69
5.1	Materials.....	69
5.2	Instrumentation.....	69
5.2.1	Nuclear Magnetic Resonance (NMR) Spectroscopy	69
5.2.2	Thin Layer Chromatography (TLC).....	70
5.2.3	Contact Angle Measurements	70
5.2.4	Gel Permeation Chromatography (GPC).....	70
5.2.5	Photophysical Measurements.....	71
5.2.5.1	Absorption Measurements	71
5.2.5.2	Emission Measurements.....	71
5.2.6	Differential Scanning Calorimetry (DSC)	71
5.2.7	Thermogravimetric analysis (TGA)	71
5.3	Syntheses	72
5.3.1	Biocide Materials	72
5.3.1.1	Mixture of <i>endo</i> and <i>exo</i> -2-(<i>tert</i> -butylamino) ethyl bicycle [2.2.1] hept-5-ene-2-carboxylate (1)	72
5.3.1.2	Mixture of <i>endo</i> and <i>exo</i> -n-dodecyl bicyclo[2.2.1]hept-5-ene-2-carboxylate (2).....	73
5.3.1.3	RuCl ₂ (pyridine) ₂ (H ₂ IMes)(CHPh) (G3).....	73
5.3.1.4	General Polymerisation Procedures for poly(1) , poly(1_x-<i>co</i>-2_{600-x}) , poly(1_x-<i>co</i>-3_{600-x}) , poly(2₃₀₀-<i>co</i>-4₃₀₀) , poly(3₃₀₀-<i>co</i>-4₃₀₀) and poly(4)	74
5.3.1.5	General Polymerisation Procedures for Test-polymerisations of 2	75
5.3.1.6	Synthesis of poly(1₃₀₀-<i>co</i>-2₃₀₀-<i>co</i>-5₃₃)	76

5.3.1.7	General Polymerisation Procedure for the Syntheses of Block- <i>cis</i> -polymers.....	77
5.3.2	Ruthenium Complexes.....	79
5.3.2.1	11-(4-Formylphenoxy)undecyl-bicyclo[2.2.1]hept-5-en-2-carboxylate (8) .	79
5.3.2.2	[1,10]-Phenanthroline-5,6-dione (10)	80
5.3.2.3	<i>endo/exo</i> -11-(4-(1H-Imidazo[4,5-f][1,10]phenanthroline-2-yl)phenoxy)undecyl - bicyclo [2.2.1]hept-5-en-2-carboxylate ⁶³	80
5.3.2.4	Chloro(<i>p</i> -cymene)ruthenium(II)complex 12	81
5.3.2.5	Synthesis of Monomer 14	82
5.3.2.6	Synthesis Monomer 15	83
5.3.2.7	Polymerisation Procedure for poly(14-<i>cis</i>-16) and poly(15-<i>cis</i>-16)	84
6	Appendix.....	86
6.1	Supporting Information	86
6.1.1	Japanese Industry Standard JIS Z 2801:2000 ⁵²	86
6.1.2	Contact Angle Measurements	88
6.1.3	Transmission Electron Microscopy	89
6.1.3.1	Sample Preparation.....	89
6.1.4	Lifetime Measurements.....	90
6.1.4.1	Time-Domain Lifetime Measurement.....	90
6.1.4.2	Frequency-Domain Lifetime Measurement.....	92
6.1.5	Humidity Measurement Set-Up.....	93
6.2	Glossary of Abbreviations	95
6.3	Glossary of Mathematical Terms.....	97
6.4	List of Figures	98
6.5	List of Schemes	100
6.6	List of Tables.....	101
6.7	Curriculum Vitae	102
6.8	List of Publications	104
6.8.1	Manuscripts.....	104
6.8.2	Proceedings.....	104
6.8.3	Presentations.....	105
6.8.3.1	Oral Contributions	105
6.8.3.2	Talks from Co-worker and Poster Presentations	105

1 Introduction

Microbial contamination and biofilm formation is a topic of great interest in many areas, such as medical devices, healthcare products, water purification systems, food packaging, food storage, etc.^{1,2} Common disinfectants or antimicrobial agents are substances of low molecular weight.³ Antibiotics,^{4,5} chlorinated phenols,⁶ Zn²⁺- and Ag⁺-based compounds,⁷ have been used for water sterilisation or food processing. With the use of these disinfectants or antimicrobial agents, the problems of residual toxicity cause serious problems to the environment. These low molecular weight antimicrobial agents, chemicals and biocides, act efficiently by affecting cell metabolism, but may exhibit human toxicity and the tendency to develop bacterial resistance. Compared to such conventional antimicrobial agents, polymeric biocide materials have the advantages of being non-volatile, chemically stable and do not release degradation products of low molecular weight into the environment.

In the food processing and packaging industries, it is important that all surfaces which come in contact with food and foodstuffs are free of potentially hazardous microorganisms. The implementation of polymeric biocide surfaces in the food industry can lead to improved cleaning and disinfection operations, by reducing the microbial load and inhibiting the proliferation of microorganisms on different surfaces.

¹ Patel, M. B.; Patel, S. A.; Ray, A.; Patel, R. M. *J. Appl. Polym. Sci.* **2003**, *89*, 895-900.

² Park, E.-S.; Lee, H.-J.; Park, H.-Y.; Kim, M.-N.; Chung, K.-H.; Yoon, J.-S. *J. Appl. Polym. Sci.* **2001**, *80*, 728-736.

³ Li, G.; Shen, J. *J. Appl. Polym. Sci.* **2000**, *78*, 676-684.

⁴ Zasloff, M. *Nature* **2002**, *415*, 389-395.

⁵ Ouellet, M.; Otis, F.; Voyer, N.; Auger, M.; *Biochim. Biophys. Acta* **2006**, *1758*, 1235.

⁶ Kassem, T.; Habib, O.; Hussein, M.; Eissa, A.; *Hungarin Journal of Industrial Chemistry* **1983**, *11(2)*, 157-162.

⁷ Breitscheidel, B.; Hartmut, H. *BASF Aktiengesellschaft* **1999**, DE19916562.

The main focus of this thesis is to avoid contaminations caused by microorganisms in the food packaging and in water pipes. In the case of food packaging, there is a risk of diffusion for antimicrobial agents of low molecular weight into the food causing various problems. Such agents may be dangerous because of their human toxicity and tendency to develop bacterial resistance, or because of the harm that they can cause by rendering undesired flavours or side-reactions. In the case of water treatment, the most common procedure to disinfect water is to use chlorine and other related chemicals. However, their residues can become concentrated in the food chain. Because of the problems associated with the use of low molecular-weight agents, the idea of polymeric antimicrobial agents appeared to be an attractive alternative.⁸ They are not volatile or soluble, applicable for long-term usage and chemically stable. Hence, the residual toxicity is minimised while the efficiency and selectivity is increased.

The ideal biocidal polymer should not be soluble in water or release any toxic residues to the environment, should not be toxic or irritating and stable in long-term usage. Furthermore it should be easily and inexpensively synthesised and exhibit a widespread activity against a broad variety of different microorganisms in short times contact.⁹

The biocide polymers presented herein are synthesised via ring opening metathesis polymerisation (ROMP). The high versatility of this polymerisation technique relies on its livingness. Hence, a broad variety of different polymer architectures can be designed.

Within this thesis the polymerisation behaviour of the presented monomers is investigated and the feasibility of designing block-*c*opolymers is addressed. Antimicrobial activity of the resultant polymers and compounds thereof using commodity materials is presented.

Furthermore, the synthesis and characterisation of luminescent ruthenium complexes bearing a norbornene functionalised imidazophenanthroline ligands is highlighted. The norbornene motif enables polymerisation of these complexes via ROMP. Random copolymers of the dye-monomers with a mixture of *endo* and *exo*-norborn-5-ene-2,3-dicarboxylic acid dimethyl ester were prepared. Photophysical properties of the transition metal complexes and the resultant polymers were investigated. The applicability of the ruthenium complexes as sensing moiety for oxygen due to their oxygen sensitive luminescence lifetime will be discussed.

The possibility of copolymerisation of the ruthenium monomers and the biocide system paves the way for the development of antimicrobial polymers while simultaneously the presence of aerobic bacteria as a function of luminescence lifetime of the copolymerised ruthenium complexes can be determined. The fact that these biocide polymers can be potentially used as antimicrobial and anti-deposit surfaces in different compositions and applications is the main driving force of this thesis.

⁸ Kenawy, E.; Mahmoud, Y. *Macromol. Biosci.* **2003**, *3*, 107-116.

⁹ Worley, S.D.; Sun, G. *Trends Polym. Sci.* **1996**, *4*, 364-370.

2 General Background

2.1 Influences on the Antimicrobial Activity

2.1.1 Species of Microorganisms

The species of the microorganism attaches great importance to antibacterial nature of biocides because not all microorganisms are equally sensitive in contact with biocidal materials.

2.1.1.1 Bacteria

Bacteria are microorganisms that can be classified as prokaryotes. In contrast to eukaryotes they do not possess a cell nucleus, separated from the rest of the cell by a cell wall. Hence the genetic material of bacteria is not membrane-bound, whereas in eukaryotes the nuclei contain the DNA. Their genetic material is typically a single circular chromosome located in the cytoplasm in an irregularly shaped body called the nucleoid.

The intracellular structures of prokaryotes consist of the cell membrane, a lipid bilayer membrane which encloses the contents of the cell and acts as a barrier to hold nutrients, the cytoplasm and the ribosome (*cf.* Figure 2.1-1). The lipid bilayer is a thin membrane made of two layers of lipid molecules. Natural bilayers consist of phospholipids, which have a hydrophilic head and two hydrophobic tails. The hydrophilic head contains the negatively charged phosphate group and may contain other polar groups (X). The hydrophobic tail usually consists of long fatty acid hydrocarbon chains (*cf.* Figure 2.1-2). When phospholipids are exposed to water, they arrange

themselves into a two-layered sheet (a bilayer) with all of their tails pointing toward the centre of the sheet (*cf.* Figure 2.1-3).

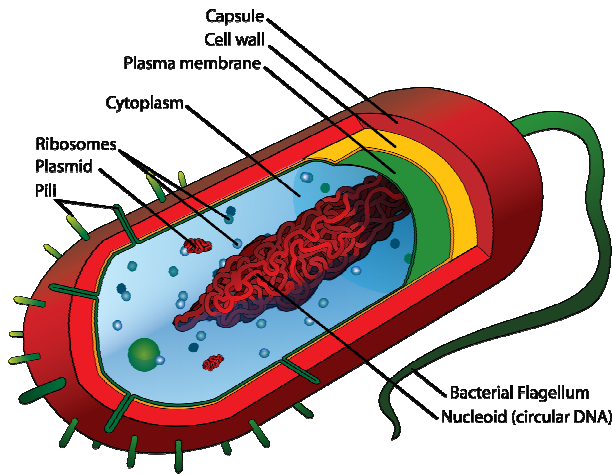


Figure 2.1-1: Schematic structure of a prokaryote.¹⁰

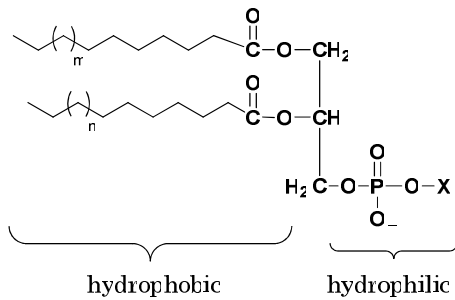


Figure 2.1-2: General structure of phospholipids.

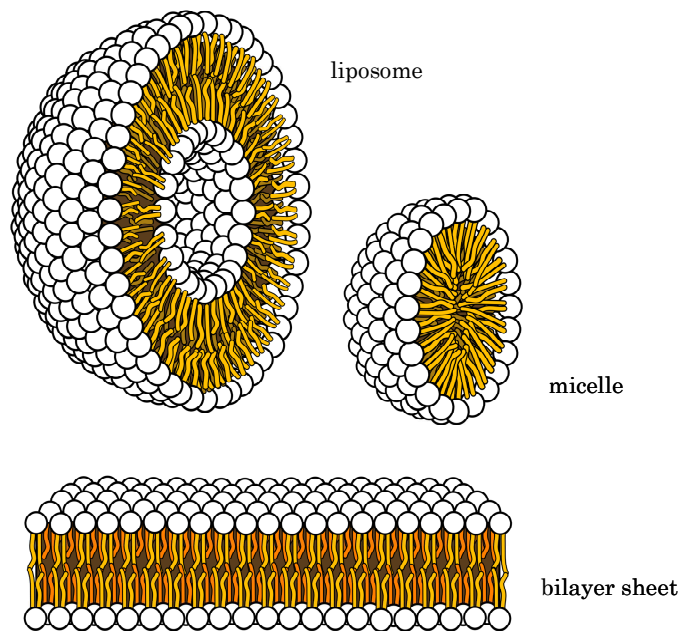


Figure 2.1-3: Three main structures of phospholipids in solution.¹¹

¹⁰ Source: http://en.wikipedia.org/wiki/File:Average_prokaryote_cell_en.svg

¹¹ Source: http://en.wikipedia.org/wiki/File:Phospholipids_aqueous_solution_structures.svg

The cell membrane is surrounded by the bacterial cell wall, describing the extra cellular structure. Bacterial cell walls consist of peptidoglycan (polysaccharide chains cross-linked by peptides containing amino acids). Due to the general lack of internal membranes electron transport occurs across the cell membrane between the cytoplasm and the periplasmic space. Depending on the sophistication of the cell wall structure, bacteria can be divided into two classes, Gram-positive (e.g. *S. aureus*) and Gram-negative (e.g. *E. coli*) by the so called Gram staining.

Gram-negative bacteria do not retain the crystal violet dye in the Gram staining protocol. Because of the very thin peptidoglycan structure the cell wall of Gram-negative bacteria is very thin. The peptidoglycan is spread through the periplasmic space, which is found between the outer and the inner membrane. The periplasmic space or periplasm is the space between the inner cytoplasmic membrane and the outer membrane of Gram-negative bacteria. The additional outer membrane of Gram-negative bacteria like *E. coli* consists of phospholipids, proteins and mainly complex lipopolysaccharides (LPs).

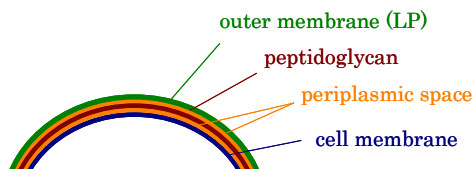


Figure 2.1-4: Gram-negative cell wall structure.

Throughout the gram staining the outer membrane is washed away and the peptidoglycan layer is exposed. Therefore the colour, which is bound in the layer is not protected anymore and washed away as well.

Gram-positive cell wall does not have an outer membrane but possesses a thick cell wall containing many layers of phospholipids, proteins, and peptidoglycan and **teichoic acids**. The periplasm in Gram-positive bacteria is the space outside the inner membrane. During the Gram staining the peptidoglycan layer gets dehydrated; the colour is trapped and cannot be washed out. Hence, the Gram-positive cell wall stain purple during the Gram staining.

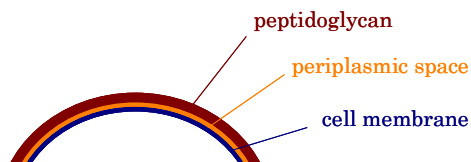


Figure 2.1-5: Gram-positive cell wall structure.

Therefore it is very important to know, if a bacterium is Gram-negative or positive. Biocides have to fulfil different requirements regarding the nature of the bacteria.

2.1.1.2 Biofilm, Biofouling Formation and Growth

A biofilm consists of microorganisms which tend to proliferate, building a matrix of extra-cellular polymeric substances (EPS) in which the different microorganisms are immobilised. This leads to an uncontrolled and exponential growth of the biofilm on different surfaces. The favoured conditions for the formation and proliferation of a biofilm are microorganisms, surfaces and interfaces, nutrients and humidity. The biofilm itself represents a shelter and living space that provides a symbiotic habitat for many different species which offers protection against environmental stresses. Nevertheless, certain conditions are necessary for the formation of a biofilm: there must be a surface or an interface in contact with water or wet air and microorganisms as well as nutrients must be present. Figure 2.1-6 shows a SEM picture of biofilm formation on silicon.

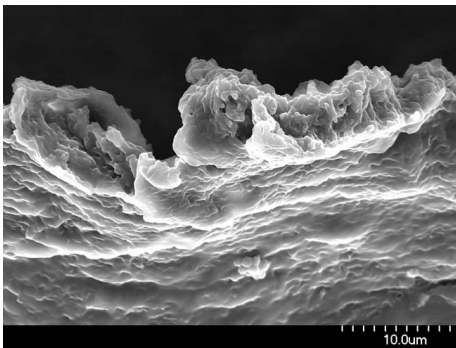


Figure 2.1-6: Biofilm formation on silicon.¹²

The term biofouling refers to a biofilm that grows within technical equipment disturbing production processes and products. Biofouling leads to significant loss of products and creates unacceptable environmental burdens for chemical cleaning. Biofouling does not only present a considerable hygiene risk in the food industry, but also causes economic losses. Therefore there is a widespread interest in biocide coatings.

Many different problems can arise from biofouling; biofilm can cause and accelerate corrosion of the affected material, pressure reductions in pipes and membrane installations. In addition, loose pieces of a biofilm contaminates products and disturb production processes and even the presence of only a few micro-organisms in purified and potable water installations may cause hygiene problems. Any method of preventing biofouling or lengthening processing time minimises downtimes and give substantial cost benefits.

¹² Source: <http://www.bacteria-world.com/biofilm.jpg>

2.1.2 Charge Effects

2.1.2.1 Electrostatic Interaction

A bacteria cell surface is usually negatively charged, demonstrated by their susceptibility to electrophoresis. Therefore, adsorption of polycations onto the negatively charged surface of bacteria takes place to a greater extent than that of monomeric cations.

Hence, the development of biocidal polymers paves the way for enhancing the biocide efficiency and selectivity while minimising the environmental problems accompanying conventional antimicrobial agents. The increased biocidal efficiency of such contact biocide polymers can be easily stated by the adsorption of polycations onto the negatively charged cell membranes taking place to a larger extent than that of monomeric cations due to the much higher charge density.

2.1.2.2 Effect of Counterions¹³

It is evident that antibacterial activity is affected by the structure of the counter anions.¹⁴ Kanazawa et al. showed that the activity was low for a counter anion, which tends to form a tight ion-pair with phosphonium ions (appearing in the cell membrane of bacteria) while it was high for those facilitating ionic dissociation to free ions. Apart from that, the only explanation for counterions having an effect on antimicrobial activity is the increased solubility of the corresponding polymers.

Adsorption of the polycationic biocide polymer appears due to electrostatic interaction with the negatively charged membrane of the microorganisms. Subsequently, the elemental counterions of the bacteria cells are displaced by the polycations. This mechanism, among others, is described in more detail in Chapter 1.1.2.3.

2.1.2.3 Biocide Mechanisms

Accordant to the broad variety of different biocides they also exhibit different antimicrobial activity and physical mechanisms of action which can be divided into four categories (*cf.* Figure 2.1-7).

¹³ Kenawy, E.-R.; Worley, S. D.; Broughton, R. *Biomacromolecules* **2007**, *8*, 1359-1384.

¹⁴ Kanazawa, A.; Ikeda, T.; Endo, T. *J. Polym. Sci., Part A: Polym. Chem.* **1993**, *31*, 1467-1472.

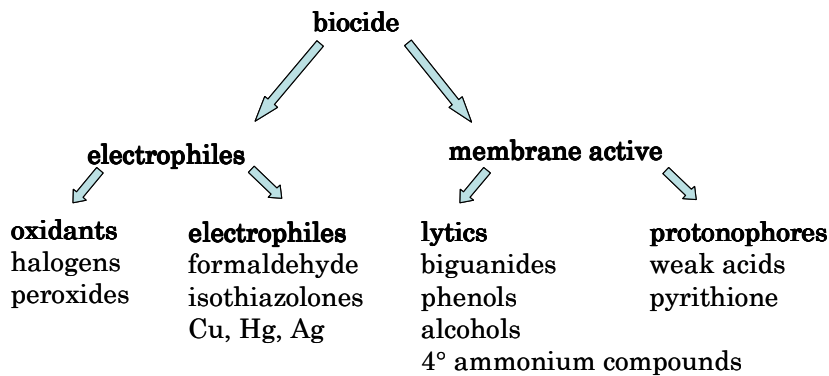


Figure 2.1-7: Mechanism of biocides.

The **oxidants** include agents such as chlorine and peroxides. They kill the bacteria rapidly via radical-mediated reactions to oxidise organic material.¹⁵

The **electrophilic** agents include inorganic ions such as silver, copper, and mercury, and organic biocides such as formaldehyde and isothiazolones. These biocides react covalently with cellular nucleophiles to inactivate enzymes.¹⁶ Furthermore this type of biocides initiates the formation of intracellular free radicals.¹⁷

Cationic **membrane active biocides** (e.g. chlorhexidine and quaternary ammonium compounds),¹⁸ and **alcohols** (e.g. phenoxyethanol)¹⁹ destabilise bacteria membranes. This effect is increased by the use of polymeric biocides due to the much higher charge density and, additionally, due to the shielding effect caused by the polymers which bind to the phospholipid membrane. This causes phase separation of charged and uncharged lipids and thus leakage of the cell constituents leading to rapid lysis of the cell (*cf.* Figure 2.1-8 to Figure 2.1-11).

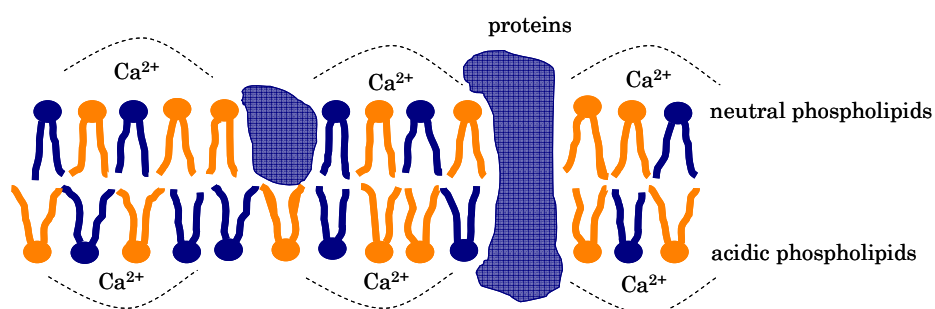


Figure 2.1-8: Cytoplasm membrane.

¹⁵ Dukan, S.; Touati, D. *J. Bacteriology* **1996**, *178*, 6145–6150.

¹⁶ Collier, P.J.; Ramsey, A.J.; Austin, P.; Gilbert, P. *J. Appl. Bacteriology* **1990**, *69*, 569–577.

¹⁷ Kimura, T.N.H. *Intracellular. Mutation Research* **1997**, *389*, 237–242.

¹⁸ Chawner, J.A.; Gilbert, P. *J. Appl. Bacteriology* **1989**, *66*, 253–258.

¹⁹ Gilbert, P.; Beveridge, E.G.; Crone, P.B. *Microbios* **1977**, *19*, 125–141.

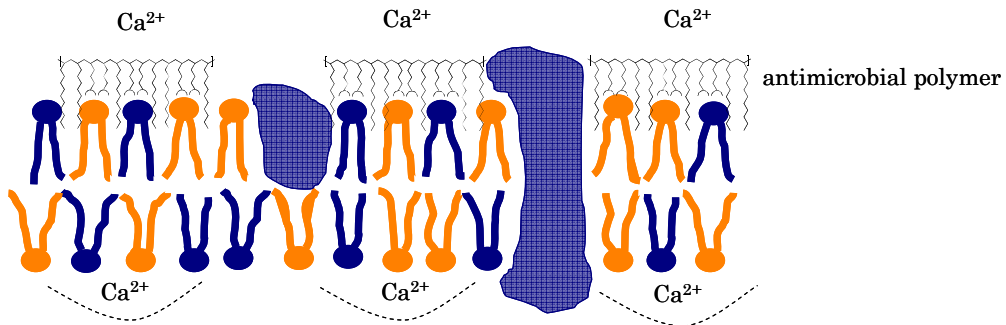


Figure 2.1-9: Adsorption onto the cytoplasmic membrane.

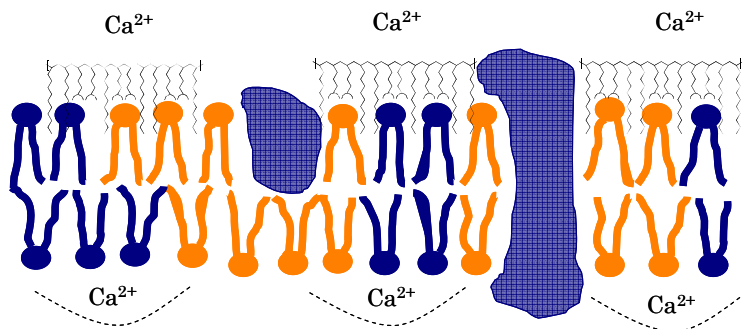


Figure 2.1-10: Disruption and phase separation of the cytoplasmic membrane.

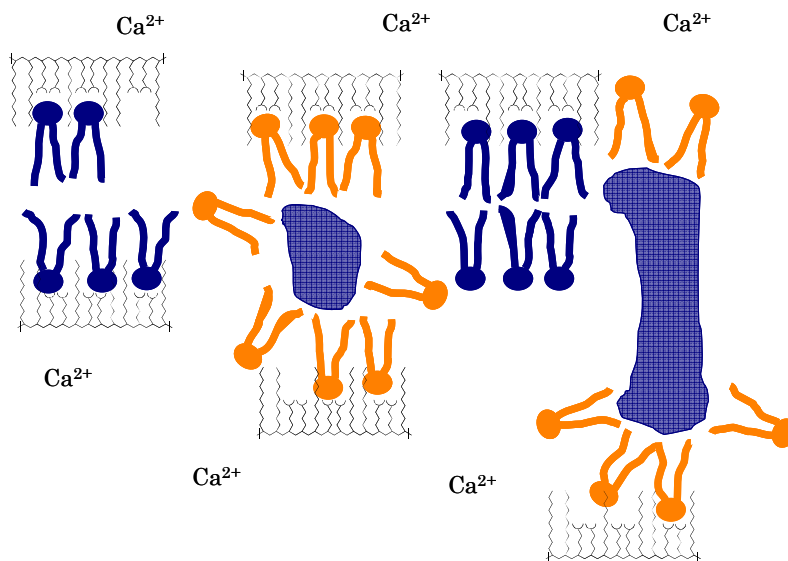


Figure 2.1-11: Leakage of the cell constituents and lysis of the cell.

Weak acids (e.g. sorbic and benzoic acid) disrupt the pH balance of the cell membrane, resulting in acidification of the cell interior and disruption of metabolism.²⁰

²⁰ Eklund, T. *J. Gen. Microbiology* **1985**, *131*, 73–76.

2.1.3 Polymer Architecture¹³

2.1.3.1 Spacer Length and Hydrophilic-Hydrophobic Balance

The spacer length between the active site and the polymer main chain affects the antimicrobial activity. In polymeric quaternary ammonium salt biocide and copolymers thereof the balance between hydrophobic and hydrophilic moieties in the polymer plays an important role. It has been shown that the antimicrobial activity increases with the length of the alkyl chain of the copolymerised hydrophobic monomer. Both, the spacer length and the hydrophilic-hydrophobic balance influence the conformation and charge density of the polymer and affect the mode of interaction with the cytoplasmic membrane.

Anti-fouling surfaces are based on minimising the intermolecular forces of interactions between extra cellular biomolecules and the synthetic surfaces. While hydrophobic surfaces show low intermolecular forces of interaction with biomolecules and thus hinder the settlement of cells, hydrophilic surfaces, with low values of polymer-water interfacial energy, show resistance to protein adsorption and cell adhesion. Ober et al. reviewed a range of polymeric coatings with promising anti-biofouling and fouling release properties. Hydrophobic poly(dimethylsiloxane)s (PDMS) and fluoropolymer surfaces are not resistant to protein adsorption, but are non-adhesive to cells and organisms due to their non-polar nature. Hydrophilic poly(ethylene glycol) (PEG) containing polymers, zwitterionic polymers incorporating oligosaccharide moieties are inherently anti-biofouling and resist protein adsorption and cell settlement.²¹ Surface hydration via hydrogen bonding and steric exclusion effects are considered to be the key factors for the resistance to non-specific protein adsorption of PEG. Nevertheless, zwitterionic materials such as betaines can bind water molecules even more strongly via electrostatically induced hydration. Thereby, surface packaging of the zwitterionic group seems to be an important factor to be considered. Future directions are aimed towards tuning the properties of zwitterionic materials by adjusting their structures, such as backbones and counterions, the distance between two charged groups and the type of positively and negatively charged groups.²²

A further, amphiphilic approach considers that the cell membranes of bacteria and fungi are hydrophobic and negatively charged (*cf.* Chapter 2.1.1.1). Consequently, long hydrophobic polymeric chains should penetrate the membranes of the microbes and disrupt the cell membrane. If these hydrophobic moieties are combined in a copolymer with positively charged groups, additionally the electrostatic interactions between the polycations and the negatively charged surface of the bacteria are increased (*cf.* Chapter 2.1.2.1). The positive charge also rigidifies the polymer and prevents

²¹ Krishnan, S.; Weinman, C.J.; Ober, C.K. *J. Mater. Chem.* **2008**, *18*, 3405-3413.

²² Jiang, S.; Cao, Z. *Adv. Mater.* **2010**, *22*, 920-932.

hydrophobic attraction between the hydrophobic moieties and forces the long alkyl chains to stay erect due to electrostatic repulsion. However, an optimal balance of hydrophobicity and charge density has to be found because a too high load of positive charge could also weaken the interaction between the polymer and the bacteria, and thus decrease antimicrobial activity.²³

2.1.3.2 Molecular Weight

Ikeda et al showed that the antimicrobial activity of polyacrylates and polymethyl acrylates with biguanide groups in the side-chain and their copolymers with acrylamide was optimal when the molecular weight range between $5 \cdot 10^4$ and $1.2 \cdot 10^5$ Da. These observations were explained by the changes in permeability through the cell wall.¹³

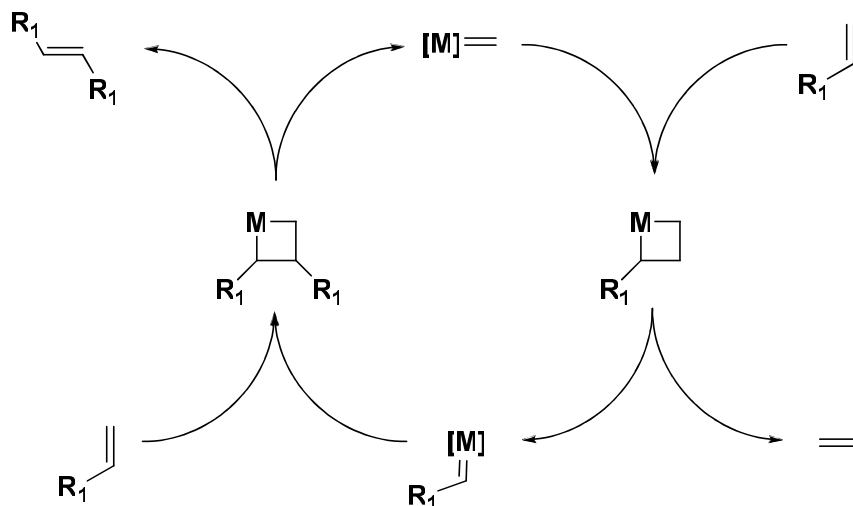
²³ Lewis, K.; Klibanov, A. M. *Trends Biotechnol.* **2005**, *23*, 343-348.

2.2 Metathesis

2.2.1 Mechanism

Olefin metathesis (from the Greek μετάθεσις "transposition") describes the exchange of alkylidene groups between two alkenes. Over the past decades and accompanied by further research and development of new catalyst systems, the olefin metathesis emerged as a mild, efficient and highly functional group tolerant method for the formation of carbon-carbon double bonds. 1971 Chauvin proposed the mechanism for the metathesis reaction as shown in Scheme 2.2-1.²⁴

Scheme 2.2-1: Mechanism of olefin metathesis.



The olefin coordinates to the metal carbene of the catalyst. By a [2+2] cycloaddition a cyclobutane ring is formed which opens under the formation of two new double bonds.

This carbon-carbon double bond formation exhibits high versatility. Cross metathesis (CM), ring closing metathesis (RCM), ring opening cross metathesis (ROCM), ring rearrangement metathesis (RRM), ene-nemetathesis, ring-expansion metathesis, ring-closing alkyne metathesis (RCAM), ring opening metathesis polymerisation (ROMP), and acyclic diene metathesis polymerisation (ADMET) are some prominent examples of possible olefin metathesis reactions.

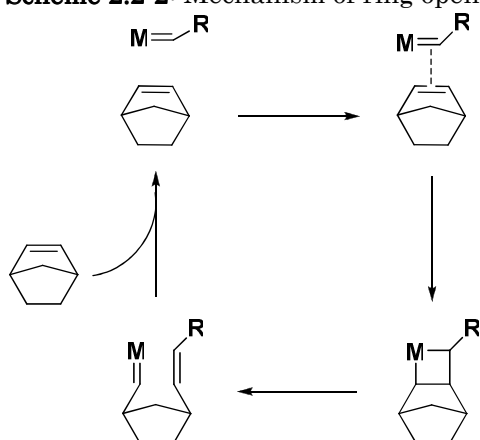
²⁴ Herisson, J-L.; Chauvin, Y.; *Makromol. Chem.* **1971**, *141*, 161-176.

2.2.2 Ring Opening Metathesis Polymerisation (ROMP)

Due to the development of new catalysts and the possibility of living polymerisation, the Ring Opening Metathesis Polymerisation gained increased importance. The characteristics of a living polymerisation include complete and rapid initiation, irreversible propagation steps and absence of chain termination or chain transfer reactions.²⁵

The norbornene motif is maybe the most prominent one for ROMP, as the equilibrium of the metathesis reaction is moved towards the growing polymer chain due to the ring strain of the norbornene derivative. As shown in Scheme 2.2-2 the growing polymer chain emerges between the initiator and the former carbene ligand of the initiator.

Scheme 2.2-2: Mechanism of ring opening metathesis polymerisation.



Due to its livingness and its high functional group tolerance ROMP allows complex polymer architectures such as block-*c*_o polymers, polymer brushes, alternating polymers, etc. Furthermore, ROMP is carried out under mild conditions, thus even sophisticated functional moieties can be easily introduced.

Depending on the initiator and the monomers used, various solvents such as benzene, toluene, dichloromethane, acetone, alcohols, water, and many others, have been used. The crucial requirement for living polymerisation, and thus, narrow molecular weight distribution, is the solubility of initiator, monomers and resultant polymer in the solvent of choice. Comparing different solvents for ROMP, a significant influence was only predominant for polymerisation rates.²⁶

²⁵ Darling, T.R.; Davis, T.P.; Fryd, M.; Gridnec, A.A.; Haddleton, D.M.; Ittel, S.D. *J. Mol. Catal. A: Chem.* **1995**, *102*, 7-21.

²⁶ Slugovc, C. *Macromol. Rapid Commun.* **2004**; *25*, 1283-1297.

2.2.2.1 Initiators

The most common initiators for ROMP are molybdenum and ruthenium carbene complexes. In the 1980ies Schrock et al.^{27,28,29,30} developed molybdenum carbene initiators (*cf.* Figure 2.2-1) which exhibit high activity and complete initiation but restricted functional group tolerance and high sensitivity towards protic solvents and air.

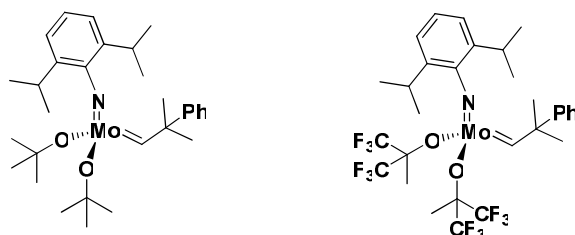


Figure 2.2-1: Schrock type initiators.

With the synthesis of the first metathesis-active ruthenium complexes by Grubbs et al.³¹ in 1992 (*cf.* Figure 2.2-2, left) the functional group tolerance was enhanced. Additionally, the ruthenium-based initiator exhibits a higher stability to air and water. Ruthenium, being a Lewis acid (electron pair acceptor), prefers soft Lewis bases and π -acids like olefins over e.g. oxygen-based ligands.

Strongly electron-donating ligands turned out to be crucial for high catalyst activity for the metal centre.³² The tricyclohexylphosphine - moieties of the 1st generation Grubbs initiator exhibit high donor attributes due to the basicity of the phosphoratom. Furthermore phosphines are strong π -acceptors and form stable complexes with electron-rich late-transition-metals. However, the activity of the 1st generation Grubbs initiators was not yet competitive compared to the Schrock metal carbene complexes.

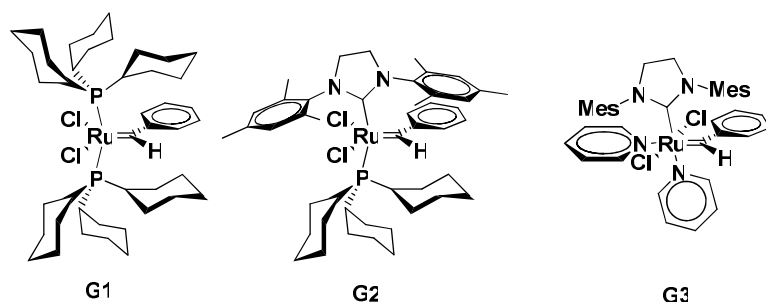


Figure 2.2-2: Grubbs type initiators.

²⁷ Schrock, R.R.; Krouse, S.A.; Knoll, K.; Feldman, J.; Murdzek, J.S.; Yang, D.C. *Journal of Molecular Catalysis* **1988**, *46*, 243-253.

²⁸ Schrock, R.R. *Tetrahedron*, **1999**, *55*, 8141-8153.

²⁹ Schrock R.R. *Acc. Chem. Res.* **1990**, *23*, 158-165.

³⁰ Schrock, R.R. *Angew. Chem.* **2006**, *118*, 3832-3844.

³¹ Nguyen, S.T.; Johnson, L.K.; Grubbs, R.H.; Ziller, J.W. *J. Am. Chem. Soc.* **1992**, *114*, 3974-3975.

³² Grubbs, R.H. *Adv. Synth. Catal.* **2007**, *349*, 34-40.

Herrmann et al.³³ introduced the thermodynamically stable N-heterocyclic carbene ligand. One of the phosphine ligands was replaced by this strong σ -donating N-heterocyclic carbene leading to a mixed ligand system. This was the birth of 2nd generation Grubbs initiators (*cf.* Figure 2.2-2, middle).³⁴ This initiator combines the high functional group tolerance of the 1st generation Grubbs carbene with the high activity of Schrock type initiators. The only disadvantageous about this type of initiator was that polymerisation propagation was high compared to initiation ($k_p \gg k_i$) resulting in high polydispersity indices (PDI - defined as the ratio of weight-average M_w and number-average M_n molecular weights: $PDI = M_w/M_n$) and a broad molecular weight distribution.

Finally, the 3rd generation Grubbs initiator and with it, the introduction of a pyridine ligand (*cf.* Figure 2.2-2, right) enhanced the initiation rate, reduced the propagation rate and suppressed secondary metathesis reactions (e.g. back-biting).

Complete and rapid initiation assures reaction of the initiator molecules with the monomer considerably faster than the rate of propagation. As a consequence, living polymerisation is feasible resulting in very narrow molecular weight distributions close to monodispersity. The average molecular weight of a polymer derived from a living polymerisation can be easily but precisely controlled through the stoichiometric initiator : monomer ratio.

The NeolystTM initiator from Umicore AG underwent an evolution, very similar to the Grubbs initiators. In these analogues the benzylidene ligand of a typical Grubbs catalyst is replaced by an indenylidene ligand (*cf.* Figure 2.2-3).³⁵

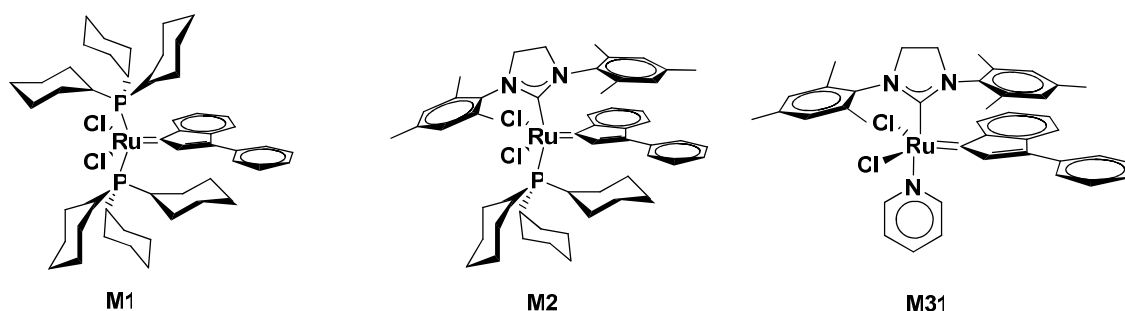


Figure 2.2-3: Neolyst initiator of Umicore AG.

The Umicore initiator show comparable activity to Grubbs initiators but are more easily and cheaper accessible for our group.

³³ Weskamp, T.; Schattenmann, W.C.; Spiegler, M.; Herrmann, W.A.; *Angew. Chem.* **1998**, *110*, 2631-2633.

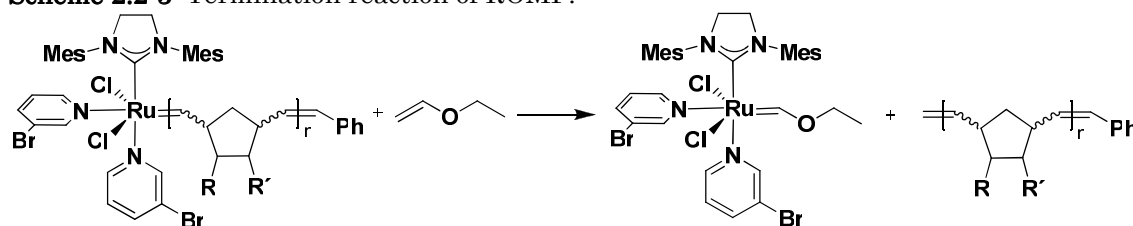
³⁴ Scholl, M.; Trnka, T. M.; Morgan, J.P.; Grubbs, R.H. *Tetrahedron Lett.* **1999**, *40*, 2247-2250.

³⁵ Schanz, H.J.; Jafapour, L.; Stevens, E.D.; Nolan, S.P. *Organometallics* **1999**, *18*, 5187-5190.

2.2.2.2 Termination

Polymerisation is easily quenched by the addition of ethyl-vinyl-ether. The mechanism is equal to the propagation reaction of the growing polymer chain. The ethyl-vinyl-ether also undergoes a metathesis reaction with the initiator under the formation of a less reactive Fisher carbene. Hence, the propagation is quenched and the initiator is removed from the polymer chain (*cf.* Scheme 2.2-3)

Scheme 2.2-3: Termination reaction of ROMP.



Furthermore, by the careful choice of different termination reagents or even by the modification of the metal carbene end-functionalisation of the polymer is possible, again increasing the tremendous field of applications.³⁶

³⁶ Lexer, C.; Saf, R.; Slugovc, C. *J. Polym. Sci. Part A: Polym. Chem.* **2008**, *47*(1), 299-305.

2.3 Luminescence

2.3.1 General information³⁷

Luminescence is the emission of light and occurs after excitation of a substance to electronically excited states. Depending on the nature of the excited state, luminescence can be divided into two categories, fluorescence and phosphorescence. The processes occurring by the absorption and emission of light are clearly demonstrated by the Jablonski diagram (cf. Figure 2.3-1)

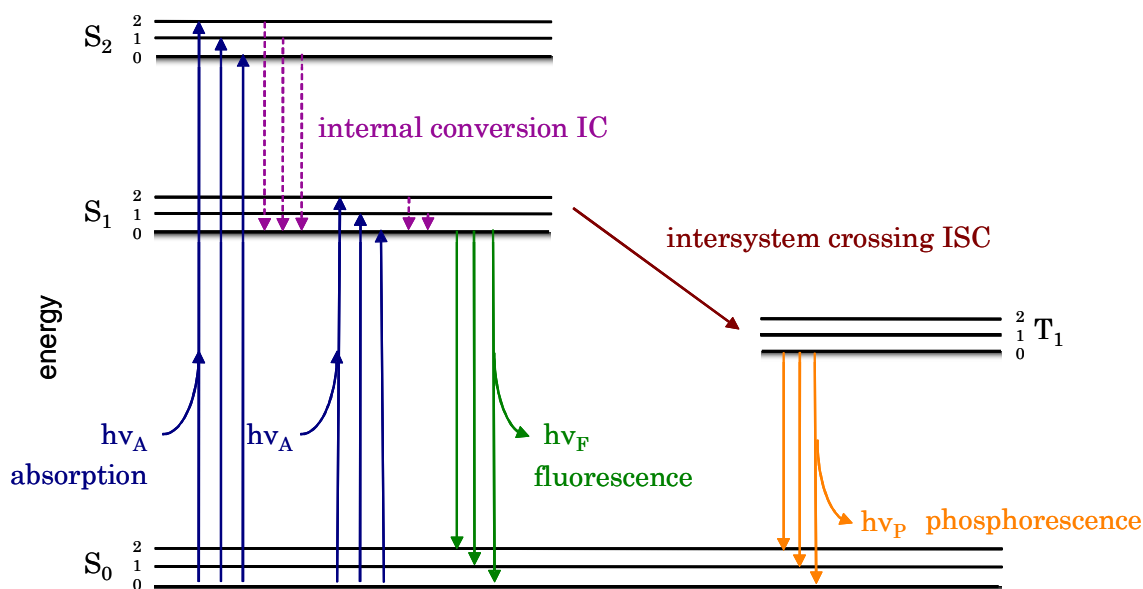


Figure 2.3-1: Jablonski diagram.

In order to induce excitation of a substance, an electron must be promoted from the singlet ground state (S_0) into an excited state (S_1 , S_2) by the absorption of light (photons) of an appropriate wavelength. At each of these electronic energy levels the molecules can exist in a number of different vibrational energy levels.

Absorption and emission usually occurs from the lowest vibrational energy levels. After the absorption of light, the fluorophore is excited to higher vibrational levels of an excited state (S_1 or S_2), but rapidly relaxes to the lowest vibrational level of S_1 . This process is called internal conversion (red arrows), usually occurs within 10^{-12} s and is therefore completed before emission. Hence, fluorescence emission generally takes place from the lowest energy vibrational state of S_1 , the thermally equilibrated excited state.

³⁷ Lakowicz, J. R. *Principles of Fluorescence Spectroscopy*, 3rd ed. Springer, Berlin, 2006.

A fluorophore usually returns to a higher vibrational level of the ground state S_0 by the emission of light, but rapidly reaches thermal equilibrium. This is the reason for the vibrational structure of the emission spectrum of the molecule and is usually similar to the absorption spectrum.

In the above mentioned excited singlet states the electron in the excited state and the second electron, in the ground-state orbital, are spin-paired. Hence these transitions are spin-allowed and are characterised by a short luminescence lifetime.

The excited molecules from the S_1 level can undergo a spin conversion to the triplet state T_1 , called inter system crossing (ISC). The emission from T_1 to the singlet ground state results in phosphorescence, which is spin forbidden and generally shifted to longer wavelength (lower energy). Transition metal atoms such as Ru, Pd, Pt or Ir usually facilitate ISC and enhance phosphorescence.

2.3.1.1 Luminescence Lifetime and Quantum Yield

The quantum yield (QY) is the number of photons emitted relative to the number of photons absorbed. Substances with a high quantum yield usually exhibit brightest emission. The lifetime of a luminophore describes the time available for interactions with other species.

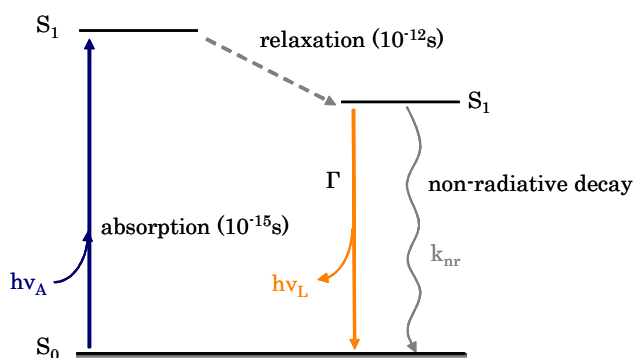


Figure 2.3-2: Simplified Jablonski diagram.

Figure 2.3-2 displays a simplified Jablonski diagram focusing on emission parameters influencing quantum yield and lifetime: the emissive rate of the fluorophore (Γ) and its rate of non-radiative decay to the singlet ground state S_0 (k_{nr}). Both constants depopulate the emissive rate. The quantum yield and accordingly the proportion of fluorophores that decay through emission is given by Equation 2.3-1.

$$Q = \frac{\Gamma}{\Gamma + k_{nr}} \quad \begin{array}{ll} Q & \text{quantum yield} \\ k_{nr} & \text{rate of non-radiative decay} \\ \Gamma & \text{emissive rate of the fluorophore} \end{array} \quad \mathbf{2.3-1}$$

The lifetime (*cf.* Equation 2.3-2) of the excited state is defined as the average time a molecule spends in the excited state before deactivation into the ground state.

$$\tau = \frac{1}{\Gamma + k_{nr}}$$

τ	lifetime of the excited state	2.3-2
k_{nr}	rate of non-radiative decay	
Γ	emissive rate of the fluorophore	

Fluorescence lifetimes are usually near 10 ns, whereas lifetimes of phosphorescent dyes range typically from a few hundred nanoseconds up to milliseconds.

2.3.1.2 Luminescence Quenching

The radiationless decrease of fluorescence intensity, called quenching, can be caused by excited-state reactions, molecular rearrangements, energy transfer, ground state complex formation (static quenching) or collisional quenching.

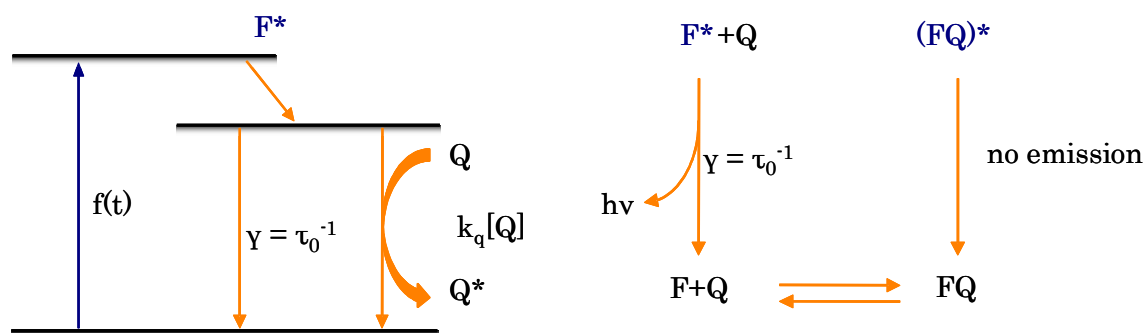


Figure 2.3-3: Collisional (left) and static quenching (right).

Dynamic quenching, also referred to as collision quenching, describes the deactivation of the excited state of the luminophore upon collision with other quencher molecules in solution (*cf.* Figure 2.2-1, left). The quencher returns to its ground state without emission of light. Hence, the intensity and luminescence lifetime of the luminophore are reduced. For collisional quenching this decrease in luminescence intensity is described by the Stern-Volmer Equation 2.3-3.

$$\frac{F_0}{F} = 1 + k_q \tau_0 [Q] = 1 + K_D [Q]$$

F_0	intensity in the absence of quencher	2.3-3
F	intensity in the presence of quencher	
k_q	bimolecular quenching constant	
τ_0	lifetime of the fluorophore in absence of quencher	
$[Q]$	concentration of quencher	
K_D	Stern-Volmer quenching constant	

In a corresponding Stern-Volmer plot, F_0/F is plotted versus the quencher concentration $[Q]$ due to the linear relation between F_0/F and the quencher concentration. For linearity of the Stern-Volmer plot the presence of a single class of fluorophores and an equal accessibility of the luminophore to the quencher are assumed. These deviations influence the x-axis while a deviation towards the y-axis indicates that the fluorophore can be quenched by static and dynamic quenching.

Well known collisional quencher include oxygen, halogen ions such as iodide and bromide, hydrogen peroxide, heavy metal ions or even olefins. But not all fluorophores are quenched by all potential quencher molecules. The individual mechanism of quenching depends on the structure of luminophore and quencher as well as on their interaction with each other.

Static quenching (*cf.* Figure 2.2-1, right) occurs by the formation of a nonfluorescent complex between the fluorophore and the quencher. This process takes place in the ground state and does not depend on diffusion processes or molecular collision. When the fluorophore-quencher-complex absorbs light, it immediately returns from the excited state into the ground state without emission of a photon.

In static quenching, a fraction of fluorophores is removed from observation leaving the uncomplexed fluorophores unperturbed. Therefore, the luminescence lifetime is independent of static quenching. In contrast, the luminescence lifetime for dynamic quenching is dependent on the quencher concentration. This effect is used in many luminescent sensors (*cf.* Equation 2.3-4).

	F_0	intensity in the absence of quencher	
	F	intensity in the presence of quencher	
	τ_0	lifetime of the fluorophore in the absence of quencher	2.3-4
	τ	lifetime of the fluorophore in the presence of quencher	
	$[Q]$	concentration of quencher	
	K_D	Stern-Volmer quenching constant	
$\frac{F_0}{F} = 1 + K_D [Q] = \frac{\tau_0}{\tau}$			

For fluorescent probes with a lifetime of 5 ns and shorter the collision with a quencher is a rather rare event compared to luminescence decay. Thus, dynamic quenching becomes rather negligible for short-lived excited state. Phosphorescent dyes with lifetimes in the range of microseconds to a few milliseconds are of particular interest for sensing purposes as the probability for collision of the excited state with a quencher is higher.

2.3.2 Ruthenium-based Metal-Ligand Complexes³⁷

Ruthenium-complexes and transition metal complexes (TMC) in general, bearing one or more diimine ligands are described as metal-ligand complex (MLC). Typical metals for these complexes are rhenium (Re), ruthenium (Ru), osmium (Os) or iridium (Ir). The luminescence intensities and characteristics vary strongly depending on the metals and the ligands.

The model complex to study excited-state charge transfer of metal-ligand complexes is $[\text{Ru}(\text{bpy})_3]^{2+}$, where bpy stands for 2,2'-bipyridine ligands. Upon absorption of light $[\text{Ru}(\text{bpy})_3]^{2+}$ becomes a metal-to-ligand charge-transfer (MLCT) species. Thereby ruthenium is oxidised to Ru^{III} and one of the bpy is reduced to the strong reductant bpy^- species (cf. 2.3-5).



Metal-ligand complexes exhibit unique electronic states (cf. Figure 2.3-4). All $[\text{Ru}(\text{bpy})_3]^{2+}$ -like metal-ligand complexes have 6 d electrons which are associated with the metal. The octahedral crystal field of the ligands splits the degenerate five d -orbitals into three triply degenerate lower (t) orbitals, filled by the 6 d electrons, and two higher, doubly degenerate, unoccupied e orbitals. The splitting arises from different orientations of the orbitals in relation to the ligands. The higher e orbitals are directed towards the ligands while the lower t orbitals point between the ligands. The extent of splitting depends on the crystal field strength Δ of the ligands which affects the electron distribution between the t and the e levels. If the crystal field of the ligands is strong and Δ is large, it is electronically more favourable to pair electrons in the t level rather than to keep them unpaired by filling the e level according to the Hund's rule. If the crystal field is weak and hence Δ smaller than the pairing energy, this would result in a maximum number of unpaired electrons which is not favourable for luminescence.

The lowest singlet and triplet ligand localised excited states are π - π^* transitions arising by promoting an electron from a π bonding to the π anti-bonding state. This transition exhibits high absorption at 250-310 nm, is largely localised at the ligand and spectroscopically similar to the free ligand, hardly showing perturbation by the metal. Lowest lying singlet and triplet d - d states arise from promoting a bonding t electron to an e level. d - d states are characterised by a low molar absorption coefficient, long radiative lifetimes and high susceptibility to environmental quenching.

Furthermore, the combination of metal and ligands leads to a new transition involving charge transfer between the metal and the ligands. In a metal-to-ligand charge transfer (MLCT) transition the electron is promoted from the d orbital of the metal to the antibonding π^* orbital of the ligand. Whereas in a ligand-to-metal charge transfer (LMCT) transition the electron is promoted from the bonding π orbital of the ligand to the e orbital of the

metal. Since ruthenium is easily oxidised and diimine ligands are easily reduced (*cf.* Chapter 2.3-5), MLCT transitions are far more likely as LMCT transitions.

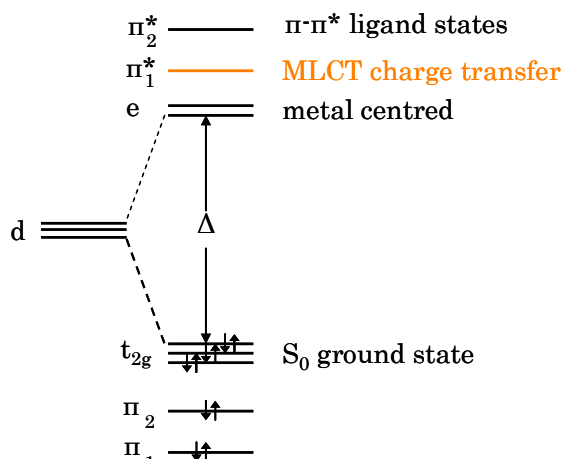


Figure 2.3-4: Electronic states of MLC.

For a metal-ligand complex to be luminescent the crystal field of the ligand must be strong enough to raise the metal centred $d-d$ state above the MLCT state (*cf.* Figure 2.3-5, left), otherwise radiationless decay is predominant.

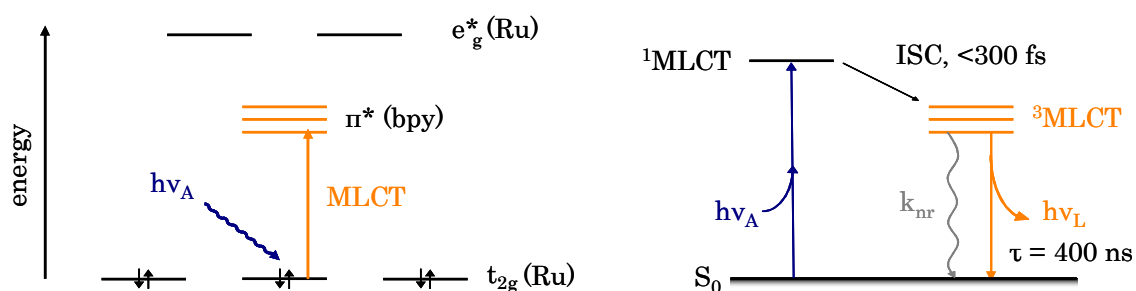


Figure 2.3-5: Crystal field dependent MLCT (left) and simplified Jablonski diagram for MLC (right).

Hence, the electrons are promoted from the metal to the ligand (metal to ligand charge transfer – MLCT) resulting in the absorption band of metal-ligand complexes at 450 nm.

Following absorption the metal-ligand complex undergoes intersystem crossing to the triplet MLCT state (*cf.* Figure 2.3-5, right).

Another important role plays the energy gap law. If the excited state energy becomes closer to the ground state, the rate of radiationless decay increases.

The emission of a TMC is also dominated by the MLCT transition. In contrast to europium complexes, absorption and emission characteristics of MLCs do not arise from the atom,³⁸ but rather from the entire complex. Thus, metal-ligand complexes behave like a single chromophoric unit. Furthermore, the metal-ligand bonds are covalent bonds, thus the ligands and the metal do not dissociate under remotely physiological conditions.

³⁸ Knall, A.-C.; Pein, A.; Noormofidi, N.; Stelzer, F.; Slugovc, C. *Polymer Preprints* **2007**, *48*, 575.

The large Stokes shift of MLC is another favourable spectral property. Consequently, excitation and emission light are easily separated and self-quenching is rather unlikely. Additionally, ruthenium complexes in general are not prone to self-association.

2.3.2.1 Applications of Transition Metal Complexes and Resulting Polymers

Ruthenium diimine complexes and ruthenium diimine complex-containing polymers have been increasingly studied and developed, owing to the unique photophysical, photochemical, and electrochemical properties. Many different applications of ruthenium bearing different bipyridyl-like ligands as well as polymeric systems have been published. Potential applications include DNA-binding properties,³⁹ sensor applications,⁴⁰ photosensitizers, electron- and energy-transfer processes, photovoltaic cells,⁴¹ and supramolecular chemistry. Schubert and Gohy issued several publications and a review on the synthesis of amphiphilic metallo-supramolecular block copolymers containing the ruthenium moiety in the polymer main chain.⁴² Star polymers with ruthenium-polypyridine complexes in the core⁴³ or on branches⁴⁴ have been prepared. O'Reilly et al. reported on hollow nano-cages derived from ruthenium micelles.⁴⁵

Polymers containing ruthenium diimine complexes can be prepared either directly from monomers containing the ruthenium complex or by coordination of preformed polymers with ruthenium complexes.⁴⁶ Weck et al. even issued a publication on ruthenium complex bearing polymers derived from ROMP.⁴⁷ Later, Metera and Sleiman conducted self-assembly studies of ruthenium-bipyridine-containing block-*c*opolymers, generated by living ROMP.^{48,49,50}

However, none of the reported polymeric systems have been investigated with respect to their potential application as sensitive layer for oxygen sensing. This is one of the main focuses of the present thesis. The aim is to develop antimicrobial polymers and simultaneously determine the presence of aerobic bacteria as a function of luminescence lifetime of the copolymerised ruthenium complexes.

³⁹ Hartshorn, R.M.; Barton, J.K. *J. Am. Chem. Soc.* **1992**, *114*, 5919-5925.

⁴⁰ Demas, J.N.; DeGraff, B.A. *Coord. Chem. Rev.* **2001**, *211*, 317-351.

⁴¹ Kalyanasundaram, K. *Coord. Chem. Rev.* **1982**, *46*, 159-244.

⁴² Gohy, J.-F.; Lohmeijer, B.G.G.; Schubert, U.S. *Chem. Eur. J.* **2003**, *9*, 3472-3479.

⁴³ Smith, A. P.; Fraser, C. L. *Macromolecules* **2003**, *36*, 5520-5525.

⁴⁴ Zhou, M.; Roovers, J. *Macromolecules* **2001**, *34*, 244-252.

⁴⁵ Ievins, A.D.; Moughton, A.O.; O'Reilly, R.K. *Macromolecules* **2008**, *41*, 3571-3578.

⁴⁶ Cho, Y.-S.; Lee, J.-S. *Macromol. Chem. Phys.* **2002**, *203*, 2495.

⁴⁷ Carlise, J.R.; Weck, M. *J. Polym. Sci. Part A: Polym. Chem.* **2004**, *42*, 2973-2984.

⁴⁸ Metera, K.L.; Sleiman, H. *Macromolecules* **2007**, *40*(10), 3733-3738.

⁴⁹ Chen, B.; Sleiman, H.F. *Macromolecules* **2004**, *37*(16), 5866-5872.

⁵⁰ Rezvani, A.; Bazzi, H.S.; Chen, B.; Rakotondradany, F.; Sleiman, H.F. *Inorg. Chem.* **2004**, *43*(16), 5112-5119.

3 Results and Discussion

3.1 Amino-Functionalised, Random ROM Polymers

3.1.1 Introduction

Our group intensively investigated the synthesis and antibacterial activity of polymeric material. Seyfriedsberger et al. first synthesised an amino-functionalised polymer, namely poly(2-tert-butylaminoethyl)methacrylate and compounded 5 wt.% with poly(ethylene). The compound exhibited high activity against *Staphylococcus aureus* (*S. aureus*) and *Escherichia Coli* (*E. Coli*).⁵¹

These results were then transferred to develop similar polymers via ROMP by Kreutzwiesner et al.⁵² ROMP was the polymerisation method of choice, not only because of the high versatility, high functional group tolerance and living nature of this polymerisation technique but also because of the decrease of functional group density on the polymeric backbone which can be achieved.

Different norbornene based monomers have been successfully synthesised. All monomers were prepared by a [4+2] cycloaddition reaction of

⁵¹ Seyfriedsberger, G.; Rametsteiner, K.; Kern, W. *Eur. Polym. J.* **2006**, *42*, 3383-3389.

⁵² Kreutzwiesner, E.; Noormofidi, N.; Seifriedsberger, G.; Wiesbrock, F.; Kern, W.; Rametsteiner, K.; Stelzer, F.; Slugovc, C. *submitted*.

cyclopentadiene with the corresponding acrylate derivative. Some of the most promising monomers are depicted in Figure 3.1-1.

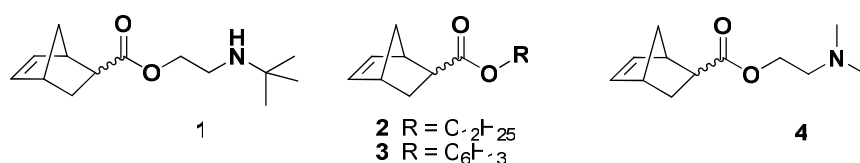


Figure 3.1-1 Monomer concepts for ROMP.

Monomers **1** and **4** were used to prepare the corresponding homopolymers **poly(1)** and **poly(4)**. Furthermore, a series of random copolymers of either **1** or **4** with **2** or **3** was prepared, aiming at a decreased water solubility of the polymers and fine-tuning of the overall polarity of the material, as an optimal balance of hydrophobicity and charge density has to be assured (*cf.* Chapter 2.1.3.1). The above mentioned random copolymers are summarised in Figure 3.1-2.

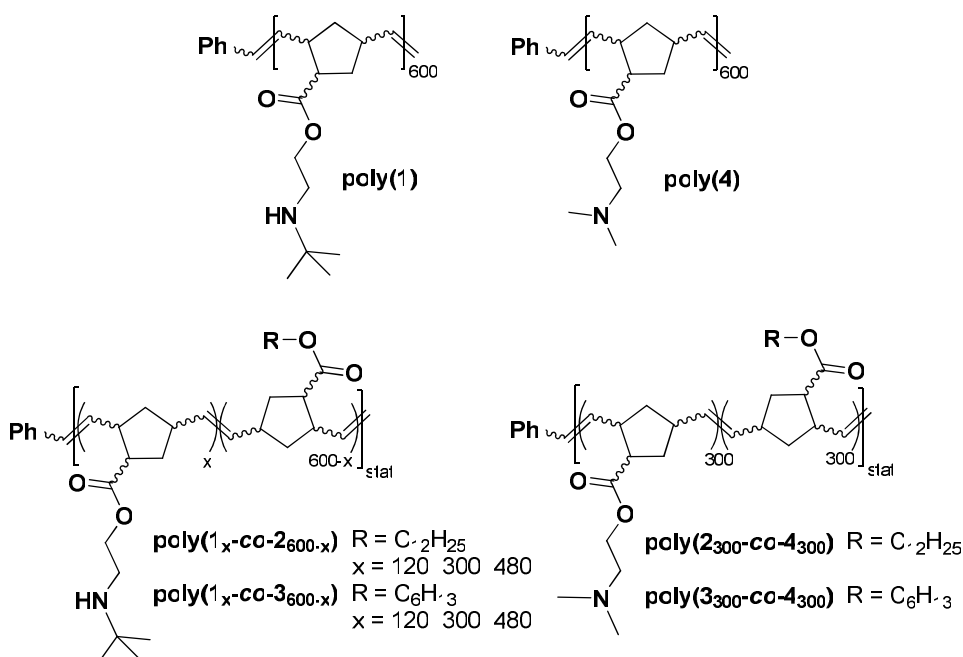


Figure 3.1-2: Resulting ROM polymers using third generation Grubbs initiator.

Polymerisation yields, average molecular weights and polydispersity indices determined by gel permeation chromatography (GPC) as well as decomposition temperature (T_{dc}) and glass transition temperature (T_g) determined by thermogravimetry are summarised in Table 3.1-1 and antimicrobial activity according to the Japanese Industry Standard (JIS Z 2801:2000)⁵³ in Table 3.1-2, respectively.

Due to high solubility and swelling in water of polymers bearing **4**, these polymers were unsuitable with regard to the intended applications.

⁵³ Suzuki, S.; Imai, S.; Kourai, H. *Biocontrol Science* **2006**, *11*, 135-145.

Thermogravimetric analysis (TGA)/ differential scanning calorimetry (DSC) measurements revealed increasing decomposition temperatures (T_{dc}) but decreasing glass transition temperature (T_g) with increasing ratio of the hydrophobic monomers **2** or **3**.

Table 3.1-1: Characteristic data of the homo- and copolymers.⁵²

polymer	Yield [%]	M_n [kDa]	PDI	T_{dc} [°C]	T_g [°C]
poly(1)	87	136	1.4	283	29
poly(4)	83	161	2.2	306	12.5
poly(1₁₂₀-<i>co</i>-2₄₈₀)	73	118	1.4	345	n.o.
poly(1₃₀₀-<i>co</i>-2₃₀₀)	74	128	1.5	320	18
poly(1₄₈₀-<i>co</i>-2₁₂₀)	73	169	1.6	292	7
poly(1₁₂₀-<i>co</i>-3₄₈₀)	68	122	1.3	338	17
poly(1₃₀₀-<i>co</i>-3₃₀₀)	77	128	1.2	293	4
poly(1₄₈₀-<i>co</i>-3₁₂₀)	79	132	1.5	279	19
poly(2₃₀₀-<i>co</i>-4₃₀₀)	75	172	1.6	351	24
poly(3₃₀₀-<i>co</i>-4₃₀₀)	76	132	1.9	333	3

Table 3.1-2: Antimicrobial activity of the homo- and copolymers.⁵²

polymer	$\Delta \lg(\text{CFU})$	$\Delta \lg(\text{CFU})$
	<i>E. coli</i>	<i>S. aureus</i>
reference	0	0
poly(1)	-1.96	-1.86
poly(4)	-3.96	0.3
poly(1₁₂₀-<i>co</i>-2₄₈₀)	-1.24	-1.79
poly(1₃₀₀-<i>co</i>-2₃₀₀)	-1.86	-2.65
poly(1₄₈₀-<i>co</i>-2₃₀₀)	-0.89	-1.79
poly(1₁₂₀-<i>co</i>-3₄₈₀)	-0.83	-0.12
poly(1₃₀₀-<i>co</i>-3₃₀₀)	-2.12	-0.37
poly(1₄₈₀-<i>co</i>-3₁₂₀)	-2.19	-0.29
poly(2₃₀₀-<i>co</i>-4₃₀₀)	-1.08	-1.2
poly(3₃₀₀-<i>co</i>-4₃₀₀)	0.41	-0.92

Hence, a compromise between water solubility and processibility had to be found, never losing sight of antimicrobial activity. Consequently, **poly(1₃₀₀-*co*-2₃₀₀)** has been selected to be the best performing and most promising candidate for further studies.

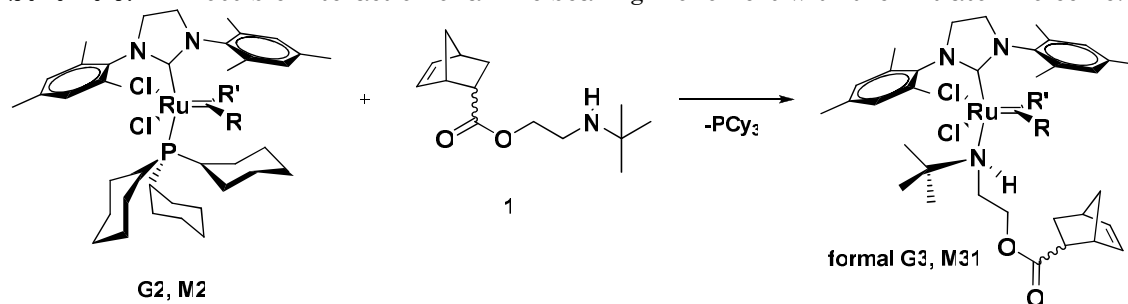
In Chapter 3.1.2 further investigations are summarised to gather deeper insights and optimise polymerisation conditions and architecture.

3.1.2 Optimisation of Polymerisation Conditions

3.1.2.1 Choice of Initiator

It was presumed that amines interfere with the polymerisation reaction in a similar manner like nitriles.^{54,55} Secondary amines tend to reduce the propagation rate and require elevated temperatures. In previous reports, pyridine functionalised initiators like **G3** gave the best results for the polymerisation of nitrogen bearing monomers.²⁶ Nevertheless, the polymerisation behaviour of the amine and their binding ability to the initiators **G2**, **G3** and **M2** was investigated. The aim of these studies was to investigate whether secondary amines could also have a positive effect on the propagation. During the development of the Grubbs initiators, pyridine ligands turned out to be good ligands and leaving groups for ruthenium and hence enhance the initiation rate and reduce the propagation rate. Other amine bearing monomers may behave similarly as shown in Scheme 3.1-1.

Scheme 3.1-1: Possible interaction of amine bearing monomers with the initiator molecule.



Test polymerisations using **G2** and **M2** lead to polymers with very high molecular weight and a broad molecular weight distribution. The polymers precipitated during polymerisation due to uncontrolled increasing molecular weight and decreased solubility. The isolated polymers exhibited such high molecular weight that even size exclusion chromatography (SEC) was unfeasible. Hence, propagation occurred much faster than initiation which makes these initiators unsuitable for the present monomer.

Most polymerisations were initiated with the 3rd generation Grubbs initiator **G3** (*cf.* Chapter 2.2.2.1) and a monomer to initiator ratio of 600 : 1 was chosen. The relatively high monomer : initiator ratio aimed at minimising the amount of initiator and in further decreasing solubility of the polymers in water due to the high molecular weight. **G3** was selected because a narrow molecular weight distribution was desired.

⁵⁴ Demel, S.; Riegler, S.; Wewerka, K.; Schoefberger, W.; Slugovc, C.; Stelzer, F. *Inorg. Chim. Acta* **2003**, *345*, 363-366.

⁵⁵ Riegler, S.; Demel, S.; Trimmel, G.; Slugovc, C.; Stelzer, F. *J. Mol. Catal. A* **2006**, *257*, 53-58.

3.1.2.2 Kinetics

For the kinetic measurements polymerisation progress, or rather monomer consumption of homo- and copolymers was monitored by NMR spectroscopy. Thereby, polymerisation of 300 equivalents of monomer **1** and **2**, respectively and a mixture of 150 equiv. of **1** and 150 equiv. of **2** were initiated by **G3** in degassed deuterated chloroform under argon atmosphere, leading to the corresponding homopolymers **poly(1)** and **poly(2)** and the random copolymer **poly(1₁₅₀-co-2₁₅₀)**, respectively as shown in Figure 2.1-6.

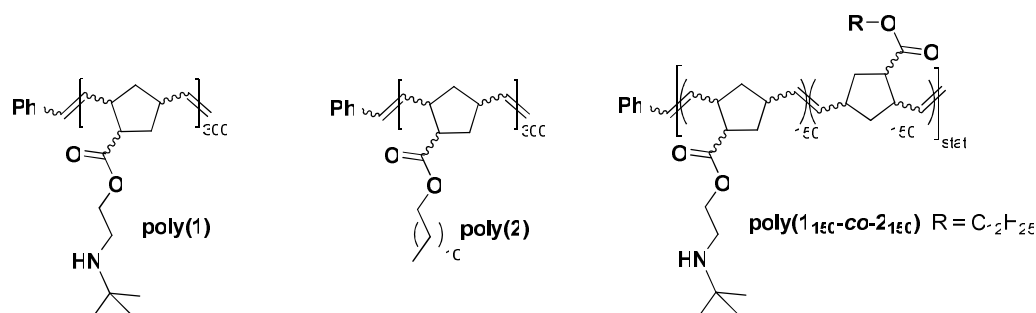


Figure 3.1-3: Synthesised polymers for kinetic measurements via NMR.

Monomer conversion was plotted versus time as shown in Figure 3.1-4. While the time in which 99% of the monomers are consumed for **1** was 6 min, it was 13 min for **2**. The polymerisation of the corresponding random copolymer **poly(1₁₅₀-co-2₁₅₀)** revealed 99% conversion after 7.5 min.

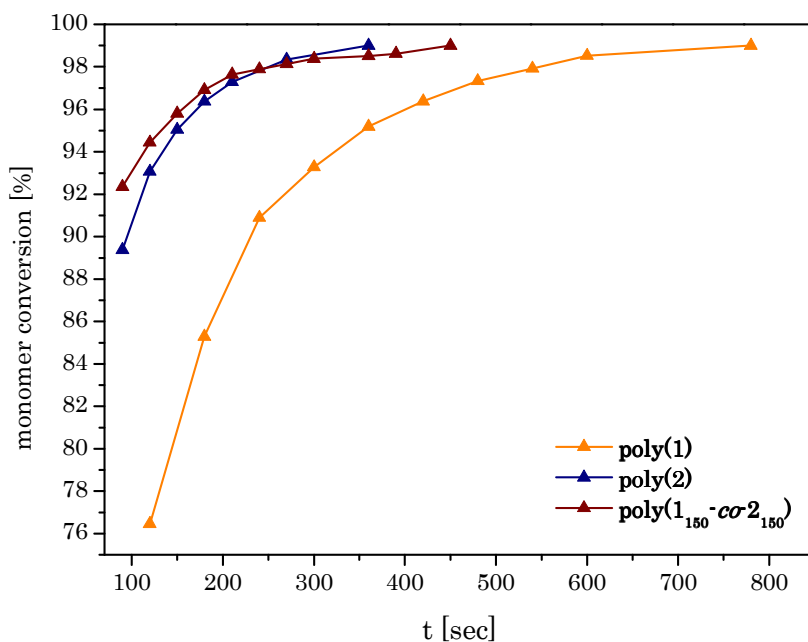


Figure 3.1-4: Monomer conversion versus time for the homopolymers **poly(1)** and **poly(2)** and the random copolymer **poly(1₁₅₀-co-2₁₅₀)**.

The polymerisation of **2** initiated by **G3** is more rapidly completed compared to **1**, giving rise to the assumption that in case of copolymerisation, **2** is consumed before are rather faster than the amine-bearing monomer **1**. In case of copolymerisation, this would lead to gradient copolymers rather than random copolymers. Surprisingly, the kinetic measurements indicate that the random copolymerisation of **1** and **2** is faster complete compared to the homopolymers.

3.1.2.3 Effect of Polymerisation Time and Temperature

Polymerisation time and temperature may be crucial factors especially in case of mono-substituted monomers. These influences on the resulting polymers were determined by test-polymerisations of **2** and subsequent GPC.

Polymerisations of **2** (300 equiv.) initiated by **G3** (1 equiv.) were performed at 0, 20 and 40°C and the polymerisation was stopped when the monomer was consumed which was continuously monitored by thin layer chromatography (TLC). Corresponding GPC data revealed polydispersity indices (PDIs) of 1.2, 1.2 and 1.4 (M_n values: 67 kDa, 68 kDa and 72.4 kDa) for the corresponding reaction temperature. Total monomer consumption was observed at 120 min, 60 min and 35 min respectively. Hence, elevated temperature accelerates the polymerisation reaction but leads to polymers with higher polydispersity.

Polymerisations of 300 equiv. **2** initiated by **G3** at 0, 20 and 40°C for 180 min each were performed and PDIs of 1.3, 1.3 and 1.6 (M_n values: 51 kDa, 66 kDa and 60 kDa, respectively) were determined for the corresponding polymers. The data show that longer reaction times lead to lower molecular weights and increasing polydispersity, which clearly approves the presumption that back biting increasingly occurs (*cf.* Table 3.1-3).

Table 3.1-3: Effect of temperature and time on molecular weight and PDI of **2**.

T [°]	t [min]	PDI	M_n [kDa]
0	120	1.2	67.2
0	180	1.3	51.4
25	60	1.2	68.1
25	180	1.3	66.3
40	35	1.4	72.4
40	180	1.6	59.3

3.1.3 Antimicrobial Activity

Antimicrobial activity of **poly(1₃₀₀-*cis*-2₃₀₀)** was tested against *Pseudomonas aeruginosa* (*P. aeruginosa* (ATCC 9027)), *S. aureus* (ATCC 6538) and the fungi *Candida albicans* (*C. albicans* (ATCC 10231)) and *Aspergillus niger* (*A. niger* (ATCC 16404)) according to the Japanese industry standard JIS Z 2801:2000.⁵³ Antimicrobial tests were performed by Hyggen (Bischofshofen, Austria).

The test sample and the control sample were prepared by spin-coating of CHCl₃ solutions containing 1 wt.% of the synthesised polymers onto 4x4 cm glass plates. The ROM polymer of *endo,exo*-dimethyl bicyclo[2.2.1]hept-5-en-2-2-carboxylate was used as the reference sample. For detailed information regarding the method see the Supporting Information (Chapter 6.1.1).

In order to classify the antimicrobial activity of a material, it is important to differ between microbiocides and microbiostatics. Microbiocides kill microorganisms while microbiostats inhibit the growth of microorganisms.⁵⁶ According to the specification of the JIS a material is referred to as microbiocide, only if a reduction of the tested microorganisms of at least two logarithmic levels is achieved. Microbiostatics, in contrast, just hinder the growth of microorganisms.

The antimicrobial activity of **poly(1₃₀₀-*cis*-2₃₀₀)** against the tested microorganisms is summarised in Table 3.1-4 and plotted as the change of amount of colony forming units (CFU) versus time in Figure 3.1-5 to Figure 3.1-8. The as 'start' identified value correlates with the theoretical starting concentration of the cell suspension (ca. 10⁶ cells mL⁻¹). The value at 0 hours was measured constantly after 15 min to guarantee equal conditions.

Table 3.1-4: Antimicrobial activity of **poly(1₃₀₀-*cis*-2₃₀₀)** after 0h, 24h and 48h according to JIS Z2801.

	lg (CFU) reference			lg (CFU) poly(1₃₀₀-<i>cis</i>-2₃₀₀)		
	0 h	24 h	48 h	0 h	24 h	48 h
<i>S. aureus</i>	5.09	5.16	5.19	5.10	2.32	1.82
<i>P. aeruginosa</i>	3.37	5.27	5.77	3.27	4.22	3.01
<i>C. albicans</i>	4.22	4.50	4.91	4.18	3.62	4.10
<i>A. niger</i>	3.49	3.82	3.48	3.41	2.01	1.29

⁵⁶ Paulus, W. *Microbiocides for the protection of materials*, 1st ed.; Chapman & Hall: London, UK, 1993.

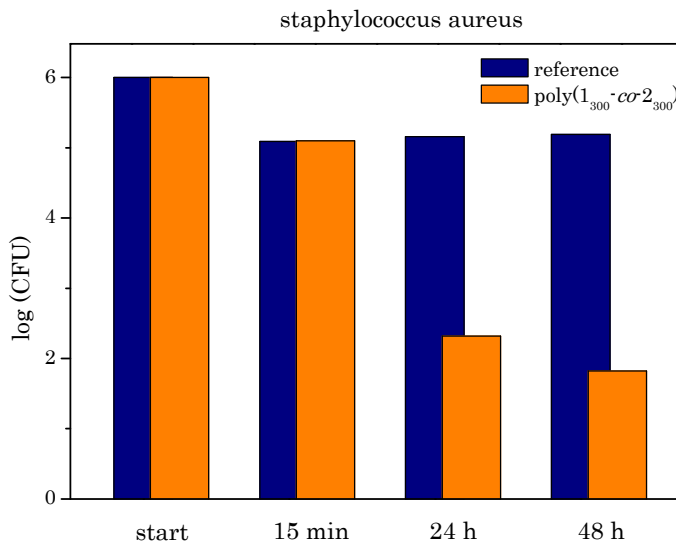


Figure 3.1-5: Antimicrobial activity of **poly(1300-co-2300)** against Gram-positive *S. aureus*.

As shown in Figure 3.1-5 microbiocidal activity of **poly(1300-co-2300)** against *S. aureus* was observed. While the amount of CFU on the reference sample stays almost constant throughout the testing period, the amount of CFU decreased 2.78 logarithmic units within 24 hours and further 0.5 logarithmic units within 48 hours. This leads to an overall decrease of 3.28 logarithmic units within two days.

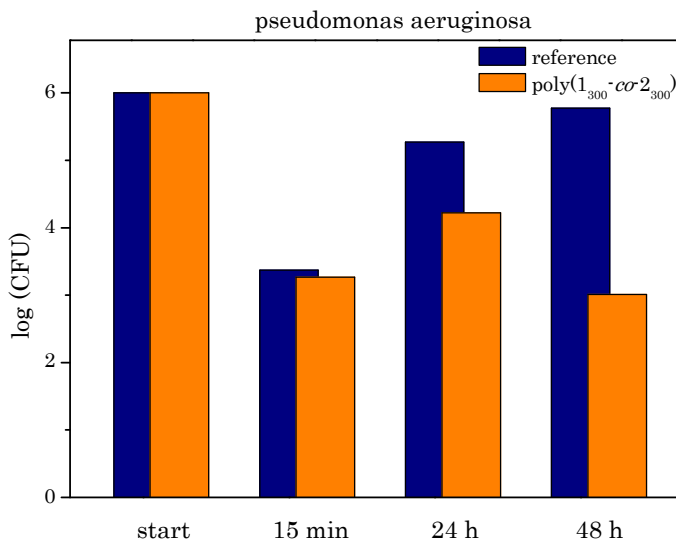


Figure 3.1-6: Antimicrobial activity of **poly(1300-co-2300)** against Gram-negative *P. aeruginosa*.

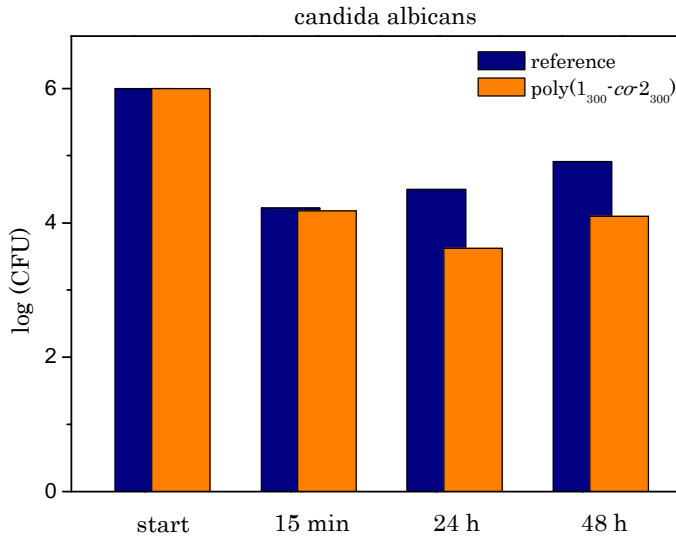


Figure 3.1-7: Antimicrobial activity of **poly(1300-co-2300)** against the fungus *C. albicans*.

As depicted in Figure 3.1-6 and Figure 3.1-7 **poly(1300-co-2300)** exhibits microbiostatic behaviour against *P. aeruginosa* and *C. albicans*. The required 2 logarithmic units for antimicrobial activity are not reached but further growth of the microorganisms is inhibited. The data for *P. aeruginosa* could even be interpreted as microbiocidal if the CFUs on the test samples are compared with the starting concentration of the cell suspension or with the amount of CFUs on the reference. After 48 hours a decrease of 2.76 logarithmic units can be determined.

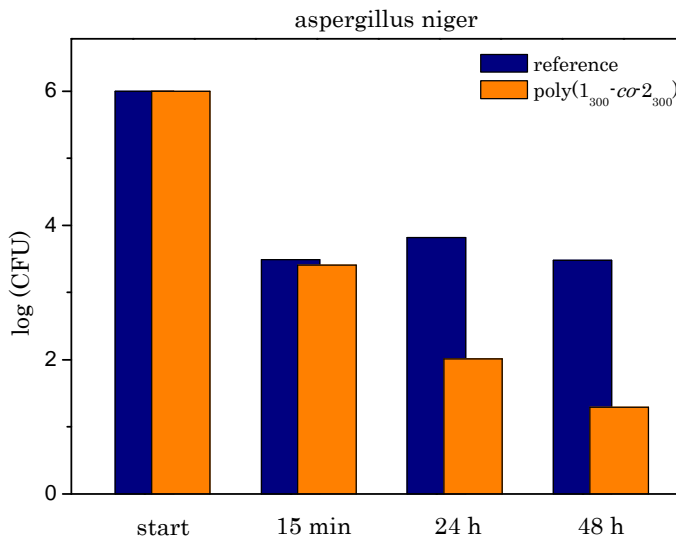


Figure 3.1-8: Antimicrobial activity of **poly(1300-co-2300)** against the fungus *A. niger*.

As shown in Figure 3.1-8 **poly(1300-co-2300)** exhibits outstanding fungicidal properties against *A. niger*. The cell population of *A. niger* on the test samples decreases to a value of 1.29 CFU while it stays more or less constant on the reference samples.

To sum up, pre-eminent microbiocidal activity of **poly(1₃₀₀-co-2₃₀₀)** films against *S. aureus* and *A. niger* was observed, while the test samples exhibited microbiostatic behaviour against *C. albicans* and *P. aeruginosa*.

3.1.4 Cytotoxicity Test

Cytotoxicity tests of extracts from prospective biomaterials play a crucial role of the initial decision, whether a proposed material is biocompatible or not.⁵⁷ To guarantee risk-less usage in food-related applications, medical devices or water pipes, possible cytotoxic effects on human health and the environment of **poly(1₃₀₀-co-2₃₀₀)** was tested, using an in vitro method in accordance with ISO 10993-5:1999. The test was performed at the Austrian Research Centre GmbH (ARC).

An extract of the copolymer was prepared by incubating the test sample with complete cell culture medium for 24 h at 37 °C in humidified atmosphere with 5% CO₂. The ratio of the test sample to complete cell culture medium was 1.25 cm² mL⁻¹. This extract was tested undiluted and diluted with complete culture medium. The extract and extract dilutions were incubated for 24 h with freshly trypsinised Balb/3T3 mouse embryo cells. The cytotoxic action was determined by visual examination of the cells, recultivation of the cells and testing their ability to re-attach and grow. Samples with complete cell culture medium served as negative controls. Dilutions of phenol and ZnSO₄ were used as positive control samples.

Test results show that the extracts of **poly(1₃₀₀-co-2₃₀₀)** did not influence the growth of the Balb/3T3-cells. The cells incubated with the extract and the extract-dilution had normal morphology, were able to reattach on the tissue culture plate, and their growth did not differ from non-treated cells. Phenol and zinc sulphate, which were used as references, showed high levels of cytotoxicity at final concentrations of 20 mg/L (and above), resulting in slower cell growth and in detached, round cells and lysis of the cells (for higher concentrations of the toxic compounds). These results also give some evidence, that the residual ruthenium content of the polymers is not cytotoxic.

⁵⁷ Rosengren, A.; Faxius, L.; Tanaka, N.; Watanabe, M.; Bjursten, L.M. *J. Biomed. Mater. Res. A* **2005**, *75*, 115-122.

3.2 Antimicrobial Compound Materials

3.2.1 Concept

As the synthesis of the antimicrobial ROM polymers is quite time consuming and expensive, the endeavours of this thesis focus on the application of such microbicidal materials as additives for low cost commodity materials such as poly(ethylene) (PE) or poly(styrene) (PS).

3.2.2 Compound Fabrication

The compounds were produced via injection- or compression moulding in close collaboration with Elisabeth Kreutzwiesner. Extrusion of thermoplastic materials leads to melting and homogenisation (*cf.* Figure 3.2-1). Thereby different additives can be added or the thermoplastic material can also be mixed with other thermoplastic or non-thermoplastic materials, mouldable at elevated temperatures. Hence, the biocide polymer **poly(1300-~~cc~~2300)** was incorporated in poly(ethylene) DOWLEX 2344 with 3, 5 and 7 wt.% of the active material in order to evaluate the minimum concentration necessary for antimicrobial performance of the compound.

For the injection-moulding the molten polymeric compound material was directly transferred into a heated cylinder with a movable plunger and injected with a piston under high pressure (*cf.* Figure 3.2-2, left) into a steel mould (*cf.* Figure 3.2-2, right).

Furthermore, after homogenisation of the compound, the moulding of thermoplastic materials and composites is possible via the compression-moulding technique. Thereby materials which are mouldable at elevated temperatures are shaped in a heat-able press under reduced pressure (*cf.* Figure 3.2-3).



Figure 3.2-1: Thermo-Haake mini-extruder.⁵⁸

⁵⁸ source: http://www.thermo.com/eThermo/CMA/Images/Product/productImg_10815.jpg.



Figure 3.2-2: Injection piston (left) and steel mould (right).



Figure 3.2-3: Collin P200PV heat-able vacuum press.

The compound samples obtained via injection- and compression-moulding are shown in Figure 3.2-4.

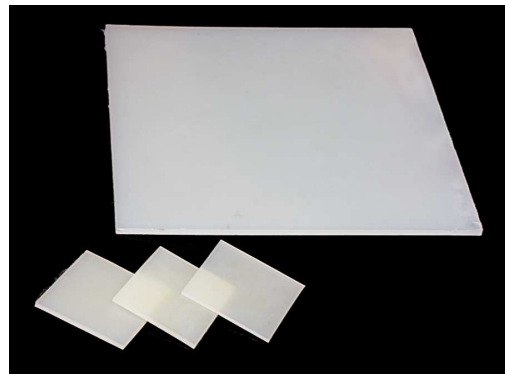


Figure 3.2-4: Compound samples produced via injection-moulding (left) and compression moulding (right).

3.2.3 Antimicrobial Activity of the Compounds

The antimicrobial activity was again tested against *P. aeruginosa* (ATCC 9027), *S. aureus* (ATCC 6538) and fungi (*C. albicans* (ATCC 10231), and *A. niger* (ATCC 16404)) according to the Japanese industry standard JIS Z 2801:2000⁵³ (cf. Chapter 6.1.1) by Hyggen (Bischofshofen, Austria).

Again, the theoretical starting concentration of the cell suspension amount to ca. 10^6 cells mL⁻¹ and the value at 0 hours was measured constantly after 15 min to guarantee equal conditions.

Table 3.2-1: Antimicrobial activity after 0h, 24h of 3, 5 and 7wt.% of **poly(1₃₀₀-co-2₃₀₀)** incorporated in PE according to JIS Z2801. 0% referred to as the reference containing no active material.

	lg (CFU) 0%		lg (CFU) 3%		lg (CFU) 5%		lg (CFU) 7%	
	0 h	24 h	0 h	24 h	0 h	24 h	0 h	24 h
<i>S. aureus</i>	4.77	5.76	4.88	5.82	4.77	5.76	4.76	5.75
<i>P. aeruginosa</i>	4.35	5.79	4.38	5.83	4.34	5.85	4.36	5.94
<i>C. albicans</i>	4.11	4.30	4.20	4.37	4.19	4.38	4.17	4.48
<i>A. niger</i>	3.96	3.99	4.05	3.67	4.04	3.76	3.89	3.53

All tests were performed in a repeat determination and showed good reproducibility of the results. Unfortunately none of the compound materials exhibit antimicrobial activity. The CFU increased within 24 hours equally for the reference as for the samples containing 3, 5 or 7 wt.% of **poly(1₃₀₀-co-2₃₀₀)** in case of *S. aureus*, *P. aeruginosa* and *C. albicans*. For *A. niger* a small reduction of the CFU 0.38, 0.28 and 0.36 logarithmic units for 3, 5 and 7 wt.% of **poly(1₃₀₀-co-2₃₀₀)** in poly(ethylene), respectively was observed while the CFUs of the reference stay almost constant. Nevertheless, according to the regulations of the JIS, requiring a reduction of CFU of at least two logarithmic units, no antimicrobial activity was observed.

3.2.4 Leaching Tests

The monomers and polymers under investigation contain an ester functionality which is generally prone to hydrolysis. Crucial points for the production of contact biocide materials are that they are long-time stable and do not release low molecular weight components into the surroundings. Hence, the hydrolysis and thus leaching behaviour of such material has to be investigated in order to assure long-term usage.

For this purpose a random copolymer of monomers **1**, **2** and 11-(2-Phenyl-1*H*-phenanthro[9,10-*d*]imidazol-1-yl) undecyl bicyclo [2.2.1]hept-5-en-2-

carboxylate **5**, a deep blue emitting chromophore,⁵⁹ was synthesised. All monomers were dissolved in degassed chloroform and polymerisation was initiated using **G3**. After total consumption of the monomers, polymerisation was quenched by an excess amount of ethyl-vinyl-ether. The resultant polymer **poly(1₃₀₀-co-2₃₀₀-co-5₃₃)** was purified by repeated precipitation of dichloromethane solutions from ethanol.

5 wt.% of **poly(1₃₀₀-co-2₃₀₀-co-5₃₃)** were compounded with poly(ethylene) via extrusion followed by compression moulding in a heat-able vacuum press. 5 g of the compound material were cut into 1x1 cm pieces and extracted using 300 mL of distilled water via Soxhlet extraction. After 24 hours the extract was freeze-dried and the residue was re-dissolved in chloroform.

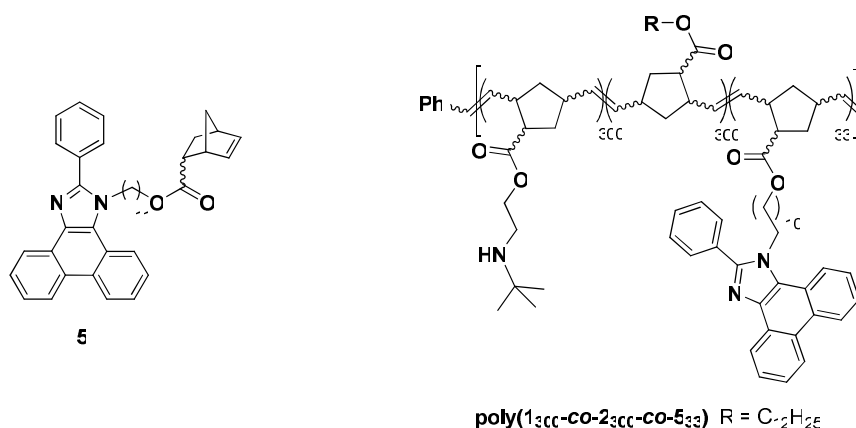


Figure 3.2-5: Chromophore **5** (left) incorporated in the random copolymer **poly(1₃₀₀-co-2₃₀₀-co-5₃₃)** (right).

The chromophore is, similar to **1** and **2**, attached to the polymerisable norbornene group or rather to the polymer back-bone via an ester group. Since luminescence spectroscopy is highly sensitive, also traces of the chromophore can be detected. It was presumed that the ester in **5** hydrolyses under equal conditions like the ester group in **1** and **2**. Thus, the synthesis and compound fabrication of the random copolymer **poly(1₃₀₀-co-2₃₀₀-co-5₃₃)** and subsequent fluorescence spectroscopy of the extract enables the detection of traces of the chromophore and allows the quantification of released chromophore.

Emission characteristic of the residue was measured after irradiation at 310 nm. Weak emission at 420 nm could be observed resulting from the chromophore. For quantification of the released amount of chromophore a calibration curve of **5** was measured (*cf.* Figure 3.2-6).

⁵⁹ Noormofidi, N.; Slugovc, C. *Macromol. Chem. Phys.* **2007**, *208*, 1093-1100.

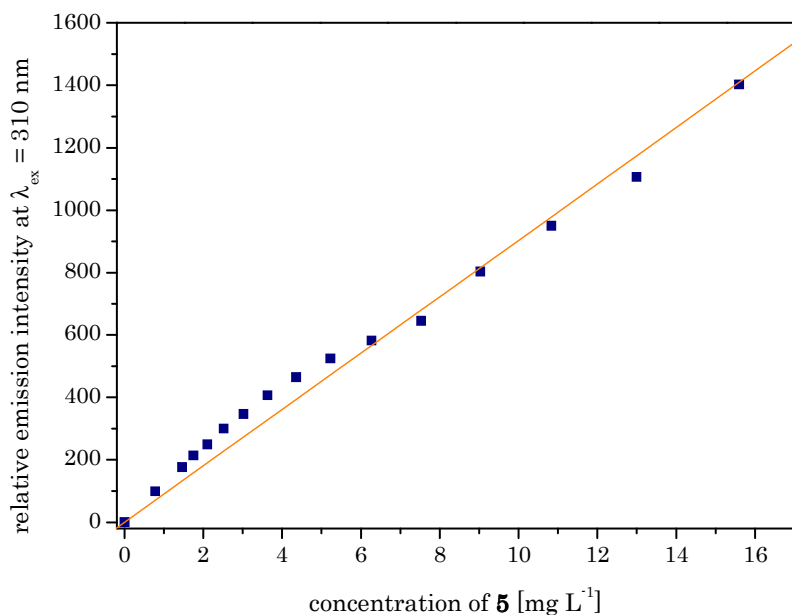


Figure 3.2-6: Relative emission intensity of **5** versus concentration.

According to this dilution series, the amount of **5** in the freeze-dried residue constitutes $1.8 \pm 0.3 \text{ mg} \cdot \text{L}^{-1}$. With respect to the applied amount of **5** for the synthesis of **poly(1₃₀₀-*co*-2₃₀₀-*co*-5₃₃)**, $0.35 \pm 0.05\%$ were detected.

Under the presumption that equal amounts of different ester groups are released under the above described conditions, 0.35% of the entire polymer would hydrolyse. In 1 kg of a compound material containing 5 wt.% of **poly(1₃₀₀-*co*-2₃₀₀-*co*-5₃₃)** or any other ester bearing poly(norbornene) 0.15 g are leached out.

3.2.5 Conclusions Drawn on Antimicrobial Compounds

None of the compound materials exhibit antimicrobial activity. The CFUs on the samples containing 3, 5 or 7 wt.% of **poly(1₃₀₀-*co*-2₃₀₀)** even increased in case of *S. aureus*, *P. aeruginosa* and *C. albicans*. According to the regulations of the JIS, requiring a reduction of CFU of at least two logarithmic units, no antimicrobial activity was observed (*cf.* Chapter 3.2.3). Consequently, emphasis was shifted to the development of block-*co*-polymers. The pursued objectives of this approach comprise the self-assembly of block-*co*-polymers and are discussed in detail in the following chapter (*cf.* Chapter 3.3).

Furthermore, the performed leaching tests evinced that the antimicrobial active groups leach out to an amount of $0.35 \pm 0.05\%$ most probably due to ester hydrolysis. For the aspired application this is still too much. Thus, non-hydrolysable groups are desired and will be focus of future investigations.

3.3 Development of Block-*c*opolymers

3.3.1 Motivation

Due to the little pleasant results presented in Chapter 3.2.3 emphasis was placed on the development of block-*c*opolymers.

Block-*c*opolymers are macromolecules with two or more different blocks of different monomers or monomer compositions. Such diblock-, triblock- or even multiblock-*c*opolymers are prone to self-assemble and self-organise.⁶⁰ Hence, new structures with novel properties and applications are accessible. The self-assembly at the nanoscale has to be very precise and homogeneous. This can only be achieved by a very well controlled synthesis of the block-*c*opolymers. The design of block-*c*opolymers requires a living polymerisation technique such as ROMP.²⁶ Therefore, ROMP is the ideal polymerisation method, latest since the development of third generation of Grubbs and Neolyst initiators which additionally exhibit high functional group tolerance.³⁵

By self-assembling, the functionality should be guided to the surface of the material enhancing the antimicrobial activity while physical properties of the commodity materials are hardly affected by the additive as shown schematically in Figure 3.3-1.

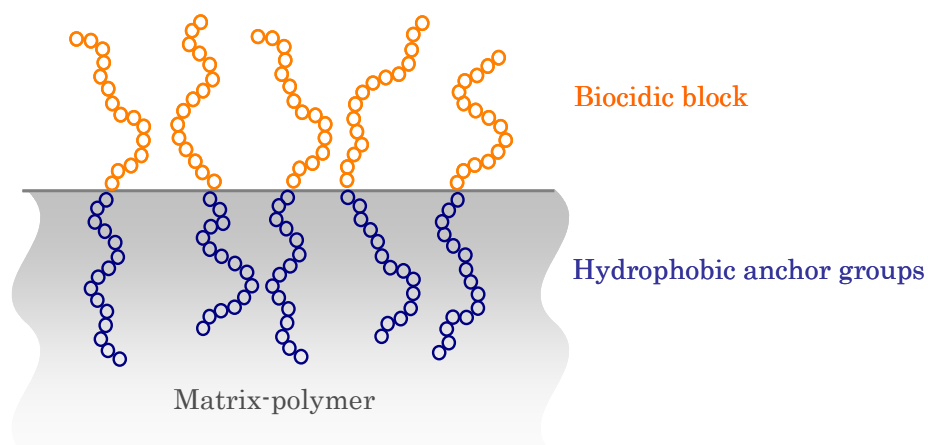


Figure 3.3-1: Self-assembling of block-*c*opolymers on the surface in compound with PE.

⁶⁰ Stubenrauch, K.; Moitzi, C.; Fritz, G.; Glatter, O.; Trimmel, G.; Stelzer, F. *Macromolecules* **2006**, *39*(17), 5865-5874.

3.3.2 Synthesis of Block-*cis*-polymers

In order to synthesise block-*cis*-polymers and thus fine-tune the self-assembly and (structural) properties, living polymerisation has to be assured. For the production of well-defined low polydispersity block-*cis*-polymers the evaluation of the PDI is necessary. Thus, the ability to synthesise block-*cis*-polymers using monomers **1** and **2** and initiator **G3** was tested using gel permeation chromatography (GPC).

To assure living polymerisation conditions, evidence for the lack of chain transfer and chain termination reactions must be demonstrated and molecular weight studies have to be performed. In living polymerisations molecular weight is directly proportional to monomer conversion, since all chain ends are growing at essentially the same rate.⁶¹

First, the polymerisation behaviour of **2** was investigated. A series of homopolymers using **G3** as the initiator and different equiv. of **2** has been synthesised, leading to the corresponding polymers **poly(2)₁₀₀**, **poly(2)₃₀₀**, **poly(2)₅₀₀**, **poly(2)₇₀₀** and **poly(2)₉₀₀**, respectively (*cf.* Scheme 3.3-1). Reaction conditions were defined with room temperature and 40 minutes reaction time for all polymerisations. Polymerisation was quenched by the addition of ethyl-vinyl-ether and the polymers were precipitated from ethanol. GPC data are summarised in Table 3.3-1.

Scheme 3.3-1: Syntheses of homopolymers of **2** of different chain lengths using **G3** initiator.

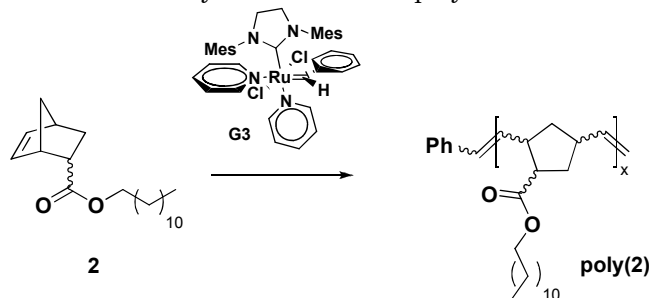


Table 3.3-1: GPC results of a series of homopolymers of **2**.

polymer	PDI	M _n [kDa]
poly(2)₁₀₀	1.10	29.7
poly(2)₃₀₀	1.20	68.1
poly(2)₅₀₀	1.37	110.7
poly(2)₇₀₀	1.34	125.6
poly(2)₉₀₀	1.45	224.6

Apart from the fact that the PDI broadened, a shift in the GPC peaks with increasing amount of monomer : initiator ratio and thus increasing chain length was observed. In Figure 3.3-2 the number average molecular weight is plotted versus the monomer : initiator ratio and evinces that the relation

⁶¹ Maughon, B.R.; Grubbs, R.H. *Macromolecules* **1997**, *30*, 3459-3469.

is almost linear, especially for chain lengths with up to 500 repeating units. Deviations increase with chain lengths above 500 monomer units indicating increased back-biting.

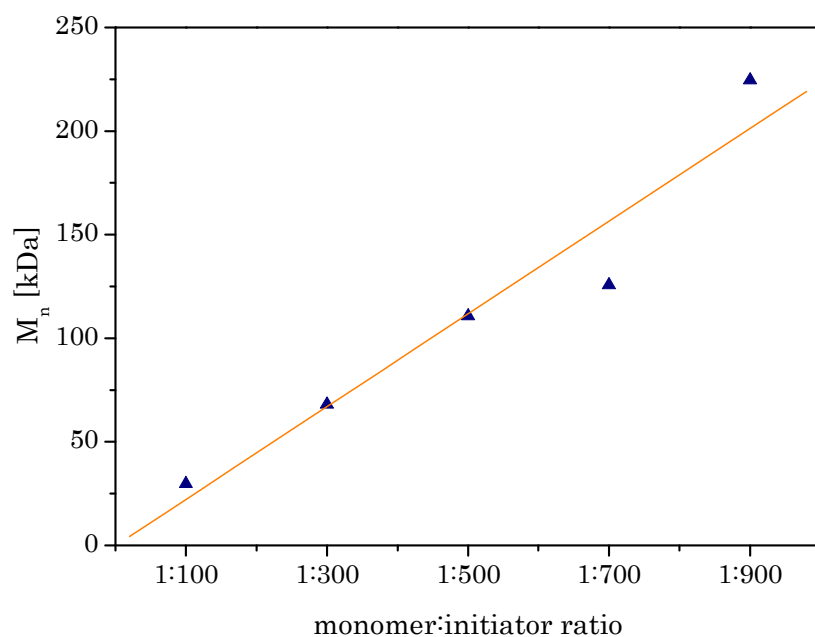


Figure 3.3-2: Linear dependence between M_n and monomer to initiator ratio.

Nevertheless, bimodal GPC traces were observed for all polymerisations except for **poly(2)₁₀₀** with the shortest chain length (*cf.* Figure 3.3-3). Thus, the absence of chain transfer and chain termination reactions, which is indicative for a living polymerisation, can not be assured. Furthermore, the bimodal molecular weight distribution indicates the occurrence of backbiting, a secondary polymerisation reaction which is increasingly observed for ROMP using mono-substituted monomers.

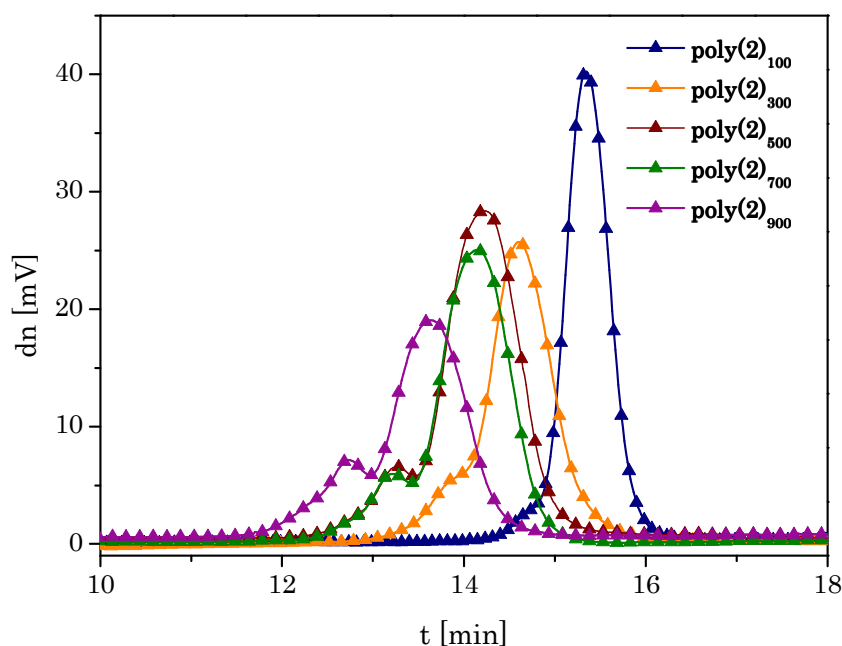


Figure 3.3-3: GPC data of **poly(2)** with different chain lengths.

As **2** seems to be prone to secondary polymerisation reactions, three block-*c*opolymers of different block lengths were synthesised starting with block **1**. The ratio of hydrophilic monomer **1** to hydrophobic monomer **2** was equal with 1:1, but the overall polymer length was varied resulting in **poly(1₁₅₀-block-2₁₅₀)**, **poly(1₃₀₀-block-2₃₀₀)** and **poly(1₅₀₀-block-2₅₀₀)** with an overall chain length of 300, 600 and 1000, respectively. All polymerisation have been performed under inert atmosphere using standard Schlenk technique. After the first monomer was consumed, which was monitored by TLC, the second monomer was added. The polymerisations were quenched by the addition of ethyl-vinyl-ether after TLC revealed full consumption of the second monomer. After repeated precipitation from ethanol, the polymers were characterised by GPC. The identifications of the different polymers, block sizes and the block ratios together with the GPC data are summarised in Table 3.3-2 and depict in Figure 3.3-4.

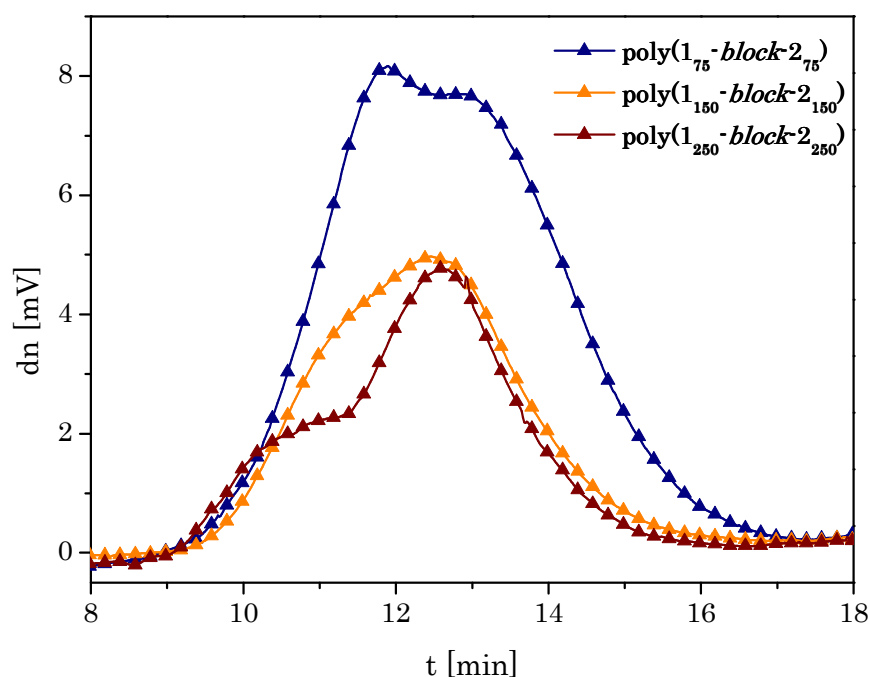


Figure 3.3-4: GPC data of block-*c*opolymers of **1** and **2**.

These GPC data demonstrate that the synthesis of block-*c*opolymers starting with **1** results in polymers of very broad and bimodal molecular weight distributions. Furthermore the M_n values are not consistent with the growing chain lengths of the polymers. Hence, chain termination processes most likely occur and living polymerisation cannot be assured.

Also, block-*c*opolymers were synthesised starting with block **2** using the same conditions as described above and a ratio of the blocks of 300:300. $^1\text{H-NMR}$ spectra of **poly(2₃₀₀-block-1₃₀₀)** was used to calculate the effective ratio of **1** to **2** by integration of corresponding characteristic peaks. The signals of the protons arising from the double bond in the main chain at 5.54-5.10 ppm and the methyl group at 0.88 ppm (s) for the methyl group of **2** were set into

correlation. This led to an effective ratio of $298 \pm 10 : 302 \pm 10$. Further information including detailed characterisation of $^1\text{H-NMR}$ peaks is given in the Experimental Section (*cf.* Chapter 5.3.1.7). In Figure 3.3-5 the molecular weight distribution of **poly(2)₃₀₀** is directly compared with **poly(2₃₀₀-block-1₃₀₀)**. Beside the fact that the PDI broadened significantly, a shift in the GPC peak to longer retention time was observed for the block-*co*-polymer, while number average molecular weight increases. These observations evince that living polymerisation is not assured and secondary metathesis reactions are predominant.

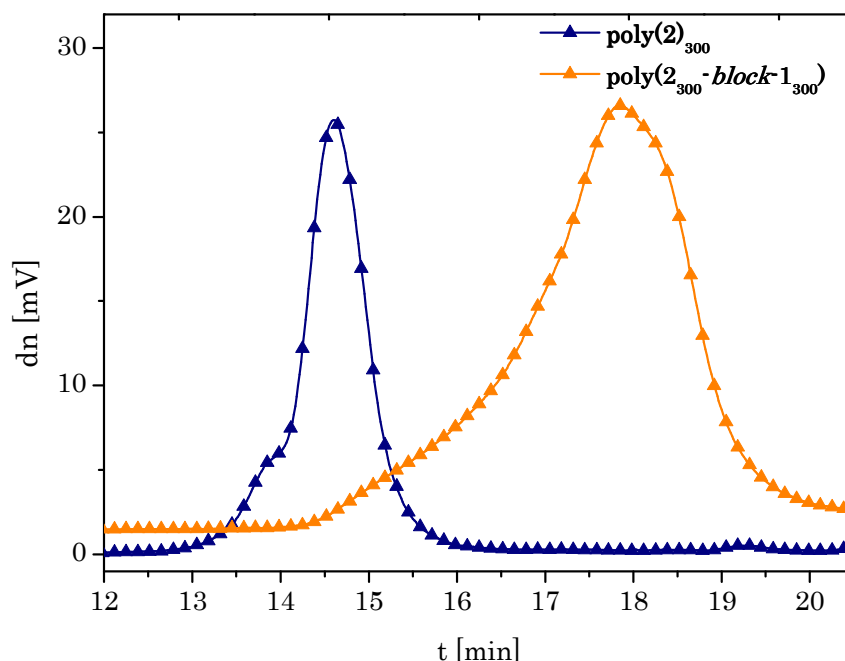


Figure 3.3-5: Comparison of molecular weight distribution of **poly(2)₃₀₀** and **poly(2₃₀₀-block-1₃₀₀)**.

Table 3.3-2: GPC Results of block-*co*-polymers.

polymer	PDI	M_n [kDa]
poly(1₇₅-block-2₇₅)	3.95	211.1
poly(1₁₅₀-block-2₁₅₀)	2.31	430.9
poly(1₂₅₀-block-2₂₅₀)	2.43	125.8
poly(2)₃₀₀	1.20	68.1
poly(2₃₀₀-block-1₃₀₀)	3.00	90.6

GPC measurements revealed that living polymerisation and thus block-*co*-polymers are difficult to obtain using monomers **1** and **2**. Kinetic measurements (*cf.* Chapter 3.1.2.2) illustrate that gradient copolymers might be obtained anyway due to different polymerisation rates of monomer **1** and **2**. Furthermore, antimicrobial activity tests showed that biocidal activity delicately depends on the ratio of hydrophilic and hydrophobic entities (*cf.* Chapter 3.1.3). Therefore it was attempted to synthesis more easily accessible block-*co*-polymers with the aim to study the influence of polymer architecture on the distribution of the biocide polymer in the poly(ethylene) matrix. Therefore, three different polymers were synthesised comprising a short hydrophobic block of **2** in order to guarantee a preferable

anchoring of the biocide polymer in the hydrophobic matrix. According to the GPC results of **poly(2)** (*cf.* Figure 3.3-3), polymerisation of 100 equiv. of **2** exhibit a rather narrow and monomodal molecular weight distribution. Thus, for the short hydrophobic block, a block length of 100 equiv. was predefined. Polymerisations were initiated with **G3** and an overall monomer : initiator ratio of 600 : 1 was chosen. After TLC revealed completeness of the polymerisation of **2**, a mixture of **1** and **2** was added to build the second block consisting of random copolymers of varied ratios of **1** and **2**. Thus the three polymers **poly(2₁₀₀-block-(1₂₅₀-*co*-2₂₅₀))**, **poly(2₁₀₀-block-(1₃₅₀-*co*-2₁₅₀))**, and **poly(2₁₀₀-block-(1₁₅₀-*co*-2₃₅₀))** were obtained and characterised by GPC and NMR spectroscopy. GPC results are summarised in Table 3.3-3 and shown in Figure 3.3-6.

Table 3.3-3: PDI and number average molecular weight of different less sophisticated block-*co*-polymers with the general structure **poly(2₁₀₀-block-(1-*co*-2)₅₀₀)**.

polymer	PDI	M _n [kDa]	effective ratio 1:2 ^a
poly(2₁₀₀-block-(1₁₅₀-<i>co</i>-2₃₅₀))	1.53	131.1	182 ± 10 : 418 ± 10
poly(2₁₀₀-block-(1₂₅₀-<i>co</i>-2₂₅₀))	1.39	117.4	254 ± 10 : 346 ± 10
poly(2₁₀₀-block-(1₃₅₀-<i>co</i>-2₁₅₀))	1.70	121.2	360 ± 10 : 240 ± 10

^a determined by integration of the corresponding NMR peaks.

As expected, all polymers exhibit almost equal retention and comparable M_n values. PDI values are broader as expected for living ROMP but far better as for the above mentioned block-*co*-polymers with the general structure **poly(1-*block*-2)**. The polymer with the highest amount of **1** exhibits the broadest molecular weight distribution, indicating that polymerisation of **1** promotes secondary metathesis reactions.

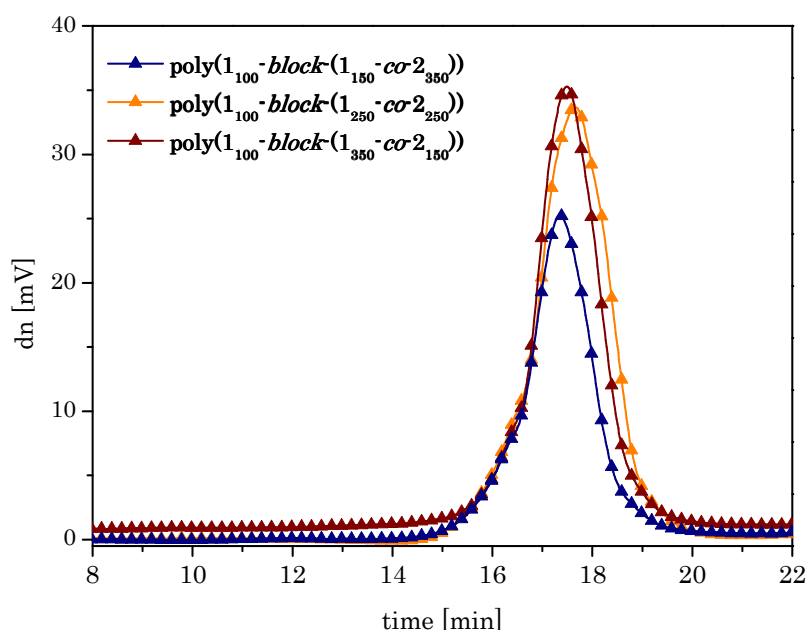


Figure 3.3-6: GPC data of **poly(2₁₀₀-block-(1₁₅₀-*co*-2₃₅₀))**, **poly(2₁₀₀-block-(1₂₅₀-*co*-2₂₅₀))** and **poly(2₁₀₀-block-(1₃₅₀-*co*-2₁₅₀))**.

The effective ratio of the copolymers was investigated by integrating appropriate peaks in the ^1H NMR spectra. The signal for the polymer's double bonds (5.52-5.10 ppm) was set in relation with the peak of the terminal methyl group (0.83 ppm) of the dodecyl-chain bearing repeating unit. The results are summarised in Table 3.3-3 and meet the expected ratios.

These results confirm the results of kinetic measurements (*cf.* Chapter 3.1.2.2) which indicate that the monomer conversion appears faster for the synthesis of a random copolymer of **1** and **2** compared to the homopolymers.

3.3.3 Determination of Distribution of the Block-*co* Polymer in the Matrix

The aim of synthesising block-*co*-polymers was to force the self-assembly of the antimicrobial polymer at the surface (*cf.* Chapter 3.3.1).

To have a better insight concerning the final distribution of the less sophisticated block-*co*-polymers with the general architecture **poly(2₁₀₀-*block*(1-*co*-2)₅₀₀)** in the poly(ethylene) matrix, contact angle and transmission electron microscopy measurements of **poly(2₁₀₀-*block*(1₂₅₀-*co*-2₂₅₀))** were conducted. For further information on the sample preparation and the measurement procedure see the Supporting Information (Chapter 6.1.2 *f*).

3.3.3.1 Contact Angle Measurements

The polarity of the surface highly influences the contact angle between the surface and the probe liquids. Hence, the incorporation of **poly(2₁₀₀-*block*(1₂₅₀-*co*-2₂₅₀))** should decrease the contact angle between the compound and a polar liquid like water. At the same time surface energy of the compound should increase. For the subsequent application an increased surface energy implies a higher interaction between the surface and the microorganisms, also due to the electrostatic interaction between the bacteria and the surface. A contrary approach is the application of surfaces of low surface energy to prevent the attachment of microorganisms. Such surfaces (e.g. poly(tetrafluorethylene)-PTFE) exhibit a high contact angle with polar probe liquids and thus a low cell adhesion.

5 wt.% of **poly(2₁₀₀-*block*(1₂₅₀-*co*-2₂₅₀))** were compounded with poly(ethylene) and processed using injection moulding forming 4 x 4 cm compound specimen. Pure poly(ethylene) specimens produced similarly were used as reference surface. Contact angle measurements and surface tension determination of the compounds were conducted using two probe liquids,

water and diiodomethane (CH₂I₂).⁶² Based on the Owens-Wendt method,⁶³ the surface tension γ was evaluated. The measurements were performed in triplicate to ensure reproducibility. Thereby contact angles were determined fivefold and average values have been taken (error within one series less than 5%). The results are summarised in Table 3.3-4.

Table 3.3-4: Determination of contact angle θ , dispersive σ^d and polar σ^p interaction and surface energy γ_{sl} of poly(ethylene) and 5 wt.% of **poly(2100-*block*-(1250-*co*-2250))** in PE.

	polymer	$\theta_{\text{CH}_2\text{I}_2}$ [°]	$\theta_{\text{H}_2\text{O}}$ [°]	σ^d [mN·m ⁻¹]	σ^p [mN·m ⁻¹]	γ_{sl} [mN·m ⁻¹]
1	poly(ethylene)	54.1	94.8	31.98	0.95	32.93
	poly(2100-<i>block</i>-(1250-<i>co</i>-2250))	50.5	79.5	34.00	4.91	38.91
2	poly(ethylene)	53.5	94.2	32.30	0.67	32.90
	poly(2100-<i>block</i>-(1250-<i>co</i>-2250))	53.2	88.1	31.90	2.48	34.39
3	poly(ethylene)	52.6	99.3	32.82	0.28	33.10
	poly(2100-<i>block</i>-(1250-<i>co</i>-2250))	54.3	93.1	31.85	1.29	33.13

In all test series the contact angle between water and the compound of **poly(2100-*block*-(1250-*co*-2250))** and poly(ethylene), material decreases while the amount of polar interactions increases, which indicates an increasing amount of polar groups on the surface. Nevertheless, only for test series 1 these effects are significantly and lead to an increased surface energy of the compound, 5.98 mN·m⁻¹ higher compared to the pure PE reference. In series 2 the surface energy increases only 1.49 mN·m⁻¹ and stays almost constant in series 3. Thus, an increase of surface energy by incorporating **poly(2100-*block*-(1250-*co*-2250))** was not observed for all three test series. These deviations of the contact angle and surface tension are assigned to the inhomogeneous incorporation of the polymer in the matrix. Furthermore, the injection-moulded specimens do not exhibit a plane surface. Thus, and due to the fact that contact angle measurements on non-reflecting surfaces are difficult, the results were not satisfactory. Therefore no reliable information could be gathered from these experiments.

3.3.3.2 Transmission Electron Microscopy Measurements

In a second step high resolution transmission electron microscopy measurements were performed. For detailed information on sample preparation and sample staining see the Supporting Information, Chapter 6.1.3. In order to directly compare the difference in distribution of the active polymers in the matrix, two polymers with equal over all chain-length but different polymer architecture were chosen. Thus, the distribution of **poly(2100-*block*-(1250-*co*-2250))** in poly(ethylene) was investigated and compared with the distribution of the random copolymer **poly(1300-*co*-2300)** in the same matrix. It was assumed that the block-*co*-polymer might self-

⁶² Ström, G.; Fredriksson, M.; Stenius, P. *J. Colloid Interf. Sci.* **1987**, *119*, 352-361.

⁶³ Owens, D.K.; Wendt, R.C. *J. Appl. Polym. Sci.* **1969**, *13*, 1741-1747.

assemble at the surface and leads to a favourable distribution of the active material in the matrix.

5 wt.% of the random copolymer **poly(1300-*co*-2300)** and the block-*co* polymer **poly(2100-*block*-(1250-*co*-2250))** were introduced into poly(ethylene). After extrusion, 4 x 4 cm compound plates were produced via injection moulding. The distribution of the two types of polymers in the matrix was determined using TEM.

The TEM pictures are shown in Figure 3.3-7. The grey appearing areas represent the poly(ethylene) matrix and the black areas are caused by the incorporated antimicrobial polymers after contrasting with ruthenium tetroxide (RuO₄).

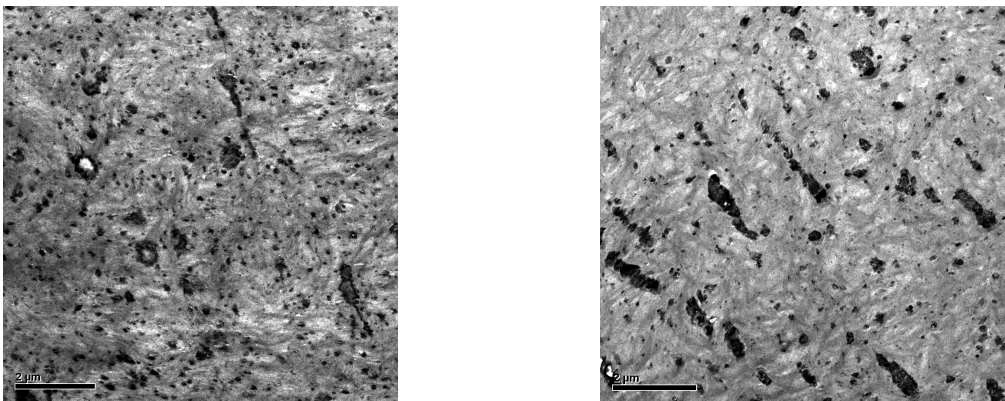


Figure 3.3-7: TEM pictures of the random copolymer **poly(1300-*co*-2300)** (left) and the block-*co* polymer **poly(2100-*block*-(1250-*co*-2250))** (right) after staining with RuO₄; 11.000 fold magnified.

Comparing the TEM pictures, a difference in terms of distribution of random and block-*co* polymer in PE is evident. This underlines the fact that block-*co* polymers were synthesised but the presumption that block-*co* polymers would self-assemble at the surface of the specimen, was not confirmed by TEM measurements. In contrast, a higher degree of agglomeration of the block-*co* polymer compared to the random copolymer was observed.

3.4 Luminescent Ruthenium Complexes

Luminescent labelling of the developed biocide systems presented in Chapter 3.1 *ff.* paves the way to further investigation of the mechanism of activity of the polymers (*cf.* Chapter 3.2.4). However, the explicit aim of this section is to determine simultaneously the presence of aerobic bacteria as a function of luminescence lifetime of the copolymerised ruthenium complexes.

3.4.1 Motivation

The condensation reaction of 9,10-phenanthrenedione with an appropriate benzaldehyde in the presence of ammonium acetate (NH₄OAc) in acetic acid (AcOH) at 100°C is a well known straight forward reaction, leading to the corresponding phenanthroimidazole derivative in high yields.^{64,65,66} Basing on the experiences reported previously in this field,⁶⁷ further research was done varying the quinone component. The condensation reaction is equally applicable for the corresponding phenanthroline-5,6-dione,⁶⁴ introducing at the same time the polymerisable norbornene derivative via the benzaldehyde moiety.

3.4.1.1 Ligand synthesis

The synthetic route leading to the educts for the condensation reaction is shown in Scheme 3.4-1. 4-Hydroxybenzaldehyde **6** was dissolved in butanone, potassium carbonate (K₂CO₃) was added and after 30 min of further stirring at 90 °C, bicyclo[2.2.1]hept-5-ene-2-carboxylic acid, 11-bromo-undecyl ester (**7**) was added.⁶⁸ TLC revealed completeness of the reaction after 10 h. Work-up and purification gave the desired product norbornene functionalised aldehyde 3-(4-formylphenoxy) undecyl bicyclo[2.2.1]hept-5-ene-2-carboxylate (**8**) in 88% yield as a mixture of 88% *endo*- and 12% *exo*-derivative as indicated by integration of the appropriate peaks in the ¹H-NMR spectrum (*cf.* Chapter 5.3). Phenanthroline-5,6-dione

⁶⁴ Steck, E.A.; Day, A.R. *J. Am. Chem. Soc.* **1943**, *65*, 452-456.

⁶⁵ Lantos, I. *J. Org. Chem.* **1975**, *40*, 1641-1642.

⁶⁶ Botana, E.; Nättinen, K.; Prados, P.; Rissanen, K.; Mendoza, *J. Org. Lett* **2004**, *6*, 1091-1094.

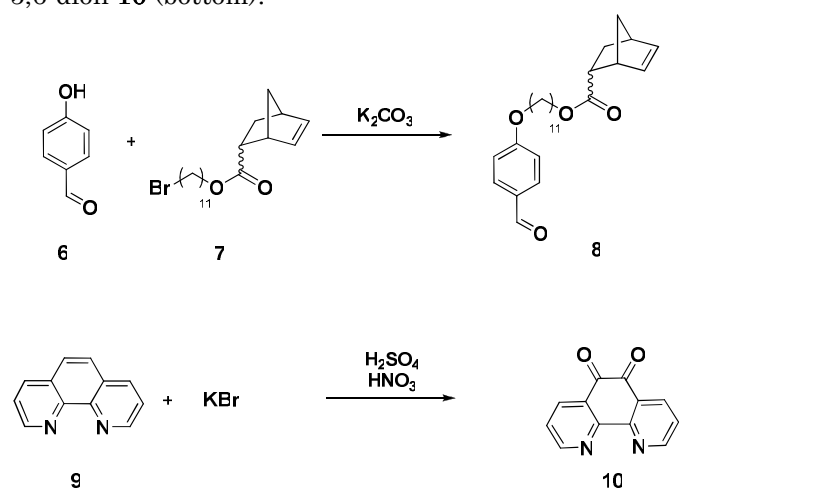
⁶⁷ Noormofidi, N.; Slugovc, C. *Eur. Polym. J.* **2010**, *46*, 694-701.

⁶⁸ Sandholzer, M.; Lex, A.; Trimmel, G.; Saf, R.; Stelzer, F.; Slugovc, C. *J Polym Sci Part A: Polym Chem* **2007**, *45*, 1336-1348.

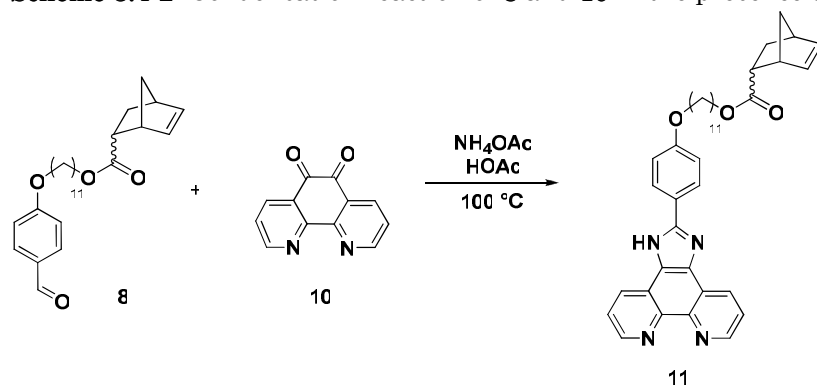
10 is commercially available but was synthesised from [1,10]-phenanthroline **9** according to literature.⁶⁹

Subsequently, the quinone **10** was reacted with the norbornene bearing aldehyde **8** as shown in Scheme 3.4-2 under the above-described condensation conditions, which led to the norbornene bearing imidazophenanthroline derivative **11** in 59.5% yield for the last step.

Scheme 3.4-1: Synthesis of the norbornene bearing aldehyde **8** (top) and phenanthroline-5,6-dione **10** (bottom).



Scheme 3.4-2: Condensation reaction of **8** and **10** in the presence of NH_4OAc in $AcOH$.



The preparation of random copolymers of **11** with (\pm)-*endo,exo*-norborn-5-ene-2,3-dicarboxylic acid dimethyl ester using the third generation Grubbs catalyst **G3** as the initiator failed repeatedly and polymerisation was not observed, most probably due to the typically strong binding between the initiator and the diimine moiety. This coordination of **11** to the initiator causes initiator poisoning and thus inactivates the initiator molecules.

Consequently, we took advantage of this strong binding-ability of diimine ligands to ruthenium and developed diimine ligands bearing ruthenium complexes for polymerisation.

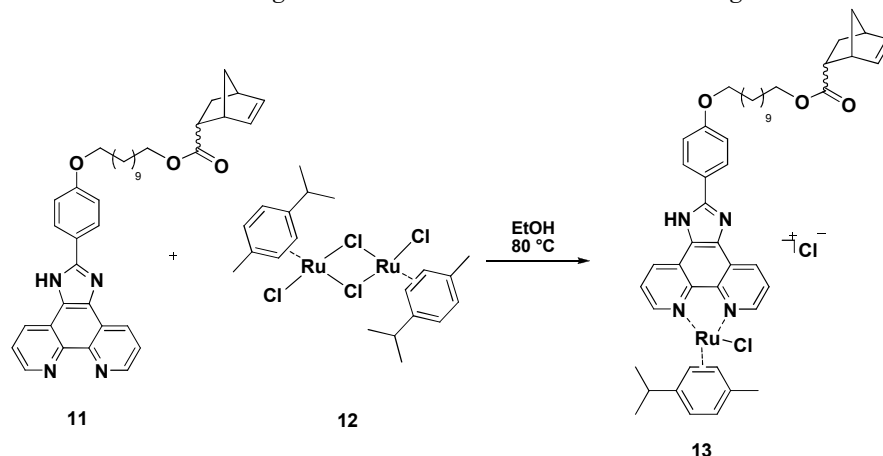
⁶⁹ Hiort, C.;Lincoln, P.; Nordén, B. *J. Am. Chem. Soc.* **1993**, *115*, 3448-3454.

3.4.2 Preparation of the Complexes

Ruthenium diimine complexes have been increasingly studied and developed and thus, applications are as versatile as the synthesis pathways (*cf.* Chapter 2.3.2). Synthesis of ruthenium complexes bearing one or more imidazophenanthroline ligands has also been reported. Thereby the condensation reaction of an aldehyde with phenanthroline-5,6-dione in presence of ammonium acetate in acetic acid is widely used. Both pathways to obtain imidazophenanthroline bearing ruthenium complex have been published, the direct complexation of the imidazophenanthroline ligand to the metal centre⁷⁰ and the synthesis of the ruthenium complex bearing one phenanthroline-5,6-dione ligand followed by the addition of the appropriate aldehyde,⁷¹ respectively.

A very convenient way to synthesise heteroleptic ruthenium complexes is the cleavage of 1 equiv. dichloro(*p*-cymene)ruthenium(II) dimer **12** with 2 equiv. of the appropriate diimine ligand - in the present case with **11** - in ethanol. After 20 hours reaction time the solvent is removed and the solid residue is washed with diethyl ether (Et₂O). This leads to the corresponding chloro(*p*-cymene) ruthenium(II) complex **13** bearing one diimine co-ligand in 82.9% yield (*cf.* Scheme 3.4-3).

Scheme 3.4-3: Cleavage of the dimer **11** with the diimine ligand **10**.



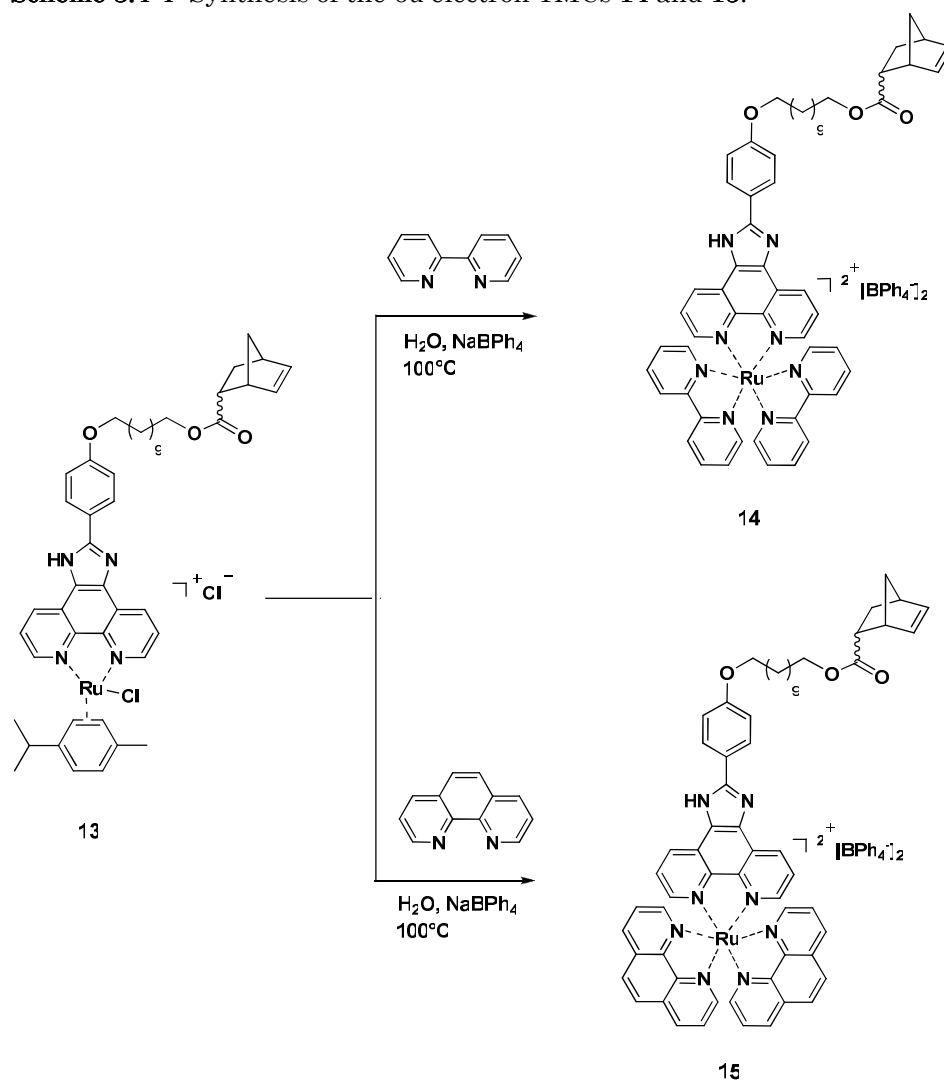
Subsequently, the *cymene* ligand is removed by the addition of 2 equiv. of further diimine ligands in aqueous media. Thereby stable *6d* electron transition metal complexes (TMC) are formed. Within this thesis two polymerisable, heteroleptic ruthenium complexes have been synthesised using 2,2' bipyridine and 1,10 - phenanthroline for the formation of the *6d* electron TMC **14** and **15**, respectively (*cf.* Scheme 3.4-4). After 20 hours, the products were precipitated by the addition of sodium tetraphenylborate

⁷⁰ Lü, Y.; Gao, L.; Han, M.; Wang, K. *Eur. J. Inorg. Chem.* **2006**, 430-436.

⁷¹ Mayer, C.R.; Dumas, E.; Miomandre, F.; Méallet-Renault, R.; Warmont, F.; Vigneron, J.; Pansu, R.; Etcheberry, A.; Sécheresse, F. *New J. Chem.* **2006**, *30*, 1628-1637.

(NaBPh₄). Thereby the chloride counter anion is exchanged by the tetraphenylborate anion (BPh₄⁻) resulting in decreased solubility in water.

Scheme 3.4-4: Synthesis of the 6d electron TMCs **14** and **15**.



The pure TMCs **14** and **15** were isolated in 75.3% and 76.5% yield, respectively. All intermediates as well as the norbornene bearing ruthenium complexes were characterised by NMR spectroscopy. By reacting the ruthenium dimer **12** with the imidazophenanthroline derivative **11** the characteristic peaks of the cymene at 6.64 and 6.41 ppm appear beside the typical imidazophenanthroline peaks. Subsequently, upon addition of the diimine ligands, these cymene peaks vanish while further diimine peaks and the intense peaks assigned to the tetraphenylborate appear. (*cf.* Chapter 5.3.2) Integration of the signals assigned to the counter anion indicates incomplete anion exchange.

3.4.3 Polymerisation of the TMCs

Monomers **14** and **15** were used to prepare random copolymers **poly(14-co-16)** and **poly(15-co-16)** with a mixture of *endo* and *exo*-norborn-5-ene-2,3-dicarboxylic acid dimethyl ester (**16**) (*cf.* Figure 3.1-2) using third generation Grubbs catalyst **G3** as the initiator and degassed dichloromethane as the solvent.^{72,73} The copolymers were prepared using a molar ratio of 300 : 3: 1 for monomer **14** or **15** : **16** : **G3**. The reaction mixture was stirred at room temperature and the progress of the polymerisation continuously monitored by TLC.

After one hour, total consumption of the monomers was determined and the polymerisation was quenched by addition of ethyl-vinyl-ether. The resultant polymers were purified by repeated precipitation of dichloromethane solutions from methanol and dried *in vacuo*. The resultant polymers **poly(14-co-16)** and **poly(15-co-16)** were isolated in 68.7% and 50.31%, respectively. Both polymers were characterised by ¹H-NMR spectroscopy. Calculation of the effective ratio of the corresponding TMC **14** or **15** to **16** by integration of characteristic NMR peaks was not possible due to the chosen ratios and the limited sensitivity of NMR spectroscopy. Hence, only the characteristic peaks of **16** were obtained. Size exclusion chromatography (SEC) failed presumably because of the polycationic nature of the polymer.

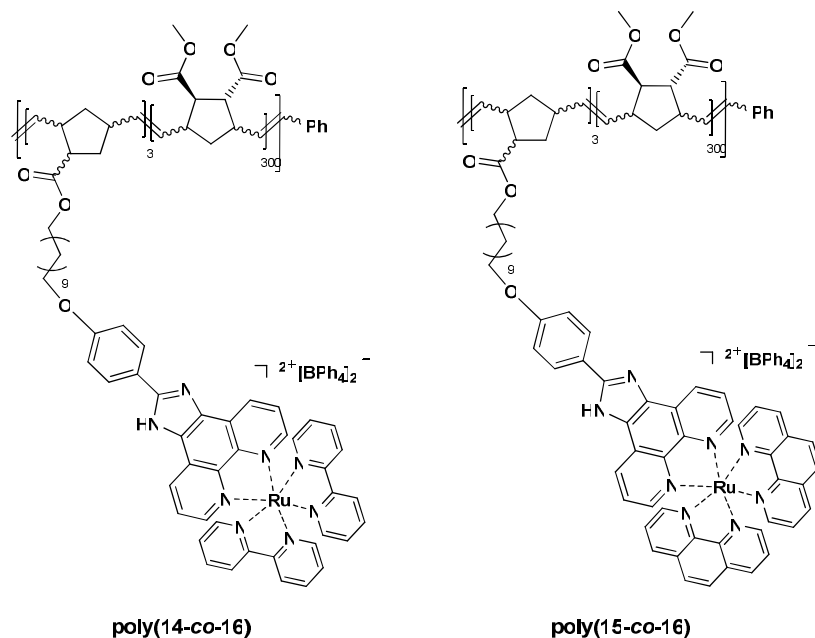


Figure 3.4-1: Random polymers **poly(14-co-16)** and **poly(15-co-16)** using third generation Grubbs initiator.

⁷² Slugovc, C.; Demel, S.; Riegler, S.; Hobisch, J.; Stelzer, F. *J Mol Catal A* **2004**, *213*, 107-113.

⁷³ Riegler, S.; Demel, S.; Trimmel, G.; Stelzer, F.; Slugovc, C. *J Mol Catal A* **2006**, *257*, 53-58.

3.4.4 Photophysical Measurements

The optical properties of the diimine ligand **11**, the monomeric TMCs **14** and **15** as well as of the resultant polymers **poly(14-co-16)** and **poly(15-co-16)** were investigated by UV-Vis and photoluminescence spectroscopy.

3.4.4.1 Optical Properties of the Imidazophenanthroline Ligand **11**

Measurements were performed in chloroform at room temperature under ambient conditions. Since chloroform may contain acidic impurities and the imidazophenanthroline chromophores are delicately affected by the pH,⁷⁴ the solvent was passed through alkaline aluminium oxide (Al_2O_3) prior to use. Additionally, 3 μL of triethyl amine (NEt_3) were added to the sample cuvettes to assure the existence of the not protonated form. Subsequently, trifluoroacetic acid (TFA) was added to the cuvettes in order to investigate the optical properties of the protonated chromophore. Absorbance and emission data of the imidazophenanthroline ligand **11** are shown in Table 3.4-1 and Figure 3.4-2.

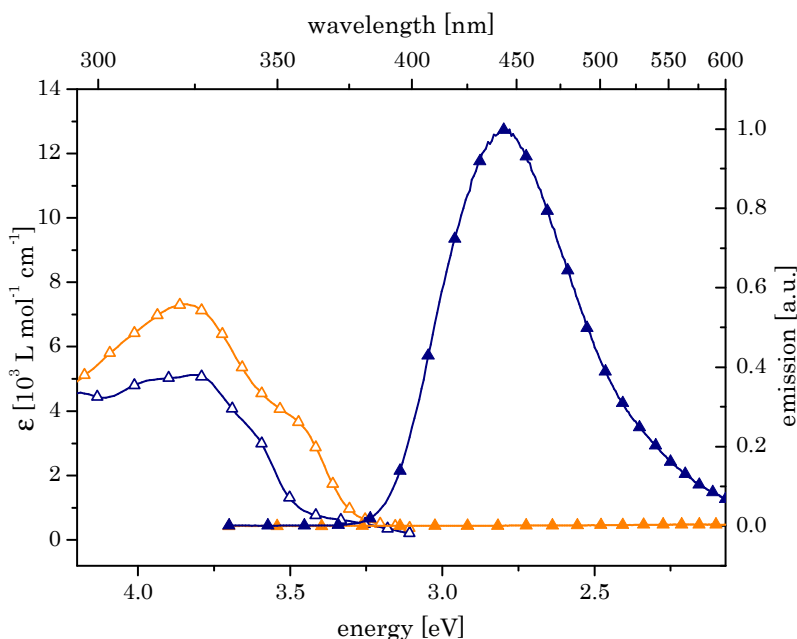


Figure 3.4-2: Absorbance (hollow symbols) and normalised emission (filled symbols) of **11** in the not protonated (blue lines) and in the protonated (orange lines) form.

Absorption spectra of **11** in the non-protonated state showed a maximum at lowest energy at 325 nm (3.81 eV, $\epsilon = 5100 \text{ L}\cdot\text{mol}^{-1}\cdot\text{cm}^{-1}$) and a shoulder at 340 nm (3.65 eV, $\epsilon = 3600 \text{ L}\cdot\text{mol}^{-1}\cdot\text{cm}^{-1}$), respectively assigned to $\pi \rightarrow \pi^*$ transitions. Upon treatment with TFA and hence complete protonation, the maximum shifted to 322 nm (3.85 eV) and the molar absorption coefficient

⁷⁴ Swaminathan, M.; Dogra, S.K. *J Chem Soc Perkin Trans II* **1983**, 1641-1644.

increased significantly up to $7300 \text{ L}\cdot\text{mol}^{-1}\cdot\text{cm}^{-1}$. This effect was ascribed to the increased ability of the protonated form to build hydrogen bonds.

Table 3.4-1: Absorption and photoluminescence data of **11** in CHCl_3 solution.

	λ_{abs} [nm]	E_{abs} [eV]	ϵ [$\text{L}\cdot\text{mol}^{-1}\cdot\text{cm}^{-1}$]	λ_{em} [nm]	E_{em} [eV]
11 not protonated	325	3.81	5100	444	2.79
	340 ^a	3.65 ^a	3600 ^a		
11 protonated	322	3.85	7300	-	-
	355 ^a	3.49 ^a	3800 ^a		

^a...shoulder.

Irradiation of compound **11** in its non-protonated form by UV-light ($\lambda_{\text{ex}} = 325 \text{ nm}$) resulted in deep blue emission. By the addition of $10 \mu\text{L}$ TFA the luminescence vanished completely and no emission was detected. The luminescence is quenched at a lower pH value when the imidazole ring is protonated as the protonated species is a better electron acceptor. It is believed that pH sensitive emission intensity of **11** upon protonation is assigned to two different mechanisms, one involving luminescence quenching arising from the positive charge and the other originating from rapid radiationless decay.

3.4.4.2 Optical Properties of the Transition Metal Complexes

Absorption and emission spectra of the monomers **14** and **15** were performed in chloroform ($\epsilon_r = 4.8$) as well as in acetone ($\epsilon_r = 20.7$) in order to investigate the solvatochromism of the complexes. The solvatochromic effect describes a dependence of absorption and emission spectra on the solvent polarity. Since polarities of the ground and excited state of a chromophore are different, a change in the solvent polarity may lead to differences regarding the stabilisation of the ground and excited states. This leads to a change in the energy gap and thus to variations in the position, intensity, and shape of the absorption and emission spectra. Especially charge transfer complexes are sensitive to solvent polarities. In solution, the transition energy and hence the colour of complexes varies with variation in solvent permittivity. This indicates variations in electron density because of the transition. The absorption and emission spectra of **14** and **15** are shown in Figure 3.4-3 and Figure 3.4-4, respectively.

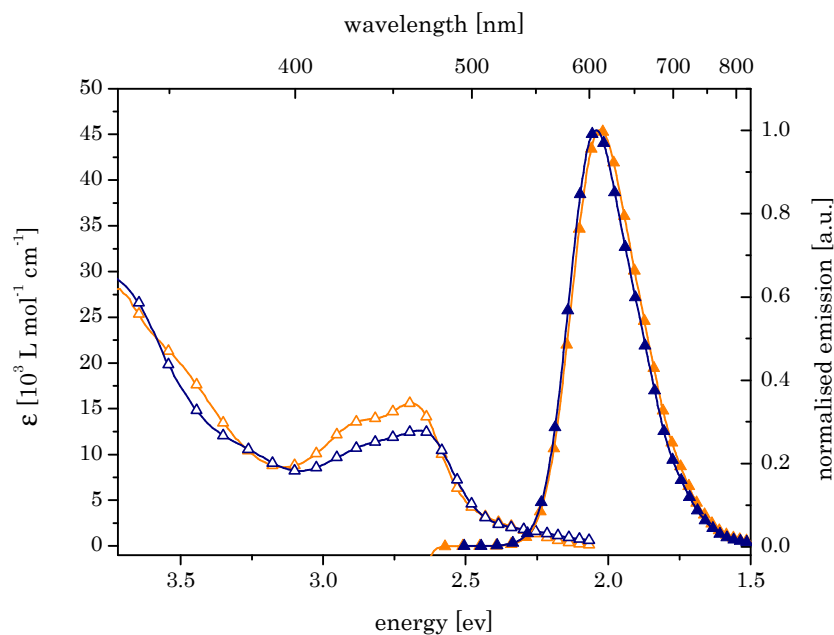


Figure 3.4-3: Absorption (hollow symbols) and emission (filled symbols) spectra of **14** in chloroform (blue lines) and in acetone (orange lines).

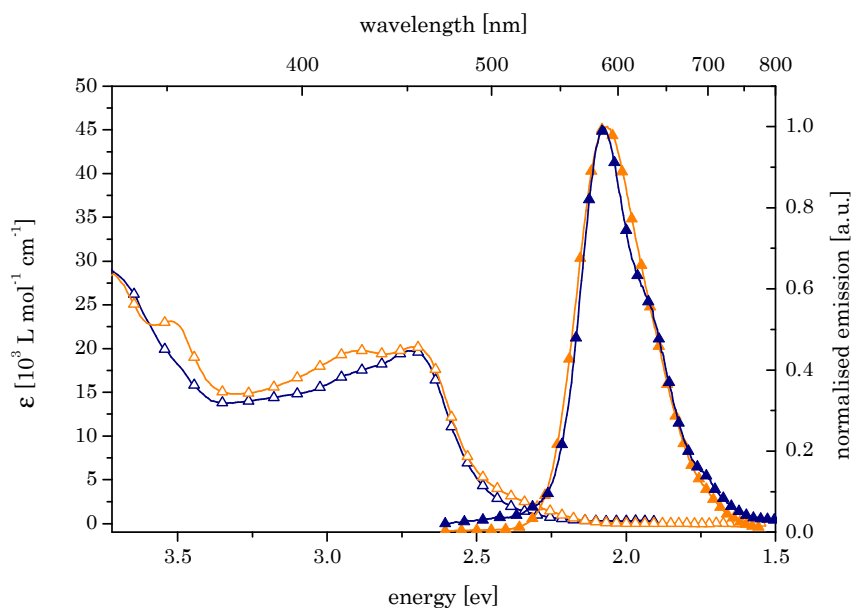


Figure 3.4-4: Absorption (hollow symbols) and emission (filled symbols) spectra of **15** in chloroform (blue lines) and in acetone (orange lines).

In general, the probability of light absorption, and thus the intensity of the correspondent absorption band, is related to the characteristics of the states involved. In metal ligand complexes (MLC) the localised absorption by the ligand, also referred to as ligand centred (LC) absorption, is assigned to a $\pi \rightarrow \pi^*$ transition and occurs at shorter wavelengths. This transition corresponds with the absorption characteristics of the free ligand and the energies of the LC bands of each ligand are usually unaffected by the other ligands. Absorption by the $d-d$ transitions of the metal is forbidden resulting in very low molar absorption coefficients. The broad absorption band around 450 nm originates from the metal-to-ligand charge transfer (MLCT)

transition. In transition metal complexes MLCT transitions are more likely to occur than ligand-to-metal charge transfer (LMCT) transitions as diimine ligands are easily reduced.⁴⁰ Thus, the highest occupied molecular orbital (HOMO) is localised on the metal centre, and the lowest unoccupied molecular orbital (LUMO) is located on the most reducible ligand. Studies on Ru(bpy)₃²⁺ and related complexes indicate that the emitting state is localised on a single ring. Temperature dependent data suggest that intermolecular (solvent-solute) and intramolecular interactions are present in single ligand localisation of Ru(bpy)₃²⁺ and Ru(phen)₃²⁺ complexes upon excitation. Resonance Raman spectroscopy provided evidence for localisation of the excitation both in mixed ligand complexes and in complexes containing equivalent ligands. Time resolved resonance Raman studies of Ru(bpy)₃²⁺ and related complexes gave evidence for a single ligand localised excited state on the time scale of molecular vibrations. Localised species is present in solution within a maximum of 1 ns after the excitation.⁷⁵ In the case of heteroleptic ruthenium complexes, more MLCT excited states, and therefore additional absorption bands, are expected due to the different orbital energies of the different ligands. Evidence that emitting state is localised on a single ring comes from shifts in absorption spectra as a function of the solvent polarity, due to instantaneous sensing of the formation of the dipolar excited state and from excited state absorption spectra.⁷⁶

Table 3.4-2: Absorption and emission characteristics of **14** and **15** in acetone and chloroform.

	λ_{abs} [nm]	E_{abs} [eV]	ϵ [L·mol ⁻¹ ·cm ⁻¹]	λ_{em} [nm]	E_{em} [eV]
14 in acetone	459	2.70	15600	611	2.03
	432	2.87	13700		
14 in chloroform	464	2.67	12600	607	2.04
15 in acetone	457	2.71	20200	597	2.08
	428	2.90	19800		
15 in chloroform	457	2.71	19700	596	2.08
				640 ^a	1.94 ^a

^a...shoulder.

In the absorption spectra of **14** the maximum of the MLCT band in acetone is located at 459 nm (2.7 eV) and displays a molar absorption coefficient of about 15600 L·mol⁻¹·cm⁻¹. In contrast, emission of **14** in chloroform exhibits a broad MLCT band around 464 nm (2.67 eV) with a slightly lower molar absorption coefficient around 12600 L·mol⁻¹·cm⁻¹.

For TMC **15** this decrease in molar absorption coefficient with decreasing solvent polarity was not observed. In acetone as well as in chloroform the maximum of the MLCT band is located at 457 nm (2.71 eV) and displays molar absorption coefficients of 20200 and 19700 L·mol⁻¹·cm⁻¹, respectively.

⁷⁵ Juris, A.; Balzani, V.; Barigelletti, F.; Campagna, S.; Belser, P.; Zelewsky, A. *Coord. Chem. Rev.* **1988**, *84*, 85-277.

⁷⁶ Yang, X.-J.; Janiak, C.; Heinze, J.; Drepper, F.; Mayer, P.; Piotrowski, H.; Klüfers, P. *Inorganica Chimica Acta* **2001**, *318*, 103-116.

The MLCT band of **14** and **15** in acetone exhibit a fine structure with one maximum at 459 nm (2.70 eV) and 457 nm (2.71 eV) and an additional absorption band at 432 nm (2.87 eV) and 428 nm (2.9 eV), respectively. The absorption in chloroform does not display any fine structure but rather one maximum at 464 nm for **14** and at 457 nm in case of **15**. This change in the absorption spectra is assigned to the increased solvent polarity and resultant solvent-chromophore interactions.³⁷

In general, absorption spectra are less sensitive to solvent polarity than emission spectra. Absorption usually occurs within 10^{-15} s, a time too short for chromophore or solvent motion. Thus, the molecules are exposed to the same local environment in the ground and in the excited states. In contrast, an emitting chromophore is exposed to a relaxed environment, as time is sufficient for solvent molecules to orient around the dipole moment of the excited state chromophore. Thus, a more pronounced effect of the solvent polarity on the emission spectra was expected. Upon irradiation of **14** and **15** at 460 nm the emission of the TMCs is also dominated by the MLCT transition. The emission does not originate from the central atom as typical for lanthanides, but rather from the entire complex. Furthermore, the metal-ligand bonds are covalent and do not dissociate under any remotely physiological conditions.³⁷

In case of **14** the emission in acetone and chloroform is centred at 611 nm (2.03 eV) and 607 nm (2.04 eV), respectively. Hence, a slight bathochromic shift of 4 nm is observed with increasing polarity of the solvent. The emission maximum of **15** displayed hardly any dependence on the solvent polarity. The emission maximum was observed at 597 nm in acetone and at 596 nm in chloroform, but with an additional shoulder in the latter case at 640 nm (1.94 eV). The appearance of a shoulder is assigned to additional absorption bands in heteroleptic ruthenium complexes originating from different orbital energies of the different ligands. Thus also emission from different MLCT triplet states might be observed.⁷⁶

Emission characteristics of **15** seem to be hardly affected by the solvent polarity, while **14** exhibit a slightly higher sensitivity towards solvent polarity. This is assigned to a lower dipole moment and a higher symmetry of **15** compared to **14**. It is plausible, that only polar chromophores display a pronounced sensitivity to solvent polarity.³⁷

On the other hand, currently known TMC systems fail to match the ideal octahedral conformation resulting in lower symmetry, which further splits the *d* levels. However, the types of excited states remain the same and the *d-d* state energies are still dictated by the average crystal field strength of all the ligands. As it was believed that **15** exhibits a higher symmetry, the ligand field strength of **15** was expected to be less compared to **14**. Consequently, the emission was also expected to be shifted to lower energies and higher wavelength compared to **14**. These expectations were not confirmed by the absorption and emission spectra, which is assigned to the fact that 2,2'-bipyridine and 1,10-phenanthroline ligands exhibit equal ligand field strength.⁴⁰

Nevertheless, it has to be pointed out that **14** displayed an increased Stoke's shift in acetone of 152 nm compared to a shift of 143 nm in chloroform. The Stoke's shift of **15** is not affected by the solvent permittivity but stays rather constant with a magnitude of 140 ± 1 nm. This is assigned to the higher dipole moment of **14**, which thus exhibit an increased sensitivity toward solvent polarity. It is well known that the Stoke's shift increases with increasing solvent polarity and increasing ability of hydrogen-bond formation due to specific solvent-chromophore interactions.³⁷ Thus, further absorbance and emission studies should be performed in protic solvents in order to investigate the ground and excited state effect of solvent polarity, but the solubility of the complexes in protic solvents is the limiting factor.

3.4.4.3 Effect of Protonation on the Optical Properties of **14**

As the photophysical characteristics of the imidazophenanthroline ligand exhibit high sensitivity to protonation, corresponding measurements of **14** have been performed in chloroform.

The lowest energy absorption at 468 nm, the metal to ligand charge transfer band, is 9 nm blue shifted and a decrease in molar absorption coefficient of $170 \text{ L}\cdot\text{mol}^{-1}\cdot\text{cm}^{-1}$ is observed upon protonation with TFA. Upon irradiation of complex **14** at 468 nm bright red emission at 613 nm was observed. In contrast to the free ligand, the emission of the TMC rises upon protonation and the emission maximum is shifted to lower wavelength.

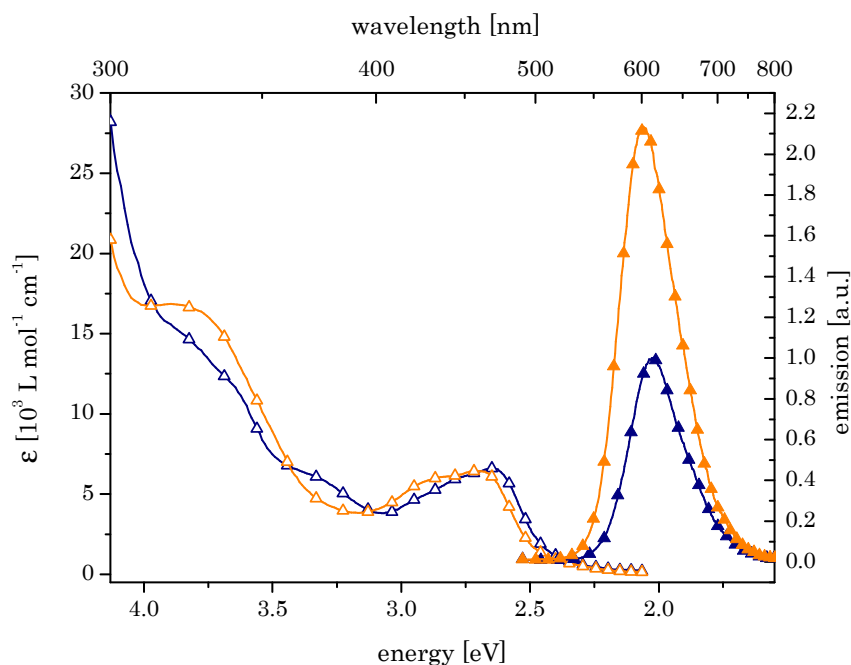


Figure 3.4-5: Absorption (hollow symbols) and emission (filled symbols) spectra of **14** in the non-protonated (blue lines) and in the protonated (orange lines) state.

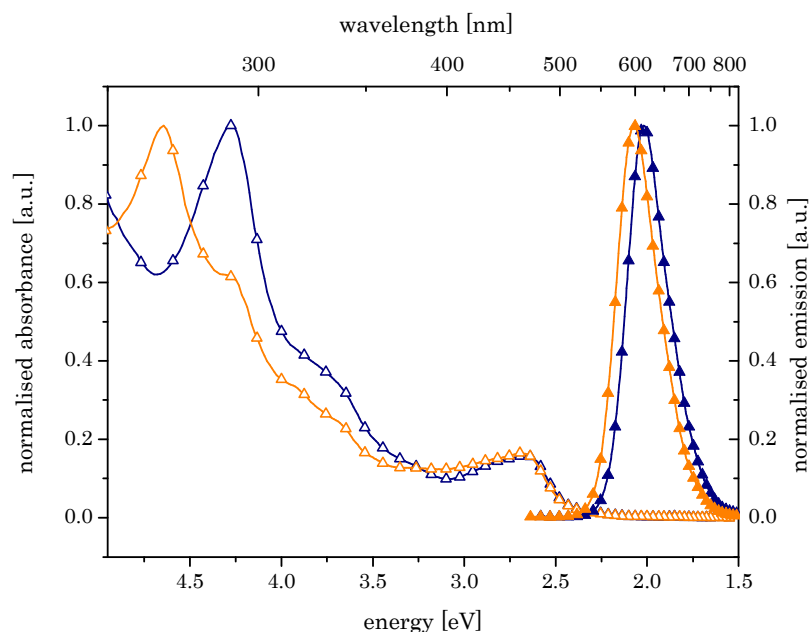
Table 3.4-3: Absorption and emission characteristics of **14** in the non-protonated state and after the addition of TFA.

	λ_{abs} [nm]	E_{abs} [eV]	ϵ [L mol ⁻¹ cm ⁻¹]	λ_{em} [nm]	E_{em} [eV]
14 not protonated	468	2.65	6610	613	2.02
14 protonated	459	2.70	6440	602	2.06

The energy of the metal-centred excited states depends on the ligand field strength, which in turn depends on the σ -donor and π -acceptor properties of the ligands. Upon protonation, the positive charge of the imidazol ring may be delocalised over the π -framework. This increases the σ -donor and decreases the π -acceptor property of the ligand, resulting in an increased ligand field strength. It is believed that the addition of a strong base capable for deprotonating the imidazol ring, would in turn lead to a non-emissive TMC species. Accordingly, the negative charge on the deprotonated imidazol is delocalised, hence the σ -donor capacity is decreased and the π -acceptor property of the ligand is increased, resulting in weakening of the ligand-field strength around the metal centre and lowering the metal σ^* orbitals.⁷⁷

3.4.4.4 Optical Properties of the Polymeric Transition Metal Complexes

Photophysical measurements of the random copolymers **poly(14-co-16)** and **poly(15-co-16)** in chloroform solutions have been performed in order to investigate whether the photophysical properties of the TMCs were preserved in the polymers. In Figure 3.4-6 normalised absorption and emission spectra of both polymers are shown entirely, in Figure 3.4-7 the low energy absorption band of the MLCT transition is zoomed in and in Table 3.4-4 all data are summarised.

**Figure 3.4-6:** Absorption (hollow symbols) and emission (filled symbols) spectra of **poly(14-co-16)** (blue lines) and **poly(15-co-16)** (orange lines) in chloroform.

⁷⁷ Gao, F.; Chao, H.; Zhou, F.; Peng, B.; Ji, L.-N. *Inorg. Chem. Comm.* **2007**, *10*, 170-173.

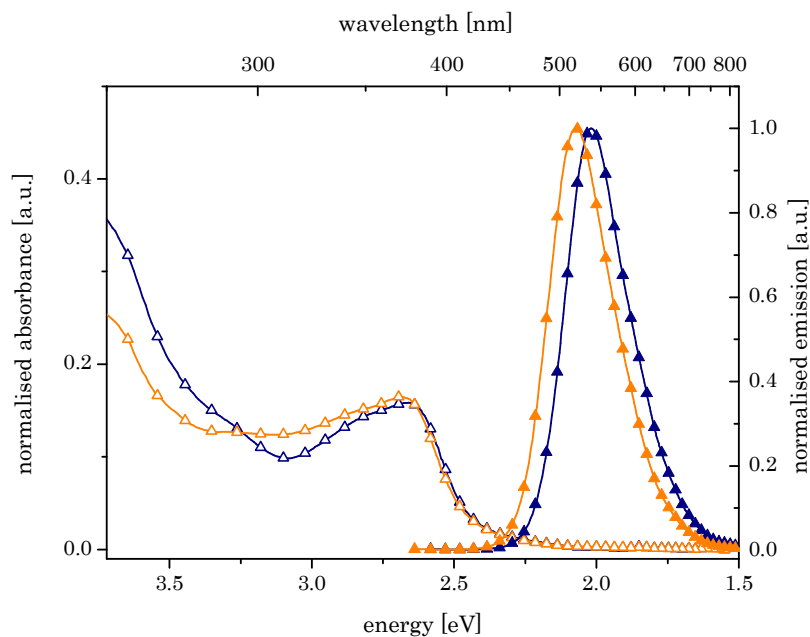


Figure 3.4-7: MLCT band (hollow symbols) and emission (filled symbols) spectra of **poly(14-co-16)** (blue lines) and **poly(15-co-16)** (orange lines) in chloroform.

Both, **poly(14-co-16)** and **poly(15-co-16)** show an absorption band of the MLCT transition at 465 nm (2.67 eV). The $\pi \rightarrow \pi^*$ state energies are dictated by the ligands. Thus, varying the π conjugation of the ligands alters the energy and intensity of the $\pi \rightarrow \pi^*$ transition. Consequently, the intense LC absorption exhibit different maxima at 290 nm (4.27 eV) and 267 nm (4.64 eV) according to the different ligands 2,2' bipyridine and 1,10-phenanthroline, respectively.

Under the presumption that the molar absorption coefficient of the monomeric materials **14** and **15** are preserved in the polymer, the effective concentration of the chromophore in the polymer can be determined. Thus, via Lambert-Beer law (*cf.* Equation 2.3-1) and the molar absorption coefficient obtained for the monomers at a certain wavelength, the effective concentration of the chromophore in the polymers is calculated and compared with the theoretical concentration.

$$E_{\lambda} = -\lg\left(\frac{I}{I_0}\right) = \varepsilon_{\lambda} \cdot c \cdot d \quad 3.4-1$$

E_{λ}	absorbance of light at the wavelength λ
I_0	intensity of the irradiating light
I	intensity of the transmitted light
ε_{λ}	molar absorption coefficient
c	concentration of the chromophore
d	cuvette width

After insertion of the known and/or measured variables, a concentration of $4.39 \cdot 10^{-5} \text{ mol} \cdot \text{L}^{-1}$ of **14** was obtained. According to the molar ratios in the polymers and under the presumption that **14** was completely incorporated into the polymer, $4.44 \cdot 10^{-5} \text{ mol} \cdot \text{L}^{-1}$ of **14** should be incorporated in the polymer. Thus, the content of **14** in **poly(14-co-16)** is as high as expected which indicates that the chromophore was incorporated into the polymer to

an expected amount. Furthermore, this also evidence that the molar absorption coefficient stays constant upon polymerisation and self-association of such complexes is unlikely to appear.

Equal calculations for **15** lead also to the assumption that the molar absorption coefficient remains constant in the polymeric material. The concentration of the chromophore calculated with Equation 2.3-1 amounts to $4.57 \cdot 10^{-5} \text{ mol} \cdot \text{L}^{-1}$ which meets perfectly the theoretically incorporated amount of $4.55 \cdot 10^{-5} \text{ mol} \cdot \text{L}^{-1}$.

Irradiation of the samples under ambient conditions at 465 nm resulted in deep red emission. The differences between **poly(14-co-16)** and **poly(15-co-16)** in the emission spectra are more pronounced compared to the monomer emission of **14** and **15**. The emission maximum of **poly(14-co-16)** is red-shifted to 614 nm (2.02 eV), while **poly(15-co-16)** exhibit the maximum at 599 nm (2.07 eV), which thus is almost unaffected by polymerisation. Absorption and emission data are shown in Table 3.4-4. Factors, which may influence emission intensity and energy, are numerous and chromophores often display multiple interactions with their environment. Beside solvent polarity and dipole moment, the emission characteristics might be delicately affected by conformational changes, viscosity of the sample and probe-probe interactions. These effects should be equally true for **poly(14-co-16)** and **poly(15-co-16)** while the emission at higher wavelength and thus lower energy of **14** and **poly(14-co-16)** is assigned to the higher dipole moment of **14**.

Table 3.4-4: Absorption and emission characteristics of **14** and **15** in chloroform compared with the corresponding polymers **poly(14-co-16)** and **poly(15-co-16)**.

	λ_{abs} [nm]	E_{abs} [eV]	ϵ [L · mol ⁻¹ · cm ⁻¹]	λ_{em} [nm]	E_{em} [eV]
14 in chloroform	464	2.67	12600	607	2.04
poly(14-co-16)	465	2.67		614	2.02
poly(14-co-16) film	475	2.61		593	2.09
15 in chloroform	457	2.71	19700	596	2.08
poly(15-co-16)	465	2.67		599	2.07

Furthermore, excitation and emission spectra of thin films of **poly(14-co-16)** were recorded and compared with the spectra obtained from solution (*cf.* Table 3.4-4 and Figure 3.4-8). For the preparation of the thin film, a chloroform solution containing 1 wt.% of **poly(14-co-16)** were spin-coated onto 0.5 x 0.5 cm glass slides. While **poly(14-co-16)** in chloroform solution exhibit a maximum of the MLCT transition at 465 nm (2.67 eV), the MLCT band of film spectrum is 10 nm red shifted to 475 nm (2.61 eV). In contrast, the emission maximum of the film is shifted to lower wavelength (higher energy) and displays a maximum of the emission at 593 nm (2.09), which is 21 nm blue shifted compared to **poly(14-co-16)** in solution. This results in a remarkable decrease of the Stoke's shift of 31 nm for **poly(14-co-16)** in the film spectrum. This effect is assigned to the increased rigidity in the film. If

the chromophore is in a rigid environment that cannot relax within the timescale of the excited state lifetime, the emission occurs from a higher, unequilibrated excited state to the initial conformation of the ground state. Thus, chromophores that have differences in energy between the initial and the relaxed excited state, differences in emission spectra are observed due to the rigidity of the environment. The emission is shifted to lower wavelength and higher energy with increasing rigidity. Effects like π -stacking and excimer formation are unlikely, as such effects for Ru-complexes, to my knowledge, have not been reported so far. Ruthenium complexes do not appear to be prone to self-association.³⁷

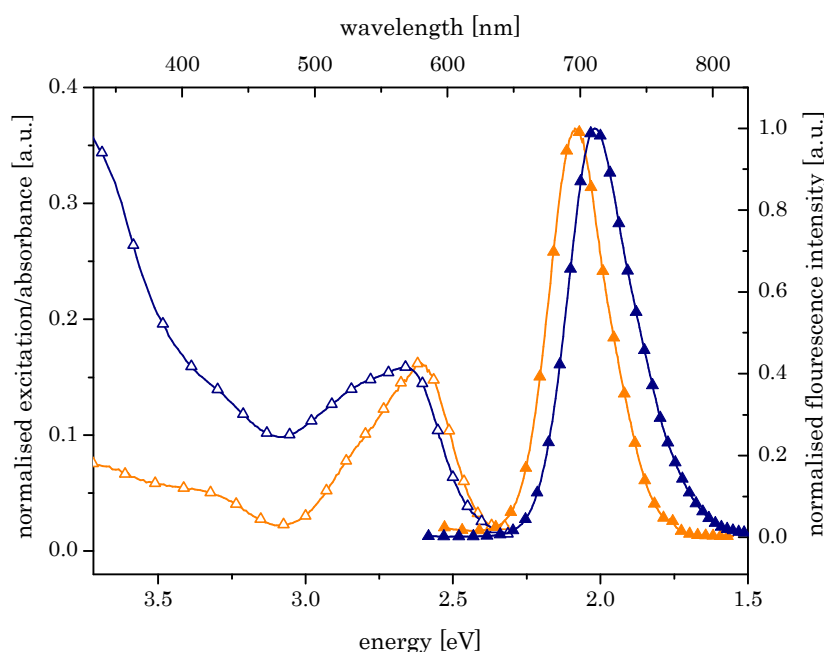


Figure 3.4-8: Comparison of absorption (hollow symbols, blue line) and excitation (hollow symbols, orange line) and emission (filled symbols) spectra of **poly(14-co-16)** in chloroform solution (blue lines) and in thin film (orange lines).

3.4.4.5 Effect of Counter Ion on the Optical Properties

In order to facilitate the interpretation of the NMR spectra and to study the influence of the counter anion on the optical properties of the complexes, analogue complexes have been synthesised using hexafluoro phosphate as the counter anion. Thereby equal reaction conditions were chosen for the synthesis of the complexes (*cf.* Chapter 3.4.2). **13** was reacted with the corresponding diimine ligands in water and subsequently the complexes were precipitated from water by the addition of 2 equiv. ammonium hexafluoro phosphate (NH_4PF_6). The monomers **17** bearing the bipyridine ligands and **18** bearing the phenanthroline ligands were isolated in 66.5% and 75.3% yield, respectively. Random copolymers were also prepared using again **16** as the second component resulting in the corresponding copolymers **poly(17-co-16)** and **poly(18-co-16)** in 60.4% and 97.8% yield, respectively (*cf.* Chapter 3.4.3).

Absorption and emission spectra of the monomers **17** and **18** in acetone and chloroform as well as of the polymers **poly(17-co-16)** and **poly(18-co-16)** in chloroform have been performed and are compared with the optical properties of monomers **14** and **15** in acetone and chloroform and the corresponding polymers. As shown in Table 3.4-5 absorption and emission maxima are hardly affected by the counter anion. It is noticeable that **17** and **18** show a loss of vibrational structure in acetone while **14** and **15** exhibit a second absorption band at 432 nm (2.87 eV) and 428 nm (2.90 eV), respectively. Furthermore, **17** exhibit higher molar absorption coefficients in acetone and chloroform compared to **14** which is assigned to the differences in molecular weight.

Table 3.4-5: Summarised absorption and emission characteristics of the TMCs in chloroform and acetone and the resultant polymers in chloroform solutions.

	λ_{abs} [nm]	E_{abs} [eV]	ϵ [L mol ⁻¹ cm ⁻¹]	λ_{em} [nm]	E_{em} [eV]
14 in acetone	459	2.70	15600	611	2.03
17 in acetone	459	2.70	17600	611	2.03
14 in chloroform	464	2.67	12600	607	2.04
17 in chloroform	463	2.68	18100	607	2.04
15 in acetone	457	2.71	20200	597	2.08
18 in acetone	457	2.71	18600	597	2.08
15 in chloroform	457	2.71	19700	596	2.08
18 in chloroform	457	2.71	20000	590	2.10
poly(14-co-16)	465	2.67		614	2.02
poly(17-co-16)	459	2.70		617	2.01
poly(15-co-16)	465	2.67		599	2.07
poly(18-co-16)	457	2.71		605	2.05

Surprisingly emission maxima are shifted to lower wavelength (higher energy) in the polymeric materials when changing the counter anion from tetraphenyl borate to hexafluoro phosphate. It was expected that the use of a smaller counter anion may accelerate relaxation and rearrangement processes and thus the emission maxima is rather shifted to lower energy.

The effective incorporation of the chromophores **17** and **18** in the polymers **poly(17-co-16)** and **poly(18-co-16)** has also been calculated using Equation 2.3-1. The thus obtained concentrations are less than expected due to the decreased molecular weight caused by the counter anions.

3.4.5 Lifetime Measurements

Time-domain lifetime measurements have been performed at Joanneum Research. The measurements were performed to investigate the behaviour of **poly(14-co-16)** and **poly(15-co-16)** in chloroform solution in absence and presence of oxygen. The aim was to study the behaviour of the complexes and evaluate their potential applicability for oxygen sensing or rather for determination of aerobic bacteria as a function of luminescence lifetime.

1 wt.% of the polymers were dissolved in chloroform. Lifetime measurements were performed before and after treatment of the solution with nitrogen. For detailed information, concerning general back-ground and set-up see Chapter 6.1.4.1. The corresponding lifetime measurements for **poly(14-co-16)** and **poly(15-co-16)** are shown in Figure 3.4-9 and Figure 3.4-10, respectively. In case of **poly(14-co-16)** a luminescence lifetime of 4.8 μs is obtained under ambient conditions which rises upon treatment with nitrogen up to 10.8 μs . **Poly(15-co-16)** exhibit a luminescence lifetime of 3.9 μs in air which increases up to 7.7 μs in nitrogen atmosphere.

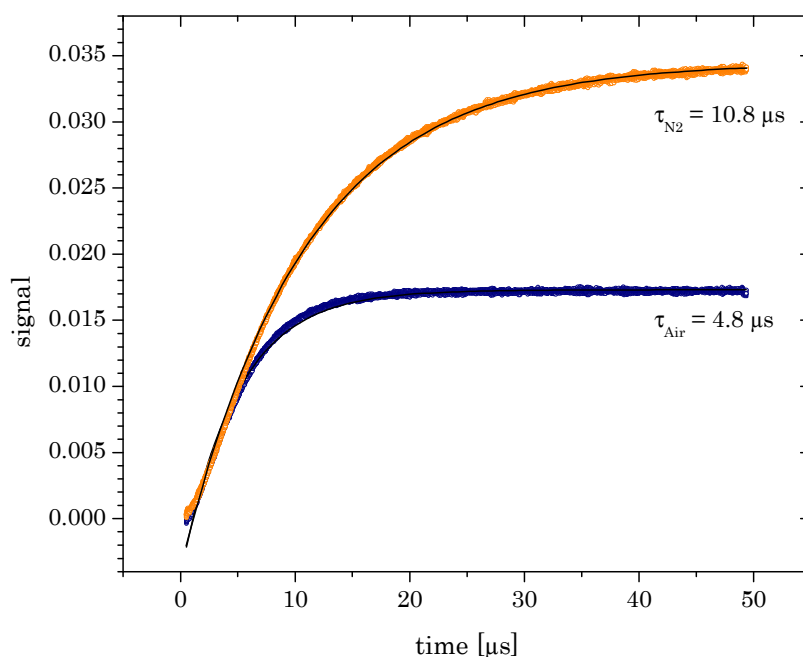


Figure 3.4-9: Time domain lifetime measurements of **poly(14-co-16)** in chloroform solution in air (blue line) and degassed in nitrogen (orange line).

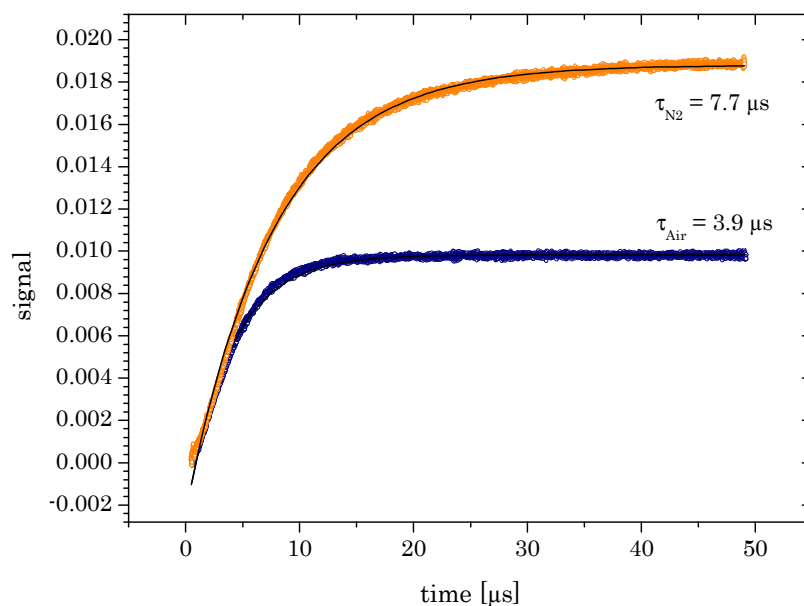


Figure 3.4-10: Time domain lifetime measurements of **poly(15-co-16)** in chloroform solution in air (blue line) and degassed in nitrogen (orange line).

These preliminary measurements evidence that **poly(14-co-16)** and **poly(15-co-16)** exhibit increased lifetimes in absence of oxygen. These results indicate that the polymeric TMCs might be applicable for measuring aerobic bacteria in water pipes.

3.4.5.1 Outlook and Future Work on Polymeric TMCs

Further time-domain lifetime measurements of the polymeric transition metal complexes **poly(14-co-16)** and **poly(15-co-16)** in thin film will be performed in future experiments using the set-up described above. Thus, real-conditions for the subsequent application are imitated and measurement errors assigned to solvent evaporation are excluded.

In order to use the developed polymeric TMCs as oxygen sensors (e.g. in water pipes and in food industry, sensitivity toward humidity of these systems has to be excluded. Hence, the cross-sensitivity of the polymeric TMCs towards humidity will be investigated. Therefore, the measuring set-up and cavity developed by Astrid Knall⁷⁸ in close cooperation with Christian Konrad and Martin Tscherner from Joanneum Research is adopted for measuring ruthenium complexes (*cf.* Chapter 6.1.4.2).

⁷⁸ Knall, A. *Doctoral Thesis*, Graz University of Technology 2008.

4 Conclusion & Outlook

4.1 Conclusion on the Biocide Polymers

Amino-functionalised random polymers were synthesised via Ring Opening Metathesis Polymerisation (ROMP) and their biocide activity against Gram-positive *S. aureus*, Gram-negative *E. coli* as well as the fungi *C. albicans* and *A. niger* was investigated. 5 wt.% of the polymers were incorporated into a poly(ethylene) matrix using injection- and compression-moulding. The pure polymers exhibit good activity against bacteria and fungi, while the compound materials with poly(ethylene) did not show any antimicrobial activity. Consequently, the feasibility of synthesising block-*co*-polymers was studied. The aim was to force the self-assembly of the resultant amphiphilic block-*co*-polymers at the surface of the compounds. Investigations led to the conclusion that the synthesis of block-*co*-polymers is quite challenging. Due to secondary metathesis reaction of the mono-substituted norbornene monomers and different polymerisation kinetics of the monomers, block-*co*-polymers are difficult to achieve. Transmission Electron Microscopy (TEM) measurements revealed that the distribution of the active ring opening metathesis polymer in poly(ethylene) is negatively affected using block-*co*-polymers. This brings us to the conclusion that block-*co*-polymers are no attractive alternative to random copolymers.

Furthermore, leaching tests were performed in order to investigate the hydrolysis behaviour of the ester groups in the ring opening metathesis polymers. Therefore, dyes, also linked to the polymerisable norbornene moiety via ester functionality, were copolymerised. Thus, leaching behaviour of ester bound moieties in general was investigated. The leaching tests evinced that the antimicrobial active groups leach out to an amount of $0.35 \pm 0.05\%$ most probably due to ester hydrolysis. For the aspired application this is still too much. Thus, non-hydrolysable groups are desired and will be focus of future research.

4.2 Conclusion on the Luminescent, Polymerisable Ruthenium Complexes

Based on the experiences gathered earlier, imidazophenanthroline ligands bearing the polymerisable norbornene motif have been synthesised. The cleavage of the dichloro(*p*-cymene)ruthenium(II) dimer with the norbornene bearing imidazophenanthroline ligand and subsequent addition of 2 equiv. of further diimine ligands (2,2' bipyridine and 1,10 - phenanthroline) lead to stable heteroleptic 6d electron ruthenium complexes in high yields. To our knowledge, this synthesis pathway had not been reported previously.

Random copolymers of the resultant monomers using a mixture of *endo* and *exo*-norborn-5-ene-2,3-dicarboxylic acid dimethyl ester as the second component and the third generation Grubbs catalyst **G3** as the initiator have been prepared leading to the polymers **poly(14-co-16)** and **poly(15-co-16)**.

Photophysical measurements of the monomers in different solvents have been performed in order to investigate the solvatochromism of the complexes. Monomer **14** exhibits an increase in Stoke's shift of 10 nm in acetone compared to chloroform. The Stoke's shift typically increases with increasing solvent polarity and increasing ability of hydrogen-bond formation due to specific solvent-chromophore interactions. Thus, the increased sensitivity toward solvent polarity is assigned to the higher dipole moment of **14**.

Photophysical measurements of the random copolymers **poly(14-co-16)** and **poly(15-co-16)** in chloroform solutions evince that the optical properties of the transition metal complexes were preserved in the polymers. Under the presumption that the molar absorption coefficient is not affected by polymerisation, the effective concentration of the chromophore in the polymer was determined by Lambert-Beer law. It has been shown that the monomers **14** and **15** have been incorporated into the polymers to the expected amount and optical properties are preserved in the polymer. Thin film measurements of **poly(14-co-16)** revealed a remarkable decrease of the Stoke's shift of 31 nm which was assigned to the increased rigidity in the film.

Time-domain lifetime measurements of the polymeric transition metal complexes **poly(14-co-16)** and **poly(15-co-16)** in chloroform solutions have been performed. These measurements evidence that **poly(14-co-16)** and **poly(15-co-16)** exhibit increased lifetimes in absence of oxygen. These results indicate that the polymeric transition metal complexes might be applicable for measuring aerobic bacteria in water pipes.

Further time-domain lifetime measurements in thin film have to be performed. Consequently, real-conditions for the subsequent application are imitated and measurement errors assigned to solvent evaporation are excluded.

For the implementation of the polymeric transition metal complexes as oxygen sensing material in water pipes and food industry, cross-sensitivity of the polymeric transition metal complexes toward humidity has to be excluded. Therefore, the measuring set-up and cavity developed by Astrid Knall in close cooperation with Christian Konrad and Martin Tscherner from Joanneum Research will be adopted for humidity measurements of ruthenium complexes.

5 Experimental

5.1 Materials

All starting materials, unless otherwise stated, were purchased from commercial sources (Aldrich, Aglycon, etc.) and used without further purification. Reactions were performed using standard Schlenk techniques under nitrogen atmosphere if required. Solvents were purified, degassed and dried if necessary using standard procedures.

5.2 Instrumentation

5.2.1 Nuclear Magnetic Resonance (NMR) Spectroscopy

^1H (500 MHz) and ^{13}C (125 MHz) spectra were performed on a VARIAN INOVA 500 MHz spectrometer. Later, ^1H (300 MHz) and ^{13}C (75 MHz) spectra were obtained on a Bruker Avance III 300 MHz spectrometer. Solvent residual peaks of the deuterated solvents were used for referencing the NMR-spectra to the corresponding values according to Gottlieb et al.⁷⁹ Multiplicity and peak shapes are indicated with s (singlet), d (doublet), dd (doublet of doublets), t (triplet), m (multiplet), b (broad), bs (broad singlet). For polymer samples, the number of scan was set to 32 for ^1H -NMR spectra

⁷⁹ Gottlieb, H. E.; Kotlyar, V.; Nudelman A.; *J. Org. Chem.* **1997**, *62*, 7512-7415.

and to 10.000 for ^{13}C -NMR spectra and the relaxation delay for ^1H -NMR spectra was set to 5 s in order to guarantee complete relaxation.

5.2.2 Thin Layer Chromatography (TLC)

Reactions were monitored by TLC (silica gel 60 F₂₅₄ on aluminium, Merck). Detection was carried out under UV-light (254 nm and 365 nm for luminescent compounds) and staining with potassium permanganate (2% in H₂O dest. for unsaturated and reducing compounds).

5.2.3 Contact Angle Measurements

Contact angle measurements on polymer compounds (5 wt.% **poly(2₁₀₀-*block*(2₂₅₀-*co*-1₂₅₀))**) in poly(ethylene) matrix, extrusion temperature 210 °C) were evaluated using a Drop Shape Analysis System DSA 100 (Krüss GmbH, Hamburg, Germany). The contact angles were obtained using the sessile drop method and were measured within two seconds after deposition of the droplet. Water and diiodomethane⁶² were used as probe liquids (drop volume approx. 3 µL). Based on the Owens-Wendt method,⁶³ the surface tension γ was evaluated (*cf.* Supporting Information, Chapter 6.1.2).

5.2.4 Gel Permeation Chromatography (GPC)

Gel permeation chromatography was used to determine the weight and number average molecular weights (M_w and M_n) as well as the polydispersity index (PDI) using THF as eluent. In case of analysis of polymers containing amine functionalities a mixture of chloroform, triethylamine and *iso*-propanol (CHCl₃ : Et₃N : *iso*-propanol = 94 : 4 : 2) was used. The instrumentation consists of a Merck Hitachi L6000A pump (delivery volume: 1 mL min⁻¹, membrane pulse attenuator between pump and injector), STV-gel-columns from Polymer Standards Service with 5 µm particle size (pre column: 8x50 mm, 100 Å pore diameter, separation column: 8 x 300 mm, 10⁶ Å, 10⁴ Å, 10³ Å pore diameter), refractive index detector from Wyatt Technology, model Optilab DSP Interferometric Refractometer. Polystyrene standards purchased from Polymer Standard Service were used for calibration.

5.2.5 Photophysical Measurements

5.2.5.1 Absorption Measurements

UV-Measurements were performed on a Cary 50 Bio UV-Visible spectrophotometer at the Institute of Analytical Chemistry, Graz University of Technology using 101-QS quartz cuvettes.

5.2.5.2 Emission Measurements

Solution luminescence spectra were recorded on a Perkin Elmer Luminescence Spectrometer LS50B or on a Hitachi F-7000 fluorescence spectrometer at Institute of Analytical Chemistry, Graz University of Technology using 104F-QS quartz cuvettes.

Thin film luminescence measurements were performed on a Shimadzu RF-5301 PC Spectrofluorophotometer. The film was prepared by dissolving 4.3 mg of **poly(14-*c*-16)** in 0.5 mL chloroform and coating onto 10 x 10 mm glass plates.

5.2.6 Differential Scanning Calorimetry (DSC)

DSC measurements were performed with a Perkin Elmer Pyris Diamond Differential Scanning Calorimeter calibrated by using an indium standard equipped with a Perkin Elmer CCA7 cooling system using liquid nitrogen. A nitrogen flow of 20 mL min⁻¹ was used. Glass transition temperatures (T_g) were read as the midpoint of the DSC traces.

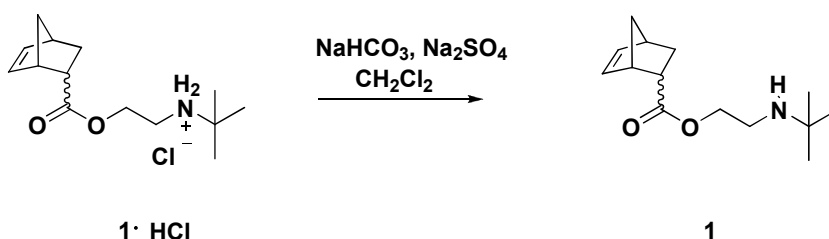
5.2.7 Thermogravimetric analysis (TGA)

TGA measurements were performed with a Netzsch Simultaneous Thermal Analyzer STA 449C (crucibles: aluminium from Netzsch). A helium flow of 50mL/min was used in combination with a protective flow of 8 mL/min.

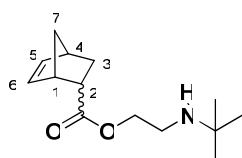
5.3 Syntheses

5.3.1 Biocide Materials

5.3.1.1 Mixture of *endo* and *exo*-2-(*tert*-butylamino) ethyl bicycle [2.2.1] hept-5-ene-2-carboxylate (1)



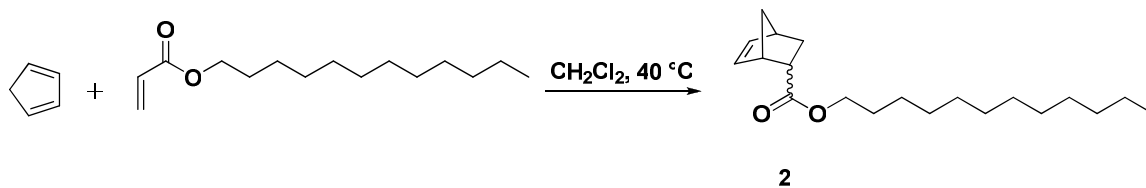
1-HCl (73.22 mmol, 1 eq., MW: 273.15 g·mol⁻¹) was dissolved in 200 mL CH₂Cl₂, Na₂CO₃·H₂O (293.53 mmol, 4 eq., MW: 124.01 g·mol⁻¹) and Na₂SO₄ (175.73 mmol, 2 eq., MW: 142.04 g·mol⁻¹) were added and the suspension was stirred for 24 h at room temperature. The solids were removed by filtration and the solution was evaporated under reduced pressure. The liquid residue is twice re-dissolved in cold *n*-pentane, filtered and the solvent was again removed *in vacuo*. The colourless, viscous liquid is dried under vacuum. Yield: 16.16 g (93%) R_f ≈ 0.4 (MeOH).



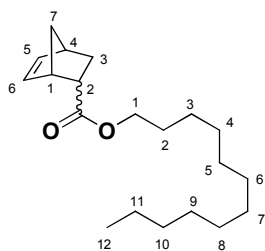
¹H-NMR (δ, 20 °C, CDCl₃, 500 MHz): 6.18, 5.92 (m, 2H, nb^{5,6}), 4.11 (t, 2H, COOCH₂), 3.19, 2.96, 2.90 (bs, m, bs, 3H, nb^{1,2,4}), 2.77 (t, 2H, CH₂NH), 1.90 (m, 1H, nb³), 1.43-1.25 (m, 4H, NH, nb^{3,7}), 1.10 (s, 9H, C(CH₃)); only signals for the *endo*-isomer are given; characteristic signals of the *exo*-isomer: 6.11 (m, 2H, nb^{5,6}), 4.17 (t, 2H, COOCH₂); *endo:exo* = 88 : 12.

¹³C{¹H} NMR (δ, 20 °C, 75 MHz, CDCl₃): 174.8, 138.0, 132.4, 64.9, 50.5, 49.8, 45.9, 43.4, 42.7, 41.5, 29.4, 29.1; characteristic signals of the *exo*-isomer: 176.3, 138.2, 135.8.

5.3.1.2 Mixture of *endo* and *exo*-n-dodecyl bicyclo[2.2.1]hept-5-ene-2-carboxylate (2)



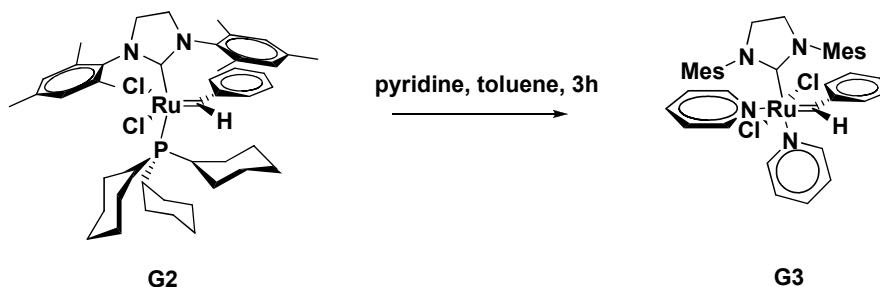
Freshly cracked and cooled cyclopentadiene (98.03 mmol, 2 eq., MW: 66.1 g·mol⁻¹) and 20 mL dry CH₂Cl₂ were added to a round bottom flask. Lauryl acrylate (49.05 mmol, 1 eq., MW: 240.38 g·mol⁻¹) was added dropwise over a period of 10 min. TLC revealed complete consumption of lauryl acrylate after 24 h at 40 °C. The crude product was purified by column chromatography (SiO₂, cyclohexane : ethyl acetate = 10 : 1). The colourless liquid was dried under reduced pressure. Yield: 12.18 g (81%), R_f ≈ 0.27 (CH:EE=30:1)



¹H-NMR (δ, 20 °C, CDCl₃, 500 MHz): 6.18, 5.92 (m, 2H, nb^{5,6}), 4.00 (m, 2H, dodecyl¹), 3.20 (bs, 1H, nb¹), 2.96-2.88 (m, 2H, nb^{2,4}), 1.90 (m, 1H, nb³), 1.59 (m, 2H, dodecyl²), 1.46-1.19 (m, 21H, nb^{3,7}, dodecyl³⁻¹¹), 0.88 (t, 3H, dodecyl¹²); only signals for the *endo*-isomer are given; characteristic signals of the *exo*-isomer: 6.11 (m, 2H, nb^{5,6}), 4.07 (t, 2H, COOCH₂); *endo*:*exo* = 80 : 20.

¹³C{¹H} NMR (δ, 20 °C, 75 MHz, CDCl₃): 176.5, 137.9, 132.5, 64.5, 49.8, 45.9, 43.5, 42.7, 32.1, 29.79, 29.78, 29.72, 29.69, 29.50, 29.38, 29.31, 28.8, 26.1, 22.8, 14.3; characteristic signals of the *exo*-isomer: 176.5, 138.2, 135.9, 64.8.

5.3.1.3 RuCl₂(pyridine)₂(H₂IMes)(CHPh) (G3)



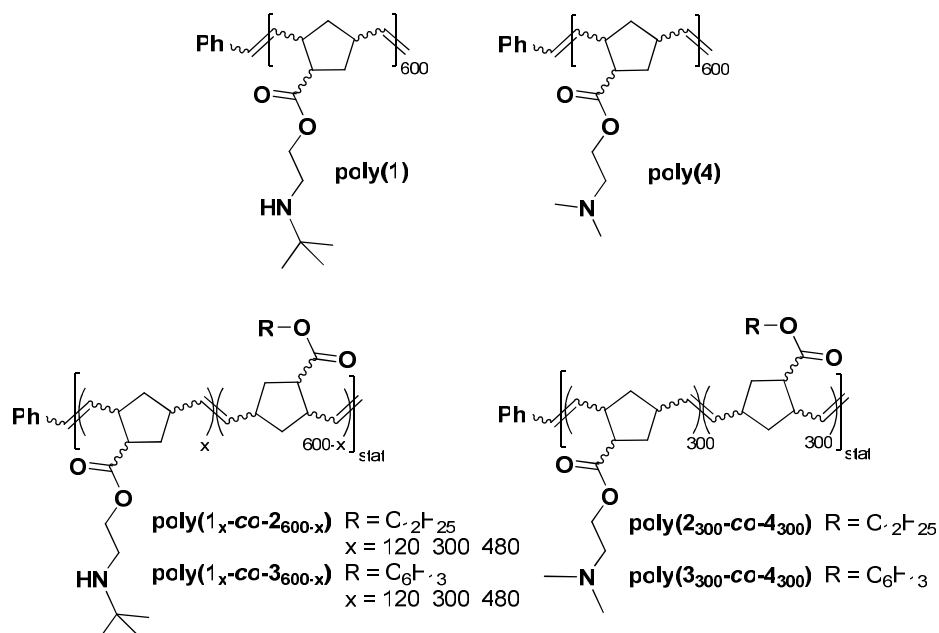
The reaction was performed under inert atmosphere in the glove-box. 155.3 mg second generation Grubbs catalyst (0.183 mmol, 1 eq., MW: 848.97 g·mol⁻¹) was dissolved in 5 mL toluene. Subsequently, 736 mg pyridine (9.305 mmol, 50 eq., MW: 79.1 g·mol⁻¹) was added dropwise. After 3 h the product was precipitated by adding dropwise into cooled *n*-heptane. The green solid was washed with *n*-heptane and dried *in vacuo*. Yield: 129.2 mg (97%).

5.3.1.4 General Polymerisation Procedures for poly(1), poly(1_x-co-2_{600-x}), poly(1_x-co-3_{600-x}), poly(2₃₀₀-co-4₃₀₀), poly(3₃₀₀-co-4₃₀₀) and poly(4)

Syntheses of polymers **poly(1)**, **poly(1_x-co-2_{600-x})** (x = 120, 300, 480), **poly(1_x-co-3_{600-x})** (x = 120, 300, 480), **poly(2₃₀₀-co-4₃₀₀)**, **poly(3₃₀₀-co-4₃₀₀)** and **poly(4)** was performed by Elisabeth Kreutzwiesner as follows:^{52,80}

Polymerisations were performed under inert atmosphere. For the syntheses of the homopolymers, **1** (2 g; 8.43 mmol; 600 eq., MW: 237.34 g·mol⁻¹) or **4** (4 g; 3.329 mmol; 602 eq., MW: 306.48 g·mol⁻¹) were dissolved in degassed, absolute CH₂Cl₂, respectively. For the copolymers **poly(1_x-co-2_{600-x})**, **1** (1.00/2.51/4.01 g; 4.21/10.57/16.90 mmol; x = 120/300/480 eq.) and **2** (5.17/3.23/1.31 g; 16.86/10.53/4.27 mmol; 600-x eq.) were dissolved in CH₂Cl₂. The copolymers **poly(1_x-co-3_{600-x})** were obtained by using **1** (1.00/2.50/4.00 g; 4.22/10.53/16.87 mmol; x = 120/300/480 eq.) and **3** (3.75/2.34/0.94 g; 16.87/10.55/4.21 mmol; 600-x eq.).

For all polymerisations, the initiator **G3** (25.75 mg, 0.035 mmol, 1 eq.) was dissolved in a small amount of CH₂Cl₂ and added to the solution. The reaction mixture was stirred at 250 rpm at room temperature for 24 h. Full conversion of monomers was assured by TLC and an excess of ethyl-vinyl-ether (1 mL) was added. The reaction mixture was stirred for further 30 min at room temperature. The solvent was partially removed *in vacuo* and the remaining solution was slowly added to stirred *n*-pentane. The obtained precipitate was re-dissolved in CH₂Cl₂ and re-precipitated from *n*-pentane. The precipitate was isolated, dried and re-dissolved in THF and precipitated in water. The final precipitate was dried *in vacuo* at 40°C.



⁸⁰ Kreutzwiesner, E. *Doctoral Thesis* 2010, Graz University of Technology.

poly(1): Yield: 87%. $^1\text{H-NMR}$ (δ , 20 °C, CDCl_3 , 500 MHz): 5.54-5.15 (m, 2H, $\text{CH}=\text{CH}$), 4.24-3.95 (m, 2H, COOCH_2), 3.23-2.36 (m, 5H, $\text{cp}^{1,2,4}$, CH_2N), 2.14-1.25 (m, 5H, NH, $\text{cp}^{3,5}$), 1.09 (bs, 6H, $\text{NC}(\text{CH}_3)_3$).

poly (1₁₂₀-*co*-2₄₈₀): Yield: 73%. $^1\text{H-NMR}$ (δ , 20 °C, CDCl_3 , 500 MHz): 5.52-5.10 (m, 2H, $\text{CH}=\text{CH}$), 4.25-3.83 (m, 2H, COOCH_2), 3.27-2.33, 2.16-0.96, 0.88 (t, 2.63H, CH_2CH_3). Determined ratio 1 : 2 = 116 \pm 10 : 484 \pm 10.

poly (1₃₀₀-*co*-2₃₀₀): Yield: 75%. $^1\text{H-NMR}$ (δ , 20 °C, CDCl_3 , 500 MHz): 5.52-5.10 (m, 2H, $\text{CH}=\text{CH}$), 4.25-3.86 (m, 2H, COOCH_2), 3.26-2.32, 2.16-0.96, 0.87 (t, 1.84H, CH_2CH_3). Determined ratio 1 : 2 = 240 \pm 10 : 360 \pm 10.

poly (1₄₈₀-*co*-2₁₂₀): Yield: 73%. $^1\text{H-NMR}$ (δ , 20 °C, CDCl_3 , 500 MHz): $^1\text{H-NMR}$ (δ , 20 °C, CDCl_3 , 300 MHz): 5.52-5.10 (m, 2H, $\text{CH}=\text{CH}$), 4.27-3.87 (m, 2H, COOCH_2), 3.25-2.31, 2.17-0.94, 0.87 (t, 0.87H, CH_2CH_3). Determined ratio 1 : 2 = 426 \pm 10 : 174 \pm 10.

poly (1₁₂₀-*co*-3₄₈₀): Yield: 68%. $^1\text{H-NMR}$ (δ , 20 °C, CDCl_3 , 500 MHz): 5.52-5.10 (m, 2H, $\text{CH}=\text{CH}$), 4.22-3.90 (m, 2H, COOCH_2), 3.27-2.33, 2.18-1.00, 0.88 (t, 2.46H, CH_2CH_3). Determined ratio 1 : 3 = 108 \pm 10 : 492 \pm 10.

poly (1₃₀₀-*co*-3₃₀₀): Yield: 77%. $^1\text{H-NMR}$ (δ , 20 °C, CDCl_3 , 500 MHz): 5.52-5.10 (m, 2H, $\text{CH}=\text{CH}$), 4.22-3.90 (m, 2H, COOCH_2), 3.27-2.33, 2.18-1.00, 0.88 (t, 1.63H, CH_2CH_3). Determined ratio 1 : 3 = 276 \pm 10 : 324 \pm 10.

poly (1₄₈₀-*co*-3₁₂₀): Yield: 79%. $^1\text{H-NMR}$ (δ , 20 °C, CDCl_3 , 500 MHz): 5.52-5.11 (m, 2H, $\text{CH}=\text{CH}$), 4.22-3.90 (m, 2H, COOCH_2), 3.27-2.32, 2.18-1.00, 0.88 (t, 0.78H, CH_2CH_3). Determined ratio 1 : 3 = 444 \pm 10 : 156 \pm 10.

poly (2₃₀₀-*co*-4₃₀₀): Yield: 75%. $^1\text{H-NMR}$ (δ , 20 °C, CDCl_3 , 500 MHz): 5.51-5.13 (m, 2H, $\text{CH}=\text{CH}$), 4.30-3.87 (m, 2H, COOCH_2), 3.25-2.22, 2.13-1.07, 0.87 (t, 1.33H, CH_2CH_3). Determined ratio 4 : 2 = 266 \pm 10 : 334 \pm 10.

poly (3₃₀₀-*co*-4₃₀₀): Yield: 76%. $^1\text{H-NMR}$ (δ , 20 °C, CDCl_3 , 500 MHz): 5.53-5.13 (m, 2H, $\text{CH}=\text{CH}$), 4.33-3.89 (m, 2H, COOCH_2), 3.24-2.24, 2.14-1.06, 0.88 (t, 1.45H, CH_2CH_3). Determined ratio 4 : 3 = 290 \pm 10 : 310 \pm 10.

Poly(4) was prepared according to the procedure for **poly(1)**. Purification of **poly(4)** was done differently: The solvent of the terminated polymerisation mixture was partially removed in vacuum and the remaining solution was slowly added to stirred *n*-pentane. The obtained precipitate was re-dissolved in CH_2Cl_2 and re-precipitated 4 times from *n*-pentane.

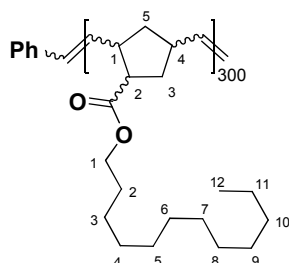
poly(4): Yield: 83% after the second precipitation. $^1\text{H-NMR}$ (δ , 20 °C, CDCl_3 , 500 MHz): 5.48-5.10 (m, 2H, $\text{CH}=\text{CH}$), 4.26-3.95 (m, 2H, COOCH_2), 3.22-2.19 (m, 11H, $\text{cp}^{1,2,4}$, CH_2N , $\text{N}(\text{CH}_3)_2$), 2.12-1.25 (m, 4H, $\text{cp}^{3,5}$).

5.3.1.5 General Polymerisation Procedures for Test-polymerisations of 2

All test-polymerisations of **2** (*cf.* Chapter 3.1.2.3) were performed in degassed CH_2Cl_2 under inert atmosphere using standard Schlenk technique. 200 mg of **2** (0.65 mmol, 300 eq., MW: 306,48 $\text{g}\cdot\text{mol}^{-1}$) were dissolved in degassed, absolute CH_2Cl_2 . In a separate flask 1.58 mg of the initiator **G3** (0.002 mmol, 1 eq., MW: 727.75 $\text{g}\cdot\text{mol}^{-1}$) was dissolved in a small amount of CH_2Cl_2 and added to the solution. The reaction mixture was stirred at 0, 20 and 40°C. Total monomer consumption was observed at 120 min, 60 min and 35 min, respectively which was assured by TLC. Half of the reaction mixture was removed and the polymerisation was stopped by the addition of an

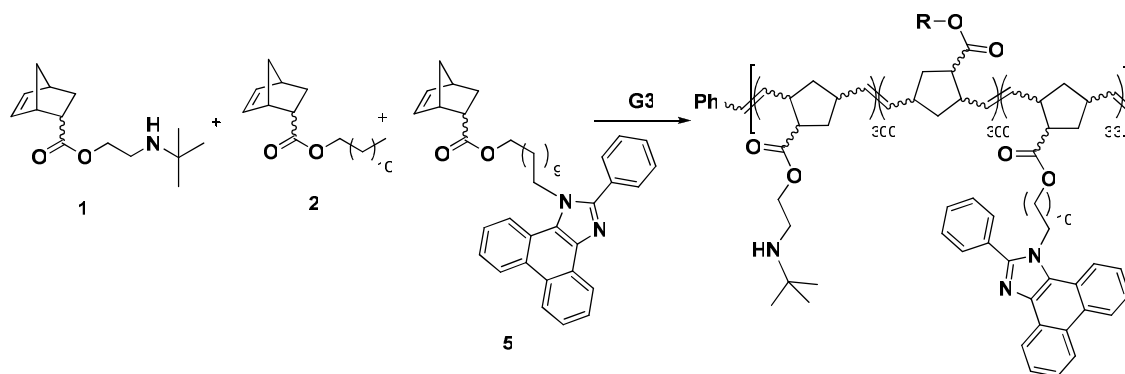
excess of ethyl-vinyl-ether (1 mL). After further stirring for 30 min the solvent was partially removed in vacuum and the remaining solution was slowly added to stirred ethanol. The obtained precipitate was re-dissolved in CH_2Cl_2 and re-precipitated from ethanol. The remaining non-quenched polymerisation reactions were further stirred, each for 180 minutes in all. Subsequently, the polymerisations were stopped and treated equally as described above.

Furthermore, a series of homopolymers using **G3** as the initiator and different equiv. of **2** were synthesised. For the polymers **poly(2)₁₀₀**, **poly(2)₃₀₀**, **poly(2)₅₀₀**, **poly(2)₇₀₀** and **poly(2)₉₀₀** 200 mg of **2** (0.65 mmol, 100/300/500/700/900 eq., MW: 306.48) were dissolved in degassed, absolute CH_2Cl_2 . The initiator **G3** (4.75/1.58/0.94/0.68/0.53 mg, 0.0065/0.0022/0.0013/0.0009/0.0007 mmol, 1 eq., MW: 727.75 $\text{g}\cdot\text{mol}^{-1}$) was separately dissolved in a small amount of CH_2Cl_2 and added to the solution. The reaction mixture was stirred at room temperature until TLC revealed complete conversion. Polymerisation was quenched by the addition of an excess of ethyl-vinyl-ether (0.5 mL). After further stirring for 30 min the solvent was partially removed *in vacuo* and the remaining solution was slowly added to stirred ethanol. The obtained precipitate was re-dissolved in CH_2Cl_2 and re-precipitated from ethanol. Yields: 23.0% for **poly(2)₁₀₀**, 85.6% for **poly(2)₃₀₀**, 70.3% for **poly(2)₅₀₀**, 69.3% for **poly(2)₇₀₀** and 64.3% for **poly(2)₉₀₀**.



$^1\text{H-NMR}$ (δ , 20 °C, CDCl_3 , 500 MHz): 5.52-5.08 (m, 2H, $\text{CH}=\text{CH}$), 3.95 (bs, 2H, COOCH_2), 3.26-2.33 (m, 3H, $\text{cp}^{1,2,4}$), 2.15-1.04 (m, 24H, $\text{cp}^{3,5}$, dodecyl²⁻¹¹), 0.87 (t, 3H, CH_2CH_3).

5.3.1.6 Synthesis of **poly(1₃₀₀-co-2₃₀₀-co-5₃₃)**



poly(1₃₀₀-co-2₃₀₀-co-5₃₃) R = C_2H_5

2.5 g of **1** (10.5 mmol, 300 eq., MW: 237.34 g·mol⁻¹), 3.23 g of **2** (10.5 mmol, 300 eq., MW: 306.48 g·mol⁻¹) and 0.68 g of **5** (1.164 mmol, 33 eq., MW: 584.8 g·mol⁻¹) were dissolved in degassed CH₂Cl₂ under inert atmosphere. In a separate vial 25.53 mg of the initiator **G3** (0.035 mmol, 1 eq., MW: 727.75 g·mol⁻¹) was dissolved in a small amount of CH₂Cl₂ and added to the solution. After 2 h monomer consumption was complete which was proven by TLC. The polymerisation was quenched by the addition of an excess of ethyl-vinyl-ether. After further stirring for 30 min the solvent was partially removed under reduced pressure and the polymer solution was repeatedly precipitated from stirred ethanol. Yield: 4.91 g, 76.6%

5.3.1.7 General Polymerisation Procedure for the Syntheses of Block-*c*o polymers

All syntheses of block-*c*o polymers were performed under inert atmosphere using standard Schlenk technique.

For the syntheses of **poly(1₁₅₀-block-2₁₅₀)**, **poly(1₃₀₀-block-2₃₀₀)** and **poly(1₅₀₀-block-2₅₀₀)** 500 mg of **1** (2.11 mmol; 150/300/500 eq.; MW: 237.34 g·mol⁻¹) were dissolved in CH₂Cl₂. The polymerisation was initiated by the addition of **G3** (10.22/5.11/3.07 mg; 0.014/0.007/0.004 mmol; 1 eq.; MW: 727.75 g·mol⁻¹). After complete consumption of **1**, which was monitored by TLC, 646 mg of **2** (2.11 mmol; 150/300/500 eq.; MW: 306.48 g·mol⁻¹) were added. After consumption of the second monomer the polymerisation was quenched by the addition of an excess of ethyl-vinyl-ether. After further stirring for 30 min the solvent was partially removed under reduced pressure and the polymer solution was precipitated from stirred ethanol. Yield: 4.91 g, 76.6%

poly(1₁₅₀-block-2₁₅₀): Yield: 72.8%. ¹H-NMR (δ, 20 °C, CDCl₃, 500 MHz): 5.51-5.11 (m, 2H, CH=CH), 4.27-3.85 (m, 2H, COOCH₂), 3.22-2.31 (m, 4H, cp^{1,2,4}, CH₂N), 2.19-1.49 (m, 5H, cp^{3,5}, dodecyl²), 1.48-1.01 (m, 11H, NH, N(CH₃)₂, dodecyl³⁻¹¹), 0.88 (t, 1.5 H, CH₂CH₃).

poly(1₃₀₀-block-2₃₀₀) : Yield: 80.1%. ¹H-NMR (δ, 20 °C, CDCl₃, 500 MHz): 5.52-5.13 (m, 2H, CH=CH), 4.22-3.84 (m, 2H, COOCH₂), 3.25-2.36 (m, 4 H, cp^{1,2,4}, CH₂N), 2.15-1.50 (m, 5H, cp^{3,5}, dodecyl²), 1.48-1.09 (m, 11H, NH, N(CH₃)₂, dodecyl³⁻¹¹), 0.87 (t, 1.5 H, CH₂CH₃).

poly(1₅₀₀-block-2₅₀₀) : Yield: 76.1%. ¹H-NMR (δ, 20 °C, CDCl₃, 500 MHz): 5.53-5.11 (m, 2H, CH=CH), 4.27-3.85 (m, 2H, COOCH₂), 3.30-2.36 (m, 4 H, cp^{1,2,4}, CH₂N), 2.21-1.51 (m, 5H, cp^{3,5}, dodecyl²), 1.51-1.12 (m, 11H, NH, N(CH₃)₂, dodecyl³⁻¹¹), 0.88 (t, 1.5 H, CH₂CH₃).

For the synthesis of **poly(2₃₀₀-block-1₃₀₀)** 645.66 mg of **2** (2.107 mmol, 300 eq., MW: 306.48 g·mol⁻¹) were dissolved in degassed CH₂Cl₂ and 5.11 mg of **G3** (0.007 mmol, 1 eq., MW: 727.75 g·mol⁻¹) were added quickly. After complete consumption of **2**, which was continuously monitored indicated by TLC, 500 mg of **1** (2.107 mmol, 300 eq., MW: 237.34 g·mol⁻¹) were added. After TLC revealed full consumption of monomer **1**, an excess of ethyl-vinyl-ether was added. After 30 min. of further stirring, solvent was partially removed *in vacuo* and the polymer solution was precipitated from stirred ethanol and centrifuged. Yield: 0.56 g, 48.6%

$^1\text{H-NMR}$ (δ , 20 °C, CDCl_3 , 500 MHz): 5.53-5.13 (m, 2H, $\text{CH}=\text{CH}$), 4.25-3.87 (m, 2H, COOCH_2), 3.27-2.35 (m, 4 H, $\text{cp}^{1,2,4}$, CH_2N), 2.19-1.51 (m, 5H, $\text{cp}^{3,5}$, dodecyl²), 1.51-1.01 (m, 11.1 H, NH , $\text{N}(\text{CH}_2)_2$, dodecyl³⁻¹¹), 0.88 (t, 1.49 H, CH_2CH_3). Determined ratio $1 : 2 = 298 \pm 10 : 302 \pm 10$

Three polymers were synthesised comprising a short hydrophobic block of **2** and a second, random block of **1** and **2**: **poly(2₁₀₀-block-(1₂₅₀-co-2₂₅₀))**, **poly(2₁₀₀-block-(1₃₅₀-co-2₁₅₀))**, and **poly(2₁₀₀-block-(1₁₅₀-co-2₃₅₀))**.

Therefore, 1 g (3mmol, 100 eq.; MW: 306.48 $\text{g}\cdot\text{mol}^{-1}$) of **2** were dissolved in dry and degassed CH_2Cl_2 (approx. 25mL). 23.9 mg **G3** (0.03 mmol, 1eq.; MW: 727.75 $\text{g}\cdot\text{mol}^{-1}$) was previously dissolved in CH_2Cl_2 (0,5mL) and added to the reaction mixture. The reaction mixtures were stirred at room temperature under constant TLC monitoring (CH:EE = 20:1 and 100% MeOH; detection: UV/VIS, 2% KMnO_4 solution.). After 20 min. TLC revealed complete consumption of **2**. Subsequently, a mixture **2** (2.516/1.511/3.521 g, 8.2/4.93/11.49 mmol; 250/150/350 eq.; MW: 306.48 $\text{g}\cdot\text{mol}^{-1}$) and **1** (1.948/2.727/1.170 g, 8.2/11.49/4.93 mmol; 250/350/150 eq.; MW: 237.34 $\text{g}\cdot\text{mol}^{-1}$) were added and stirred at room temperature for further 35 minutes. The polymerisations were quenched by the addition of an excess of ethyl-vinyl-ether. After 15 min. the solvent was partially removed under reduced pressure and the polymer was precipitated from stirred ethanol dried *in vacuo*.

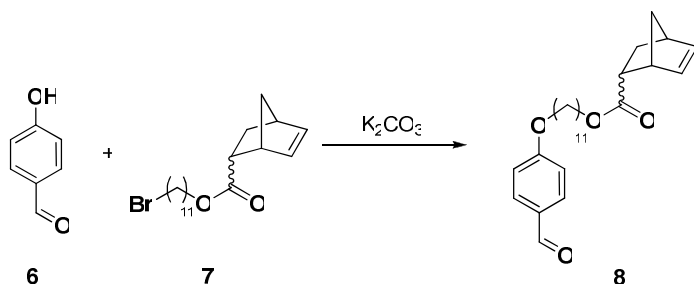
poly(2₁₀₀-block-(1₂₅₀-co-2₂₅₀)): Yield: 71.4%. $^1\text{H-NMR}$ (δ , 20 °C, CDCl_3 , 300 MHz): 5.57-5.09 (m, 2H, $\text{CH}=\text{CH}$), 4.31-3.87 (m, 2H, COOCH_2), 3.31-2.25 (m, 4.3 H, $\text{cp}^{1,2,4}$, CH_2N), 2.24-0.99 (m, 21H, $\text{cp}^{3,5}$, NH , $\text{N}(\text{CH}_2)_3$, dodecyl²⁻¹¹), 0.87 (t, 1.73 H, CH_2CH_3). Determined ratio $1 : 2 = 254 \pm 10 : 346 \pm 10$.

poly(2₁₀₀-block-(1₃₅₀-co-2₁₅₀)): Yield: 59.8%. $^1\text{H-NMR}$ (δ , 20 °C, CDCl_3 , 300 MHz): 5.50-5.05 (m, 2H, $\text{CH}=\text{CH}$), 4.23-3.80 (m, 2H, COOCH_2), 3.21-2.26 (m, 4.4 H, $\text{cp}^{1,2,4}$, CH_2N), 2.14-0.93 (m, 18.6H, $\text{cp}^{3,5}$, NH , $\text{N}(\text{CH}_2)_3$, dodecyl²⁻¹¹), 0.81 (t, 1.20 H, CH_2CH_3). Determined ratio $1 : 2 = 360 \pm 10 : 240 \pm 10$.

poly(2₁₀₀-block-(1₁₅₀-co-2₃₅₀)): Yield: 78.4%. $^1\text{H-NMR}$ (δ , 20 °C, CDCl_3 , 300 MHz): 5.51-5.04 (m, 2H, $\text{CH}=\text{CH}$), 4.21-3.74 (m, 2H, COOCH_2), 3.23-2.25 (m, 3.70H, $\text{cp}^{1,2,4}$, CH_2N), 2.11-0.93 (m, 21H, $\text{cp}^{3,5}$, NH , $\text{N}(\text{CH}_2)_3$, dodecyl²⁻¹¹), 0.81 (t, 2.09H, CH_2CH_3). Determined ratio $1 : 2 = 182 \pm 10 : 418 \pm 10$.

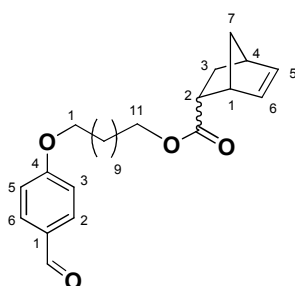
5.3.2 Ruthenium Complexes

5.3.2.1 11-(4-Formylphenoxy)undecyl-bicyclo[2.2.1]hept-5-en-2-carboxylate (8)



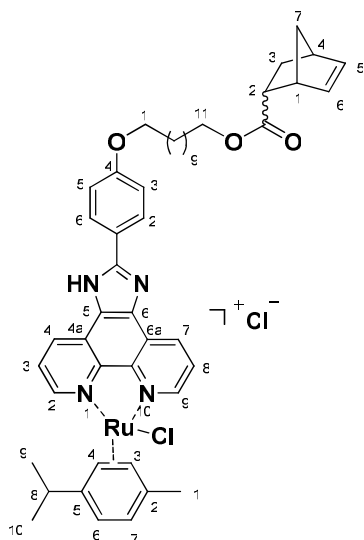
1.288 g 4-hydroxybenzaldehyde (10.55 mmol, 1 eq., MW: 122.12 g·mol⁻¹) were dissolved in 60 mL butanone and 2,186 g potassium carbonate (15.81 mmol, 1.5 eq., MW: 138.2 g·mol⁻¹) and after 30 min of further stirring at 90 °C, 4.311 g (11,60 mmol, 1.1 eq., MW: 371.35 g·mol⁻¹) bicyclo[2.2.1]hept-5-ene-2-carboxylic acid, 11-bromo-undecyl ester (**7**) was added. TLC (mobile phase Cy:EE = 3:1) revealed completeness of the reaction after 10 hours.

The solvent was removed under reduced pressure, the dried residue dissolved in dichloromethane and extracted three times with 10% hydrochloric acid and three times with deionised water. The organic phase was dried over anhydrous sodium sulphate, and evaporated under reduced pressure. The crude product was purified by column chromatography (stationary phase: silica gel, mobile phase: Cy:EE = 10:1). Yield: 3.35 g, 88.1%; 88% *endo*- and 12% *exo*-derivative.



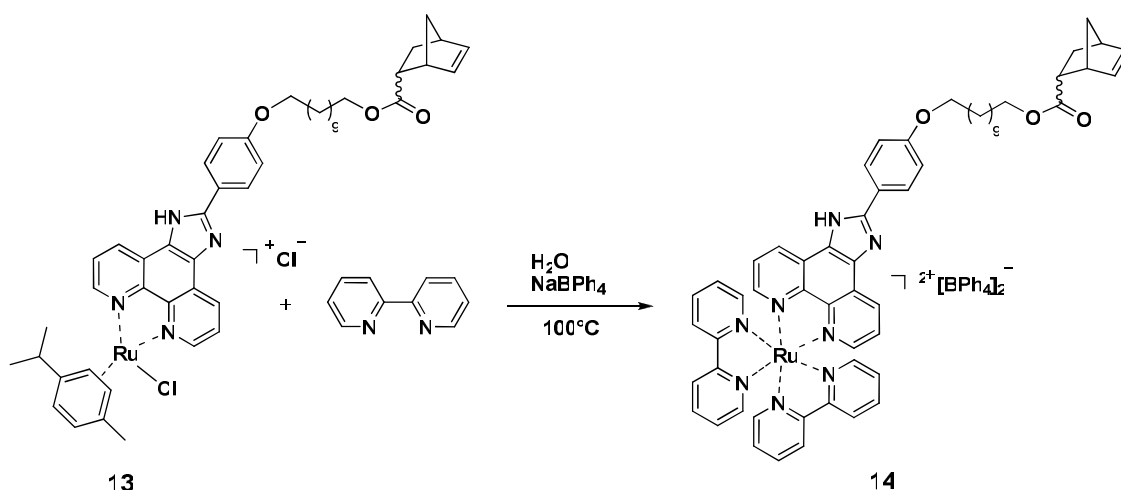
¹H-NMR (δ, 20°C, CDCl₃, 500 MHz): 9.88 (s, 1H, C=O) 7.83 (d, ³J_{HH} = 8.77 Hz, 2H, ph^{2,6}); 6.99 (d, ³J_{HH} = 8.72 Hz, 2H, ph^{3,5}); 6.19 und 5.92 (m, m, 1H, 1H, nb⁵, nb⁶); 4.02 (m, 4H, CH₂^{1,11}); 3.20 und 3.03 (bs, bs, 1H, 1H, nb¹, nb⁴); 2.90 (m, 1H, nb²); 1.89 (m, 1H, nb⁷); 1.81 (m, 2H, CH₂¹⁰); 1.57 – 1.29 (m, 18H, nb³, CH₂^{2,3,4,5,6,7,8,9}). **7** is a mixture of 88% *endo*- and 12% *exo*-derivative (characteristic signals for *exo*-**7**: 6.13, 6.11 (m, 2H, nb^{5,6}))

¹³C-NMR (δ, 20°C, CDCl₃, 125 MHz): 190.8 (1C, CH=O); 174.9 (1C, C=O); 164.2 (1C, ph⁴); 137.7 (2C, nb^{5,6}); 132.3; 132.0; 129.7 (3C, ph^{1,2,6}); 114.7 (2C, ph^{3,5}); 68.4 (1C, CH₂¹); 64.3 (1C, CH₂¹⁰); 49.6; 45.7; 43.4; 42.5 (4C, nb^{1,2,4,7}); 29.49; 29.46; 29.32; 29.20; 29.16; 29.04; 28.66; 26.90; 25.95; 25.93 (10C, CH₂^{2,3,4,5,6,7,8,9,10}, nb³).



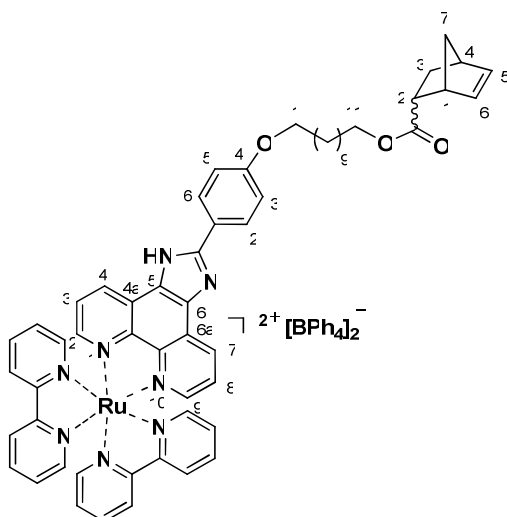
$^1\text{H-NMR}$ (δ , 20°C , DMSO-d_6 , 500 MHz): 10.15 (d, $^3J_{\text{HH}} = 5.04$ Hz, 2H, iphen^{2,9}); 9.65 (m, 2H, iphen^{4,7}); 8.63 (d, $^3J_{\text{HH}} = 8.72$ Hz, 2H, ph^{2,6}); 8.50 (bs, 2H, iphen^{3,8}); 7.48 (d, $^3J_{\text{HH}} = 8.75$ Hz, 2H, ph^{3,5}); 6.64 (d, $^3J_{\text{HH}} = 6.31$ Hz, 2H, cym^{4,6}); 6.45 (m, 1H, nb⁵); 6.41 (d, $^3J_{\text{HH}} = 6.25$ Hz, 2H, cym^{3,7}); 6.15 (m, 1H, nb⁶); 4.38 (t, $^3J_{\text{HH}} = 6.35$ Hz, 2H, CH_2^1); 4.23 (m, 2H, CH_2^{11}); 3.40 (bs, 1H, nb¹); 3.28 (m, 1H, cym⁸); 3.14 (bs, 1H, nb²); 2.91 (m, 1H, nb⁴); 2.80 – 1.19 (m, 31H, cym^{1,9,10}, $\text{CH}_2^{2,3,4,5,6,7,8,9,10}$, nb^{3,7}).

5.3.2.5 Synthesis of Monomer 14



0.1000 g chloro(*p*-cymene)ruthenium(II)complex **13** (0.1099 mmol, 1 eq., MW: 909.86 $\text{g}\cdot\text{mol}^{-1}$) and 0.0343 g 2,2'-bipyridine (0.2198 mmol, 2 eq., MW: 156.19 $\text{g}\cdot\text{mol}^{-1}$) were suspended in 10 mL of deionised water and heated to reflux. After 20 hours the reaction was completed according to TLC (mobile phase: methanol).

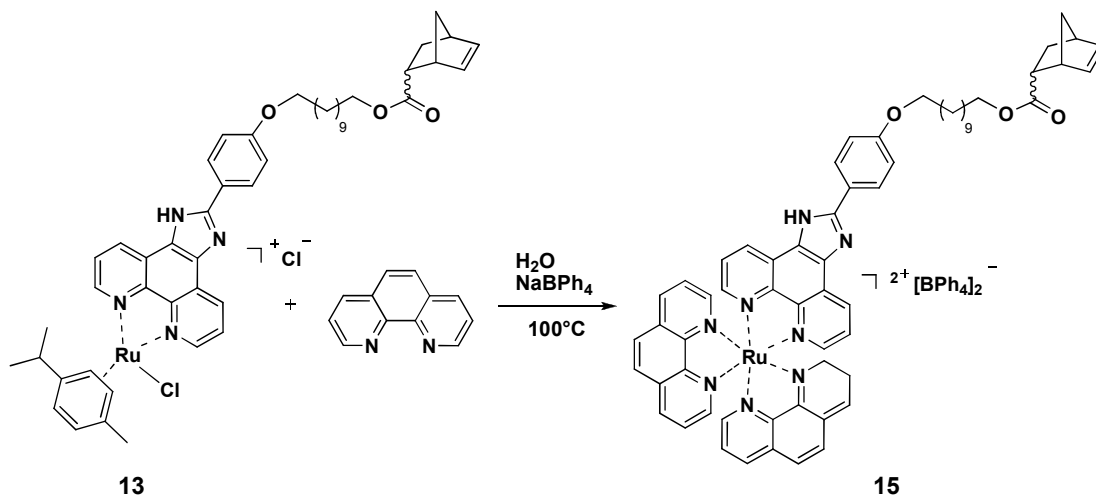
By the addition of 0.0752 g sodium tetraphenylborate (0.2198 mmol, 2 eq., MW: 342.23 $\text{g}\cdot\text{mol}^{-1}$) the product was precipitated, filtered, washed with water and recrystallised from acetone to give the product as fine red powder. Yield: 138.8 mg, 75.3%



$^1\text{H-NMR}$ (δ , 20°C , acetone d_6 , 500 MHz): 9.08 (d, $^3J_{\text{HH}} = 8.19$ Hz, 2H, iphen^{2,9}); 8.63 (m, 4H, bpy^L); 8.29 (d, $^3J_{\text{HH}} = 8.61$ Hz, 2H, bpy^L); 8.17 (d, $^3J_{\text{HH}} = 4.87$ Hz, 2H, bpy^L); 8.08 (m, 4H, bpy^L); 7.99 (t, $^3J_{\text{HH}} = 7.45$ Hz, 2H, iphen^{4,7}); 7.84 (d, $^3J_{\text{HH}} = 5.51$ Hz, 2H, ph^{2,6}); 7.71 (m, 2H, iphen^{3,8}); 7.45 (t, $^3J_{\text{HH}} = 6.36$ Hz, 2H, ph^{3,5}); 7.31 (bs, 13H, BPh₄); 7.25 (t, $^3J_{\text{HH}} = 6.48$ Hz, 2H, bpy^L); 7.11 (d, $^3J_{\text{HH}} = 8.70$ Hz, 2H, bpy^L); 6.86 (t, $^3J_{\text{HH}} = 7.37$ Hz, 13H, BPh₄); 6.72 (t, $^3J_{\text{HH}} = 7.16$ Hz, 7H, BPh₄); 6.13, 5.89 (m, 2H, nb^{5,6}); 4.10 bis 3.93 (m, 4H, CH₂^{1,11}); 3.40 (m, 1H, nb¹); 2.97 (m, 1H, nb²); 2.85 (bs; 1H, nb⁴); 1.90 – 1.11 (m, 22H, CH₂^{2,3,4,5,6,7,8,9,10}, nb^{3,7}).

$^{13}\text{C-NMR}$ (δ , 20°C , acetone d_6 , 125 MHz): 175.5 (1C, C=O); 166.5, 166.1, 165.7, 165.3 (BPh₄); 162.9 (1C, ph⁴); 159.2 (4C, bpy^L); 159.0, 156.2 (BPh₄); 153.7 (6C, iphen^{2,9}, bpy^L); 153.5 (BPh₄); 151.5 (1C, N-C=N); 147.2 (1C, N=C iphen^{10a}); 139.9 (BPh₄); 139.7 (4C, bpy^L); 139.2 (2C, nb^{5,6}); 137.8 (2C, iphen^{4,7}); 134.2 (BPh₄); 132.4 (1C, N=C iphen^{10b}); 130.2 (2C, ph^{2,6}); 129.6 (1C, iphen^{4a}); 129.5 (1C, iphen^{6a}); 12.7 (1C, iphen⁶); 127.0 (4C, bpy^L); 126.2 (2C, iphen^{3,8}); 126.1 (1C, iphen⁵); 124.5 (BPh₄); 123.2 (4C, bpy^L); 116.8 (3C, ph^{1,3,5}); 69.9 (1C, CH₂¹); 65.5 (1C, CH₂¹¹); 51.1 (1C, nb⁷); 47.4 (1C, nb¹); 44.8 (1C, nb²); 44.2 (nb⁴); 30.8 bis 27.7 (10C, CH₂^{2,3,4,5,6,7,8,9,10}, nb³).

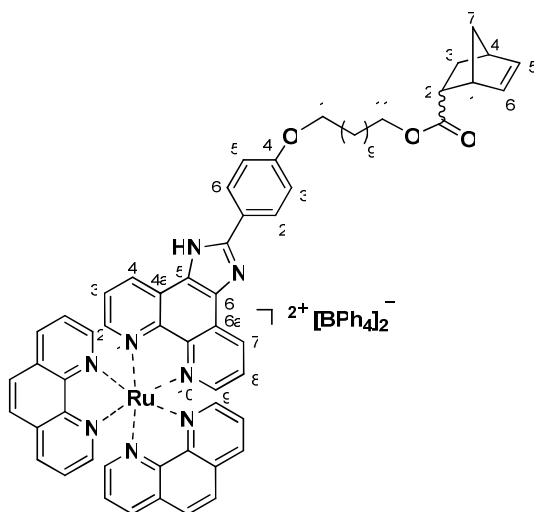
5.3.2.6 Synthesis Monomer 15



0.1000 g chloro(*p*-cymene)ruthenium(II)complex **13** (0.1099 mmol, 1 eq., MW: 909.86 g·mol⁻¹) and 0,0396 g 1,10-phenanthroline (0.2198 mmol, 2 eq., MW: 180.21 g·mol⁻¹) were suspended in 10 mL of deionised water and heated to reflux. After 20 hours TLC (mobile phase: methanol) revealed completeness of the reaction.

By the addition of 0.0752 g sodium tetraphenylborate (0.2198 mmol, 2 eq., MW: 342.23 g·mol⁻¹) the product was precipitated, filtered, washed with

water and recrystallised from acetone and washed with ethanol. Yield: 143.1 mg, 76.5%.



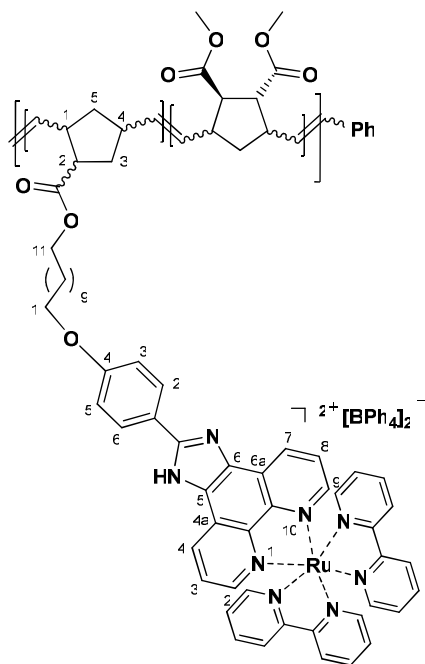
$^1\text{H-NMR}$ (δ , 20°C , acetone d_6 , 500 MHz): 9.05 (d, $^3J_{\text{HH}} = 8.06$ Hz, 2H, iphen^{2,9}); 8.67 (t, $^3J_{\text{HH}} = 6.59$ Hz, 4H, phen^L); 8.36 – 8.26 (m, 10H, phen^L); 8.12 (d, $^3J_{\text{HH}} = 5.05$ Hz, 2H, iphen^{4,7}); 7.70 (m, 2H, phen^L); 7.64 (m, 2H, ph^{2,6}); 7.58 (m, 2H, iphen^{3,8}); 7.29 (bs, 12H, BPh⁴); 7.03 (d, $^3J_{\text{HH}} = 7.53$ Hz, 2H, ph^{3,5}); 6.85 (t, $^3J_{\text{HH}} = 7.37$ Hz, 12H, BPh₄); 6.71 (t, $^3J_{\text{HH}} = 7.16$ Hz, 6H, BPh₄); 6.13, 5.88 (m, 2H, nb^{5,6}); 4.08 – 3.93 (m, 4H, CH₂^{1,11}); 3.40 (m, 2H, nb^{1,2}); 3.15 (bs, 1H, nb⁴); 1.87 – 1.11 (m, 22H, CH₂^{2,3,4,5,6,7,8,9,10}, nb^{3,7}).

$^{13}\text{C-NMR}$ (δ , 20°C , acetone d_6 , 125 MHz): 175.5 (1C, C=O); 166.5, 166.1, 165.7, 165.3 (BPh₄); 162.6 (1C, ph⁴); 154.9 (BPh₄); 154.8 (6C, iphen^{2,9}, phen^L); 151.6 (1C, N=C=N); 149.9, 149.8 (BPh₄); 147.4 (1C, N=C iphen^{10a}); 139.2 (BPh₄); 138.7 (2C, nb^{5,6}); 138.0 (8C, phen^L); 134.2 (BPh₄); 132.9 (2C, iphen^{4,7}); 132.3 (1C, N=C iphen^{10b}); 130.1 (2C, iphen^{4a,6a}); 128.1 (2C, ph^{2,6}); 127.4 (1C, iphen⁵); 127.0 (4C, phen^L); 123.2 (8C, iphen^{3,8}, phen^L); 116.6 (3C, ph^{1,3,5}); 67.1 (1C, CH₂¹); 65.5 (1C, CH₂¹¹); 51.0 (1C, nb⁷); 47.3 (1C, nb¹); 44.8 (1C, nb²); 44.2 (1C, nb⁴); 31.4 - 27.7 (7C, CH₂^{2,3,4,5,6,7,8,9,10}, nb³).

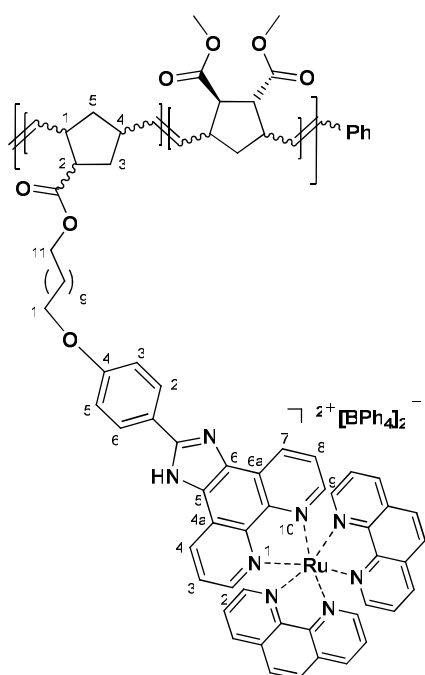
5.3.2.7 Polymerisation Procedure for poly(14-*cø*-16) and poly(15-*cø*-16)

Both polymerisations were performed under inert atmosphere of argon. 40 mg of the TMCs **14** or **15** (0.0242 mmol of **14** or 0.0235 mmol of **15**, 3 equiv., MW₁₄: 1653.65 g·mol⁻¹, MW₁₅: 1702.70 g·mol⁻¹) and 508.5 mg respectively 493.9 mg of dimethyl bicyclo[2.2.1]heptane-2,3-dicarboxylate **16** (2.419 mmol for poly(14-*cø*-16) and 2.349 mmol for poly(15-*cø*-16), 300 equiv., MW: 210.23 g·mol⁻¹) were dissolved in 7 mL of absolute and degassed dichloromethane. The polymerisations were initiated with 5.9 mg of 3rd generation Grubbs-type initiator RuCl₂(pyridine)₂(H₂IMes)(CHPh) **G3** (0.0081 mmol, 1 equiv., MW: 726.0 g·mol⁻¹).

After one hour TLC (CH₂Cl₂ : MeOH = 5 : 1) revealed total conversion and the polymer spot exhibited red emission. The polymerisation was quenched by the addition of 100 μL of ethyl-vinyl-ether. The solution was partly evaporated, purified by repeated precipitation of dichloromethane solutions from methanol and dried *in vacuo*. Yield: 376.8 mg, 68.7% for poly(14-*cø*-16) and 268,6 mg, 50.31% for poly(15-*cø*-16).



$^1\text{H-NMR}$ (δ , 20°C , CDCl_3 , 500 MHz): 5.58-5.10 (m, 2H, CH=CH); 3.82-3.56 (m, 6H, COO-CH₃); 3.40-2.86 (m, 4H, cp^{1,2,3,4}); 2.12-1.82 (bs, 1H, cp⁵); 1.54-1.36 (bs, 1H, cp⁵). Only the characteristic peaks of the poly(nornornene-dimethylester) repeating unit were observed in the NMR spectra.



$^1\text{H-NMR}$ (δ , 20°C , CDCl_3 , 500 MHz): 5.56-5.12 (m, 2H, CH=CH); 3.80-3.58 (m, 6H, COO-CH₃); 3.40-2.90 (m, 4H, cp^{1,2,3,4}); 2.12-1.84 (bs, 1H, cp⁵); 1.60-1.38 (bs, 1H, cp⁵). Only the characteristic peaks of the poly(nornornene-dimethylester) repeating unit were observed in the NMR spectra.

6 Appendix

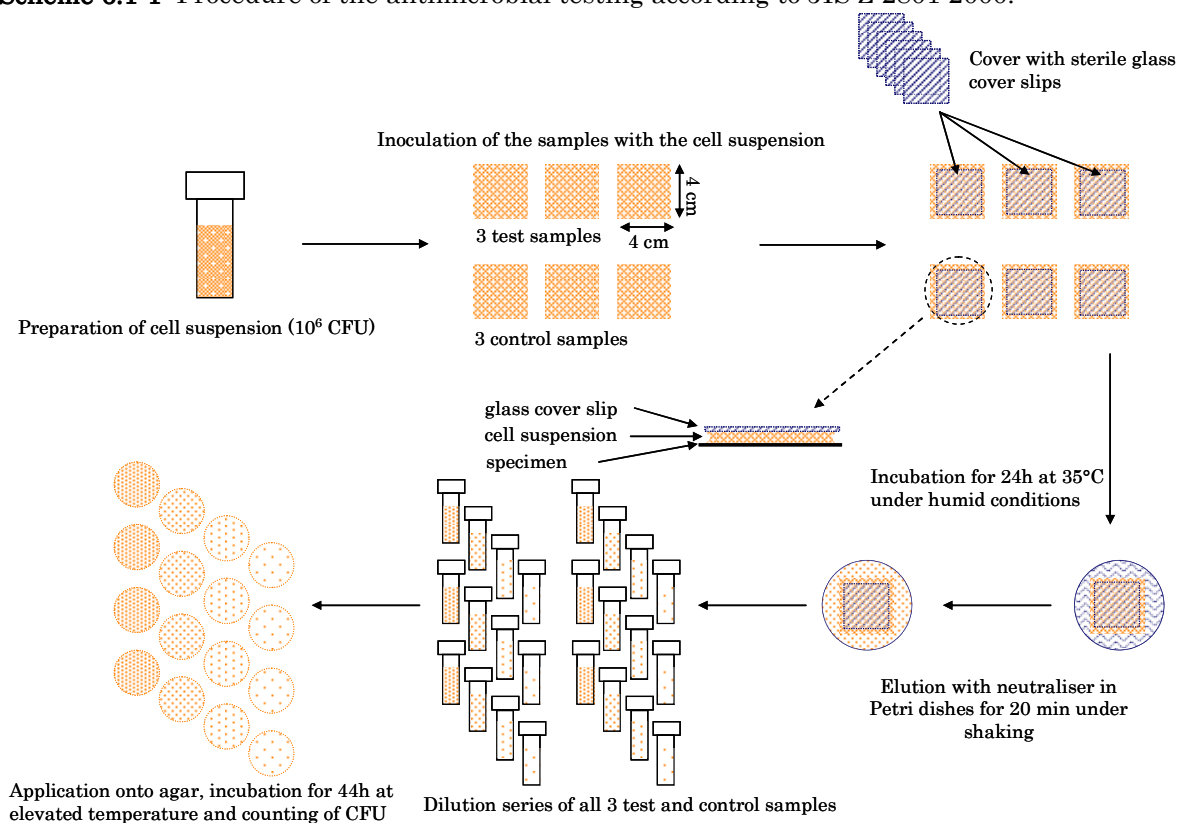
6.1 Supporting Information

6.1.1 Japanese Industry Standard JIS Z 2801:2000⁵³

The antimicrobial activity was tested against *P. aeruginosa* (ATCC 9027), *S. aureus* (ATCC 6538) and fungi (*C. albicans* (ATCC 10231), and *A. niger* (ATCC 16404) according to the Japanese industry standard JIS Z 2801:2000 method as described below and shown in Scheme 6.1-1:

The test sample and the control sample were prepared by spin-coating of CHCl_3 solutions containing 1 w-% of the synthesised polymers onto 4x4 cm glass plates. The ROM polymer of *endo,exo*-dimethyl bicyclo[2.2.1]hept-5-en-2-2-carboxylate was used as the control sample.

Each sample was inoculated with a suspension of the test organisms (ca. 10^6 cells mL^{-1}). The inoculum is held in contact with the test sample by covering it with a sterile cover slip. The use of glass covers instead of polyethylene films describes a minor deviation from the JIS Z 2801:2000 but still meets its requirement. The glass covers do not affect the bacteria suspension and assure a homogenous, planar bacteria film without entrapped air between the sample and the glass cover. All test samples are inoculated in triplicate, with additional three replicates of the control samples.

Scheme 6.1-1: Procedure of the antimicrobial testing according to JIS Z 2801:2000.

The bacterial population was determined at three different times, 0, 24 and 48 hours for the test and the control samples. The value at 0 hours was measured constantly after 15 min. Due to operational expenditure of time a constant immediate measurement following inoculation could not be reliably realised. The measured value of the control sample after 15 min assumed to be the initial population on the test samples.

The remaining samples are incubated for the test period (24 hours) at 35°C. Thereby, the required humid conditions were guaranteed by carrying out the incubation in Petri dishes over water.

After incubation each sample together with the glass cover were transferred into with neutraliser and glass beads filled Petri dishes and eluted for 20 min under continuous shaking. A dilution series (1 mL, 0.1 mL, 0.1 mL of a 10^{-1} dilution and 0.1 mL of a 10^{-2} dilution) were applied onto casein peptone-soybean flour agar (CSA) at $36 \pm 1^\circ\text{C}$ for 44 ± 4 hours in case of the tested bacteria, *C.albicans* at $30 \pm 1^\circ\text{C}$ for 44 ± 4 hours and *A. niger* $30 \pm 1^\circ\text{C}$ for 92 ± 4 hours, respectively.

Finally, a comparison of the bacterial population at the beginning and end of the test period was made.

In order to classify the antimicrobial activity of a material, it is important to differ between microbiocides and microbiostats. Microbiocides kill microorganisms while microbiostats inhibit the growth of microorganisms. According to the specification of the JIS a material is referred to as microbiocide, if a reduction of the tested microbes of at least two logarithmic levels is achieved.

6.1.2 Contact Angle Measurements

Contact angle measurements were performed on a Drop Shape Analysis System DSA 100 (Krüss GmbH, Hamburg, Germany) using the sessile drop technique. A droplet of liquid with a known surface energy is placed on the solid surface using a syringe. The shape of the drop, arising from the contact angle which is defined as the angle between the liquid/solid interface and the liquid/air interface, and the known surface energy of the liquid are the parameters which were used to calculate the surface energy of the solid sample.

The interfacial tension at the interface of the probe liquid and the solid surface is the result of different types of intermolecular forces. Thus, surface energies are divided in surface energy due to dispersive and polar interactions. The Owens-Wendt model (*cf.* Equation 6.1-1), which was used for the calculation of the interfacial tension, considers both types of interactions.

$$\gamma_{sl} = \sigma_s + \sigma_l - 2 \cdot (\sqrt{\sigma_s^d \cdot \sigma_l^d} + \sqrt{\sigma_s^p \cdot \sigma_l^p})$$

γ_{sl}	interfacial tension	6.1-1
σ^d	dispersive interaction	
σ^p	polar interaction	

The combination of Equation 6.1-1 with the Young's relation (*cf.* Equation 2.3-1) allows the determination of the surface energy of solids from contact angle data.

$$\sigma_s = \gamma_{sl} + \sigma_l \cdot \cos \theta$$

γ_{sl}	interfacial tension	6.1-2
σ_s	surface tension solid	
σ_l	surface tension liquid	
θ	contact angle	

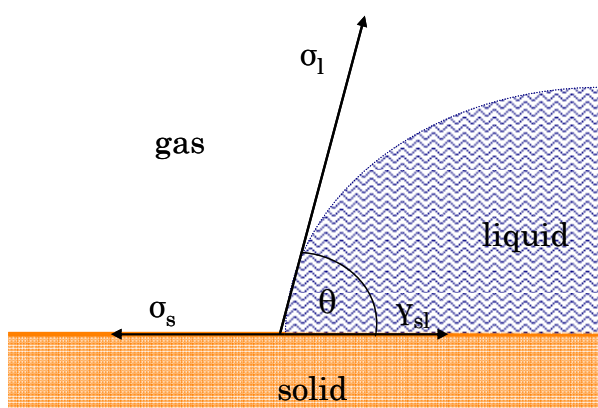


Figure 6.1-1: Contact angle formation on a solid surface according to Young.

4 x 4 cm test samples of the compound material containing 5 wt.% of **poly(2₁₀₀-block-(2₂₅₀-co-1₂₅₀))** were used for the contact angle measurements. The test samples were made according to the procedure described in Chapter 3.2.2. The volume of the probe liquid was set 3 μL. After setting the

droplets, the drops were recorded immediately with a camera to facilitate the analysis of the contact angles and the surface tension, respectively and to avoid deviations of the contact angles due to evaporation of the probe liquid. The probe liquids used for this experiment were water and diiodomethane.⁶² Depending on the polarity of both the probe liquid and the solid surface, different contact angles were obtained as shown in Figure 6.1-2.

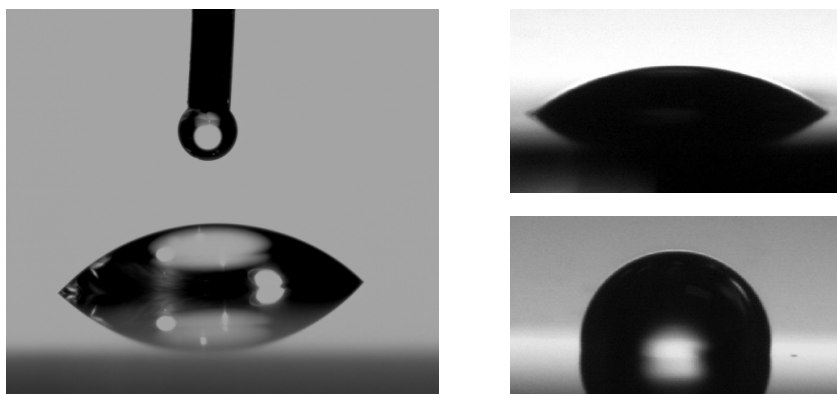


Figure 6.1-2: Images of the probe liquid drops on the solid surface.⁸¹

6.1.3 Transmission Electron Microscopy

Transmission electron microscopy (TEM) is a high resolution imaging technique providing resolutions up to 0.2 nm. TEM measurements were performed to determine the distribution of random copolymer **poly(1₃₀₀-*co*-2₃₀₀)** and the block-*co*-polymer **poly(2₁₀₀-*block*-(2₂₅₀-*co*-1₂₅₀))** in the matrix polymer poly(ethylene).

6.1.3.1 Sample Preparation

In order to facilitate trimming of the sample the compound material was embedded in an epoxy resin. During trimming, the embedded sample was sharpened and thus prepared for cryo-ultra-microtomy at low temperatures, which enables the preparation of ultra-thin cuts of soft, organic samples by moving the tip of the sample above the cuneiform edge of the diamante cutter (*cf.* Figure 6.1-3, left).

⁸¹Sources: http://en.wikivisual.com/images/d/d3/Video_contact_angle.gif, http://betterthandiamond.com/asha5/asha_water_angle.jpg, http://betterthandiamond.com/asha5/cz_water_angle.jpg.



Figure 6.1-3: Microtome for ultra-thin cuts (left) and TEM (right).⁸²

The ultra-thin cuts float on the water surface and are transferred onto a copper carrier grid. Subsequently the specimen is treated with a ruthenium tetroxide (RuO_4) solution to increase the contrast of such ultra-thin cuts. Now the specimen is ready for TEM measurement, conducted in the microscope shown in Figure 6.1-3, right.

6.1.4 Lifetime Measurements

For the measurement of lifetime changes, two different methods for time-resolved measurement are predominant: the direct time domain and the indirect frequency domain method.

6.1.4.1 Time-Domain Lifetime Measurement

In the time domain method, the chromophore is usually excited with a very short light pulse which is preferably much shorter than the luminescence lifetime. This results in an initial population n_0 of chromophores in the excited state, which decays according to Equation 6.1-3.

$$\frac{dn(t)}{dt} = (\Gamma + k_{nr})n(t)$$

$n(t)$	number of excited molecules at time t	6.1-3
Γ	emissive rate	
k_{nr}	non-radiative decay rate	

Emission is a random process and each excited chromophore exhibit equal probability to emit a photon in a given period of time. Consequently, an exponential decay of the excited state population is given by Equation 6.1-4.

$$n(t) = n_0 e^{-(t/\tau)}$$

n_0	initial population of excited state	6.1-4
t	time	
τ	lifetime	

⁸² Source: Haber, T., *FELMI-ZFE*, Graz University of Technology.

In practice fluorescence intensity, which is proportional to $n(t)$, is measured rather than an exact number of excited molecules. Thus, integration of Equation 6.1-3 and substitution of number of molecules by intensity leads to the expression for a single exponential decay (*cf.* Equation 6.1-5 and Figure 6.1-4)

$$I(t) = I_0 e^{-(t/\tau)} \quad \begin{array}{ll} I_0 & \text{intensity at time 0} \\ t & \text{time} \\ \tau & \text{lifetime} \end{array} \quad 6.1-5$$

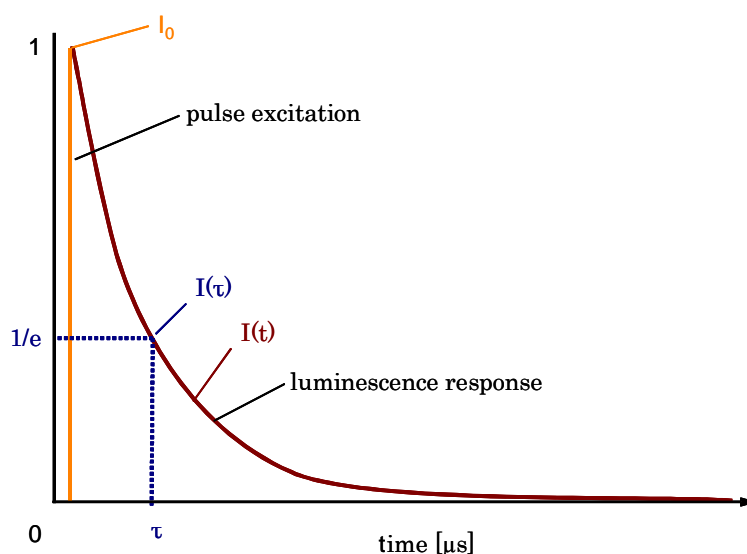


Figure 6.1-4: Exponential decay of pulse-excited luminescence and definition of luminescence lifetime.

Usually, measurements in the time-domain require sophisticated equipment, such as flash-lamps, lasers or synchrotron radiation sources for short excitation pulses. In order to avoid such sophisticated instrumentations a light emitting device (LED) with a sharp emission maximum at 461 nm was used. The LED was actuated by the trigger which generates the signal. Furthermore, photomultiplier tubes (PMT) with a wide bandwidth were used as the detector in combination with an oscilloscope for signal sampling circuits. A schematic of the set-up is shown in Figure 3.4-9.

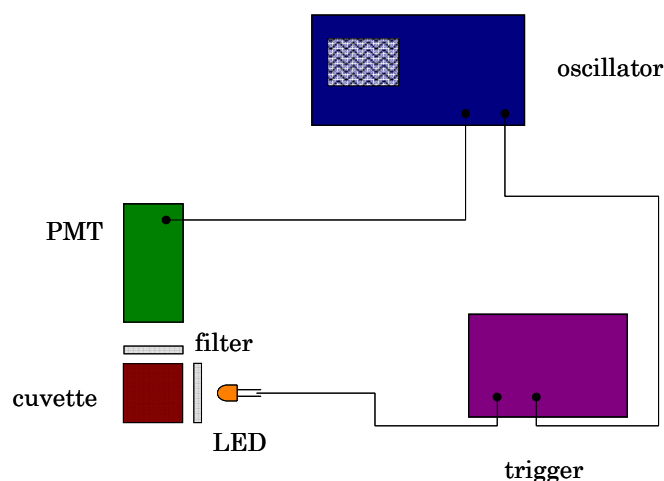


Figure 6.1-5: Schematic set-up for time domain lifetime measurements.

The signal generated by the trigger and the corresponding response signal of the TMC is shown in Figure 6.1-6. Lifetime is calculated using Equation 6.1-5.

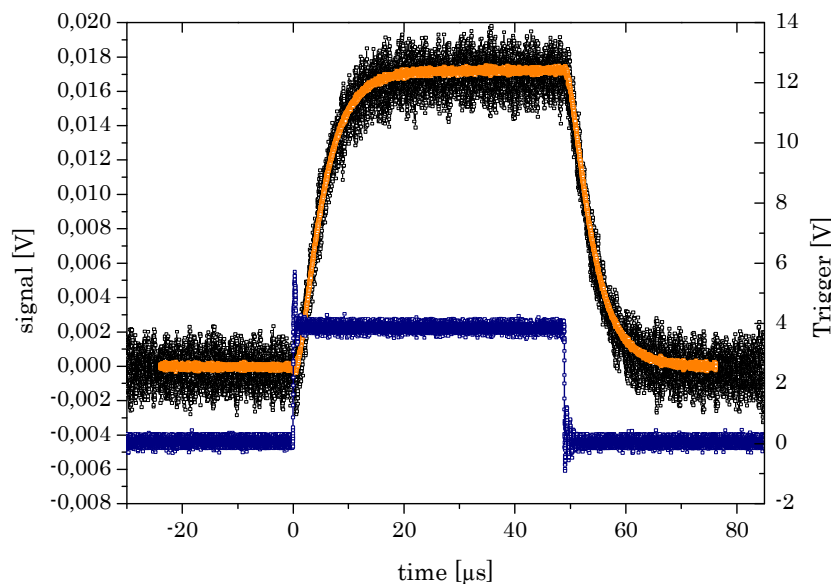


Figure 6.1-6: Signal generated by the trigger (blue line) and average response signal of the chromophore (orange line).

6.1.4.2 Frequency-Domain Lifetime Measurement

The frequency-domain lifetime measurement, also referred to as phase modulation method, is the second commonly used method for lifetime measurements.

The excitation light is intensity modulated with a sine function. The corresponding luminescent signal is also intensity-modulated, but the response signal of the chromophore is time-delayed due to the time lag between absorption and emission. This delay can be expressed as the phase shift (*cf.* Equation 6.1-6 and Figure 6.1-7).

$$\tan \phi = 2\pi f \tau$$

ϕ	phase shift	6.1-6
f	frequency	
τ	lifetime	

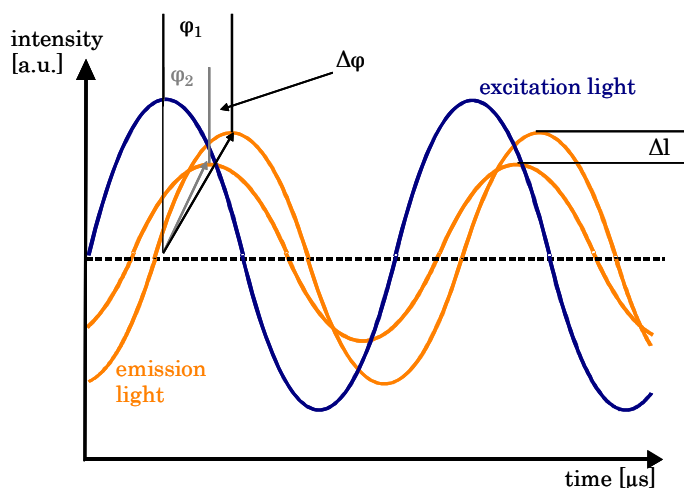


Figure 6.1-7: Principle of frequency-domain lifetime measurements and definition of phase shift φ .

6.1.5 Humidity Measurement Set-Up

Initially a flow-through and injection cell measuring set-up was developed by Astrid Knall supported by Christian Konrad and Martin Tscherner from Joanneum Research.⁷⁸ These set-ups turned out to be time-consuming and reproducibility had to be enhanced. Thus the measuring system or rather the water vapour generation was further improved. For the generation of defined amounts of moisture a set-up consisting of a thermo-stabilised bubbler and a gas mixer was employed. Furthermore, a reference system was included in the measuring cavity. The resultant measurement set-up is shown in Figure 6.1-8.

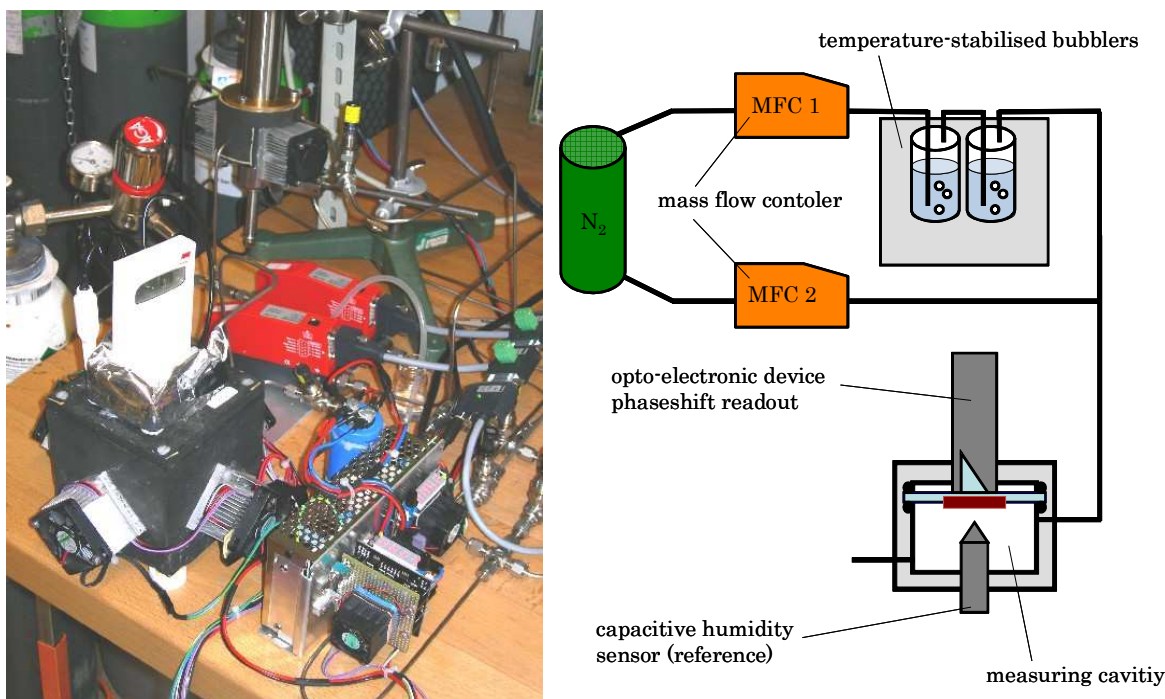


Figure 6.1-8: Picture (left) and schematic (right) of the measuring set-up.⁷⁸

A detailed schematic of the measuring cavity is shown in Figure 6.1-9.

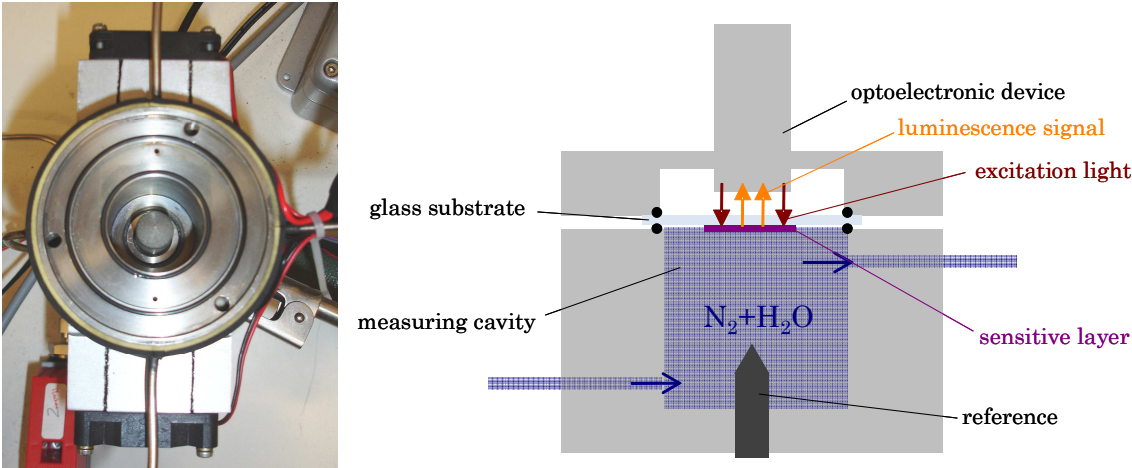


Figure 6.1-9: Top-view picture of the measuring cavity (left) and schematic of the measuring cavity (right).⁷⁸

As reference system a capacitive humidity sensor was purchased. This sensor was placed directly in the cavity opposite to the sensitive layer and the optical readout device for monitoring the water vapour concentration in the measuring cavity.

An existing LabView based program, used by Joanneum Research was modified by Martin Tscherner. The software allows simultaneous logging of phase shift and amplitude and on-line viewing of three parameters. Furthermore, different sequences for water vapour concentration levels can be programmed by addressing the two mass flow controllers.

6.2 Glossary of Abbreviations

AcOH	acetic acid
ADMET	acyclic diene metathesis polymerisation
Al ₂ O ₃	aluminium oxide
<i>A. niger</i>	<i>Aspergillus niger</i>
ARC	Austrian Research Centre GmbH
bs	broad singlet, NMR multiplicity and shape
BPh ₄ ⁻	tetraphenylborate anion
bpy	bipyridyl
<i>C. albicans</i>	<i>Candida albicans</i>
CDCl ₃	deuterated chloroform
CH ₂ Cl ₂	dichloromethane
CH ₂ I ₂	diiodomethane
CFU	colony forming unit
CM	cross-metathesis
Cy	cyclohexane
cym	p - cymene
d	doublet, NMR multiplicity
dd	doublet of doublets, NMR multiplicity
DNA	deoxyribonucleic acid
DSC	differential scanning calorimetry
<i>E. coli</i>	<i>Escherichia coli</i>
EE	ethyl acetate
EPS	extra-cellular polymeric substance
eq	equivalent
Et ₂ O	diethyl ether
G1	1 st generation Grubbs-type initiator
G2	2 nd generation Grubbs-type initiator
G3	3 rd generation Grubbs-type initiator
	RuCl ₂ (pyridine) ₂ (H ₂ IMes)(CHPh)
GPC	gel permeation chromatography
H ₂ O	water
HOMO	highest occupied molecular orbital
IC	internal conversion
iphen	imidazophenanthroline
ISC	intersystem crossing
JIS	Japanese Industry Standard
LC	ligand centred
LED	light emitting device
LMCT	ligand -to- metal charge-transfer
LP	lipopolysaccharide
LUMO	lowest unoccupied molecular orbital
m	multiplet, NMR multiplicity

M1	1 st generation Umicore initiator
M2	2 nd generation Umicore initiator
M31	3 rd generation Umicore initiator
MeOH	methanol
MFC	mass flow controller
MLC	metal-ligand complex
MLCT	metal-to-ligand charge-transfer
MW	molecular weight
NaBPh ₄	sodium tetrakisphenylborate
nb	norbornene
Net ₃	triethyl amine
NH ₄ OAc	ammonium acetate
NMR	nuclear magnetic resonance
n.o.	not observed
<i>P. aeruginosa</i>	<i>Pseudomonas aeruginosa</i>
PDI	polydispersity index
PDMS	poly(dimethylsiloxane)
PE	poly(ethylene)
PEG	poly(ethylene glycol)
ph	phenyl
phen	phenanthroline
PMT	photo multiplier tube
PP	poly(propylene)
PS	poly(styrene)
PTFE	poly(tetrafluorethylene)
QY	quantum yield
RCAM	ring-closing alkyne metathesis
RCM	ring-closing metathesis
ROCM	ring opening cross metathesis
ROMP	ring opening metathesis polymerisation
RRS	ring rearrangement metathesis
RuO ₄	ruthenium tetroxide
s	singlet, NMR multiplicity
<i>S. aureus</i>	<i>Staphylococcus aureus</i>
SEC	size exclusion chromatography
SEM	scanning electron microscopy
t	triplet, NMR multiplicity
TFA	trifluoro acetic acid
TGA	thermogravimetric analysis
THF	tetrahydrofuran
TLC	thin layer chromatography
TMC	transition metal complex
UV	ultra violet

6.3 Glossary of Mathematical Terms

c	concentration of the chromophore
d	cuvette width
E_{λ}	absorbance of light at the wavelength λ
ϵ_{λ}	molar absorption coefficient
F_0	intensity in the absence of quencher
F	intensity in the presence of quencher
Γ	emissive rate of the fluorophore
γ_{sl}	interfacial tension
I_0	intensity of the irradiating light at time 0
I	intensity of the transmitted light
J_{HH}	coupling constant (NMR)
K_D	Stern-Volmer quenching constant
k_{nr}	rate of non-radiative decay
k_q	bimolecular quenching constant
M_n	number average molecular weights
M_w	weight average molecular weights
n_0	initial population of excited state at the time 0
$n(t)$	number of excited molecules at the time t
Q	quantum yield
$[Q]$	concentration of quencher
σ^d	surface energy due to dispersive interactions
σ_l	surface tension liquid
σ^p	surface energy due to polar interactions
σ_s	surface tension solid
τ	lifetime of the excited state
τ_D	lifetime of the fluorophore in absence of quencher
θ	contact angle
$\theta_{CH_2I_2}$	contact angle diiodomethane – solid surface
θ_{H_2O}	contact angle water – solid surface

6.4 List of Figures

Figure 2.1-1: Schematic structure of a prokaryote.	4
Figure 2.1-2: General structure of phospholipids.	4
Figure 2.1-3: Three main structures of phospholipids in solution.	4
Figure 2.1-4: Gram-negative cell wall structure.	5
Figure 2.1-5: Gram-positive cell wall structure.	5
Figure 2.1-6: Biofilm formation on silicon.	6
Figure 2.1-7: Mechanism of biocides.	8
Figure 2.1-8: Cytoplasm membrane.	8
Figure 2.1-9: Adsorption onto the cytoplasmic membrane.	9
Figure 2.1-10: Disruption and phase separation of the cytoplasm membrane.	9
Figure 2.1-11: Leakage of the cell constituents and lysis of the cell.	9
Figure 2.2-1: Schrock type initiators.	14
Figure 2.2-2: Grubbs type initiators.	14
Figure 2.2-3: Neolyst initiator of Umicore AG.	15
Figure 2.3-1: Jablonski diagram.	17
Figure 2.3-2: Simplified Jablonski diagram.	18
Figure 2.3-3: Collisional (left) and static quenching (right).	19
Figure 2.3-4: Electronic states of MLC.	22
Figure 2.3-5: Crystal field dependent MLCT (left) and simplified Jablonski diagram for MLC (right).	22
Figure 3.1-1 Monomer concepts for ROMP.	25
Figure 3.1-2: Resulting ROM polymers using third generation Grubbs initiator.	25
Figure 3.1-3: Synthesised polymers for kinetic measurements via NMR.	28
Figure 3.1-4: Monomer conversion versus time for the homopolymers poly(1) and poly(2) and the random copolymer poly(1₁₅₀-co-2₁₅₀) .	28
Figure 3.1-5: Antimicrobial activity of poly(1₃₀₀-co-2₃₀₀) against Gram-positive <i>S. aureus</i> .	31
Figure 3.1-6: Antimicrobial activity of poly(1₃₀₀-co-2₃₀₀) against Gram-negative <i>P. aeruginosa</i> .	31
Figure 3.1-7: Antimicrobial activity of poly(1₃₀₀-co-2₃₀₀) against the fungus <i>C. albicans</i> .	32
Figure 3.1-8: Antimicrobial activity of poly(1₃₀₀-co-2₃₀₀) against the fungus <i>A. niger</i> .	32
Figure 3.2-1: Thermo-Haake mini-extruder.	34
Figure 3.2-2: Injection piston (left) and steel mould (right).	35
Figure 3.2-3: Collin P200PV heat-able vacuum press.	35
Figure 3.2-4: Compound samples produced via injection-moulding (left) and compression moulding (right).	35
Figure 3.2-5: Chromophore 5 (left) incorporated in the random copolymer poly(1₃₀₀-co-2₃₀₀-co-5₃₃) (right).	37
Figure 3.2-6: Relative emission intensity of 5 versus concentration.	38
Figure 3.3-1: Self-assembling of block-co-polymers on the surface in compound with PE.	39
Figure 3.3-2: Linear dependence between M_n and monomer to initiator ratio.	41
Figure 3.3-3: GPC data of poly(2) with different chain lengths.	41
Figure 3.3-4: GPC data of block-co-polymers of 1 and 2 .	42
Figure 3.3-5: Comparison of molecular weight distribution of poly(2)₃₀₀ and poly(2₃₀₀-block-1₃₀₀) .	43
Figure 3.3-6: GPC data of poly(2₁₀₀-block-(1₁₅₀-co-2₃₅₀)) , poly(2₁₀₀-block-(1₂₅₀-co-2₂₅₀)) and poly(2₁₀₀-block-(1₃₅₀-co-2₁₅₀)) .	44
Figure 3.3-7: TEM pictures of the random copolymer poly(1₃₀₀-co-2₃₀₀) (left) and the block-co-polymer poly(2₁₀₀-block-(1₂₅₀-co-2₂₅₀)) (right) after staining with RuO ₄ ; 11.000 fold magnified.	47
Figure 3.4-1: Random polymers poly(14-co-16) and poly(15-co-16) using third generation Grubbs initiator.	52
	98

Figure 3.4-2: Absorbance (hollow symbols) and normalised emission (filled symbols) of 11 in the not protonated (blue lines) and in the protonated (orange lines) form.	53
Figure 3.4-3: Absorption (hollow symbols) and emission (filled symbols) spectra of 14 in chloroform (blue lines) and in acetone (orange lines).	55
Figure 3.4-4: Absorption (hollow symbols) and emission (filled symbols) spectra of 15 in chloroform (blue lines) and in acetone (orange lines).	55
Figure 3.4-5: Absorption (hollow symbols) and emission (filled symbols) spectra of 14 in the non-protonated (blue lines) and in the protonated (orange lines) state.	58
Figure 3.4-6: Absorption (hollow symbols) and emission (filled symbols) spectra of poly(14-co-16) (blue lines) and poly(15-co-16) (orange lines) in chloroform.	59
Figure 3.4-7: MLCT band (hollow symbols) and emission (filled symbols) spectra of poly(14-co-16) (blue lines) and poly(15-co-16) (orange lines) in chloroform.	60
Figure 3.4-8: Comparison of absorption (hollow symbols, blue line) and excitation (hollow symbols, orange line) and emission (filled symbols) spectra of poly(14-co-16) in chloroform solution (blue lines) and in thin film (orange lines).	62
Figure 3.4-9: Time domain lifetime measurements of poly(14-co-16) in chloroform solution in air (blue line) and degassed in nitrogen (orange line).	64
Figure 3.4-10: Time domain lifetime measurements of poly(15-co-16) in chloroform solution in air (blue line) and degassed in nitrogen (orange line).	65
Figure 6.1-1: Contact angle formation on a solid surface according to Young.	88
Figure 6.1-2: Images of the probe liquid drops on the solid surface.	89
Figure 6.1-3: Microtome for ultra-thin cuts (left) and TEM (right).	90
Figure 6.1-4: Exponential decay of pulse-excited luminescence and definition of luminescence lifetime.	91
Figure 6.1-5: Schematic set-up for time domain lifetime measurements.	92
Figure 6.1-6: Signal generated by the trigger (blue line) and average response signal of the chromophore (orange line).	92
Figure 6.1-7: Principle of frequency-domain lifetime measurements and definition of phase shift φ .	93
Figure 6.1-8: Picture (left) and schematic (right) of the measuring set-up.	93
Figure 6.1-9: Top-view picture of the measuring cavity (left) and schematic of the measuring cavity (right).	94

6.5 List of Schemes

Scheme 2.2-1: Mechanism of olefin metathesis.	12
Scheme 2.2-2: Mechanism of ring opening metathesis polymerisation.	13
Scheme 2.2-3: Termination reaction of ROMP.	16
Scheme 3.1-1: Possible interaction of amine bearing monomers with the initiator molecule.	27
Scheme 3.3-1: Syntheses of homopolymers of 2 of different chain lengths using G3 initiator.	40
Scheme 3.4-1: Synthesis of the norbornene bearing aldehyde 8 (top) and phenanthroline-5,6-dion 10 (bottom).	49
Scheme 3.4-2: Condensation reaction of 8 and 10 in the presence of NH ₄ OAc in AcOH.	49
Scheme 3.4-3: Cleavage of the dimer 11 with the diimine ligand 10 .	50
Scheme 3.4-4: Synthesis of the 6 <i>d</i> electron TMCs 14 and 15 .	51
Scheme 6.1-1: Procedure of the antimicrobial testing according to JIS Z 2801:2000.	87

6.6 List of Tables

Table 3.1-1: Characteristic data of the homo- and copolymers. ⁵¹	26
Table 3.1-2: Antimicrobial activity of the homo- and copolymers. ⁵¹	26
Table 3.1-3: Effect of temperature and time on molecular weight and PDI of 2 .	29
Table 3.1-4: Antimicrobial activity of poly(1300-co-2300) after 0h, 24h and 48h according to JIS Z2801.	30
Table 3.2-1: Antimicrobial activity after 0h, 24h of 3, 5 and 7wt.% of poly(1300-co-2300) incorporated in PE according to JIS Z2801. 0% referred to as the reference containing no active material.	36
Table 3.3-1: GPC results of a series of homopolymers of 2 .	40
Table 3.3-2: GPC Results of block-co-polymers.	43
Table 3.3-3: PDI and number average molecular weight of different less sophisticated block-co-polymers with the general structure poly(2100-block-(1-co-2)₅₀₀) .	44
Table 3.3-4: Determination of contact angle θ , dispersive σ^d and polar σ^p interaction and surface energy γ_{sl} of poly(ethylene) and 5 wt.% of poly(2100-block-(1250-co-2250)) in PE.	46
Table 3.4-1: Absorption and photoluminescence data of 11 in CHCl ₃ solution.	54
Table 3.4-2: Absorption and emission characteristics of 14 and 15 in acetone and chloroform.	56
Table 3.4-3: Absorption and emission characteristics of 14 in the non-protonated state and after the addition of TFA.	59
Table 3.4-4: Absorption and emission characteristics of 14 and 15 in chloroform compared with the corresponding polymers poly(14-co-16) and poly(15-co-16) .	61
Table 3.4-5: Summarised absorption and emission characteristics of the TMCs in chloroform and acetone and the resultant polymers in chloroform solutions.	63

6.7 Curriculum Vitae

Name: Nadja Noormofidi
 Adresse: Goethestrasse 22
 PO: 8010 Graz
 Phone: 0043 650 7416821
 Email: noormofidi@tugraz.at
 Place and date of birth: Graz 05.10.1980



Core Competence

Project management
 Congress management
 Communications and collaboration
 Scientific working
 Social competence
 Networking

Professional Achievements

Scientific project manager and coordinator of the EU-project ‚BIOSURF - Development and implementation of a contact biocide polymer for its application as antimicrobial and anti-deposit surfaces in the food industry’. Submitted to the European Commission within the 7th Framework Program ‚Research for the benefit of SMEs’.

Start of the project: June, 1st, 2009

Project period: 24 months

Budget: 1.12 Mio Euro

December, 16th, 2009: Honour from The Austrian Research Promotion Agency (FFG) for successful Austrian coordinators of FP7 projects.

Project manager of the FEMtech-Karierewege project ‘erfinderin – Erfolgreiche Frauen in der Industrie – Entwicklung, Research, Innovation’

Start of the project: March, 1st 2009

Project period: 24 months

Budget: 354.526 Euro

Member of the Steering Committee of the **European Polymer Congress 2009 (epf09)** and organisation of the **STIPOMAT-Workshop 2007** (European Science Foundation – ESF).

Studies assistance at the Institute for Chemistry and Technology of Materials, summer 2007

Education

Scientific assistance at the Institute for Chemistry and Technology of Materials, start: 2009 (ongoing), research area: biocide polymers

PhD thesis at the Institute for Chemistry and Technology of Materials, SS 2007, research area: end-functionalisation of ROM polymers, synthesis of luminescent and biocide polymers
(June 2006 – November 2009)

Diploma thesis at the Institute for Chemistry and Technology of Materials
(February 2005 – January 2006)

Studies abroad within the scope of an ERASMUS fellowship in **Sevilla (Spain)**
(January 2004 – June 2004)

Studies of Technical Chemistry at the University of Technology Graz, Graduation Date: January, 26th, 2006

School certificate examination at BG/BRG Körösisstrasse July, 6th, 1998

High school at BRG Körösisstrasse 1994-1998

Secondary school at BG/BRG Carnerigasse 1990-1994

Elementary school at Volksschule Hitzendorf 1986-1990

Professional Experience

Laboratory assistant at **Fresenius Kabi Graz**
May 2000 – December 2005

Summer job at the **Institute for Inorganic Chemistry** at TU-Graz.
Juli 2003

Summer job at **Roche Diagnostics** (formaly AVL List)
summer 1999, 1998, 1997

Languages

German: native
English: high
Spanish: good
Farsi: basic

Leisure activity

running, traveling, reading books, friends, skiing, music.

6.8 List of Publications

6.8.1 Manuscripts

Non-Cytotoxic Contact Bactericides and Fungicides on the Basis of Amino-Functionalized Poly(norbornene)s.

Kreuzwiesner, E.; Noormofidi, N.; Wiesbrock, F.; Kern, W.; Rametsteiner, K.; Stelzer, F.; Slugovc, C. **2010**, *submitted*.

Optical Response of Phenantroimidazole-Dyes Covalently Linked to a Polynorbornene-Backbone to Acid and Base.

Noormofidi, N.; Slugovc, C. *Eur. Polym. J.* **2010**, *46*, 594-701.

Acid-Base Sensitive Ring Opening Metathesis Polymers Based on Phenanthroimidazole-Dyes.

Noormofidi, N.; Slugovc, C. *Macromol. Chem. Phys.* **2007**, *208*, 1093.

Open, cyclic, and bicyclic compounds of double silylated phosphorus and boron. Markov, J.; Fischer, R.; Wagner, H.; Noormofidi, N.; Baumgartner, J.; Marschner, C. *Dalton Trans.* **2004**, 2166.

6.8.2 Proceedings

Europium-containing polymers as humidity-sensing materials.

Knall, A.-C.; Pein, A.; Noormofidi, N.; Stelzer, F.; Slugovc, C. *Polymer Preprints* **2007**, *48*, 575.

Towards acid/base stimuli responsive materials: ROM polymers side chain functionalized with phenanthroimidazoles.

Noormofidi, N.; Stelzer, F.; Slugovc, C. *World Polymer Congress – Proceedings of the Macro 2006, 41st International Symposium on Macromolecules, Rio de Janeiro, 16-21 July, 2006*, 747.

Fluorescence labelled olefin metathesis polymerization initiators.

Burtscher, D.; Noormofidi, N.; Stelzer, F.; Slugovc, C. *World Polymer Congress – Proceedings of the Macro 2006, 41st International Symposium on Macromolecules, Rio de Janeiro, 16-21 July, 2006*, 0863.

6.8.3 Presentations

6.8.3.1 Oral Contributions

Towards acid/base stimuli responsive materials: ROM polymers side chain functionalized with phenanthroimidazoles.

Noormofidi, N.; Stelzer, F.; Slugovc, C. *World Polymer Congress – Macro 2006, 41st International Symposium on Macromolecules, Rio de Janeiro, 16-21 July, 2006*, Book of Abstracts p.12.

Phenanthroimidazoles and Imidazophenanthrolines as Luminescent Moieties in ROM-Polymers.

Noormofidi, N.; Stelzer, F.; Slugovc, C. *8th Austrian Polymer Meeting, Linz, 20-22 Sept., 2006*, S1-L8.

Antimicrobial Polymer Blends via ROMP.

Noormofidi, N.; Kreutzwiesner, E.; Stelzer, F.; Slugovc, C. *1st Joint Austrian & Slovenian Polymer Meeting (ASPM 2008), Graz, March 26-28, 2008*, PM2 OP5.

6.8.3.2 Talks from Co-worker and Poster Presentations

Condensed Results from SENSMAT.

Blas, M.; Lex, A.; Noormofidi, N.; Waich, K.; Kappaun, S.; Niedermair, F.; Stubenrauch, K.; Zelzer, M.; Klimant, I.; Mayr, T.; Slugovc, C.; Trimmel, G. *ISOTEC Progress Meeting, Weiz 1-2 December, 2005*.

Ring Opening Metathesis Polymers Side Chain Functionalized with Phenanthroimidazoles.

Noormofidi, N.; Stelzer, F.; Slugovc, C. *1st European Chemistry Congress, Budapest, Hungary, 27-31 Aug. 2006*, Book of Abstracts, p294 / M-PO-64.

Fluorescence labeled olefin metathesis polymerization initiators.

Burtscher, D.; Noormofidi, N.; Stelzer, F.; Slugovc, C. *World Polymer Congress – Macro 2006, 41st International Symposium on Macromolecules, Rio de Janeiro, 16-21 July, 2006*, Book of Abstracts p. 48.

Ring Opening Metathesis Polymers with Fluorescent End Groups.

Burtscher, D.; Saf, R.; Noormofidi, N.; Slugovc, C. *8th Austrian Polymer Meeting, Linz, 20-22 Sept., 2006*, S1-P36.

Towards acid/base stimuli responsive materials: ROM polymers side chain functionalized with phenanthroimidazoles.

Noormofidi, N.; Slugovc, C. *2nd STIPOMAT Workshop, Seggau, 23.-25. October, 2006*, P14.

ROM-polymers incorporating imidazophenanthrolines and their ruthenium(II) complexes.

Noormofidi, N.; Slugovc, C. *106. Hauptversammlung der Deutschen Bunsen-Gesellschaft für Physikalische Chemie, May 17-19, 2007*, P119.

ROM Polymers as Scaffold for Phosphorescent Transition Metal Complexes.

Noormofidi, N.; Pein, A.; Knall, A. C.; Slugovc, C. *European Polymer Congress (EPF), Portoroz, Slovenia, 2nd-6th July, 2007*, Book of Abstracts P5.4.46.

Towards Asymmetrically End-Group Functionalized Ring Opening Metathesis Polymers.

Slugovc, C.; Lexer, C.; Burtscher, D.; Noormofidi, N. *European Polymer Congress (EPF), Portoroz, Slovenia, 2nd-6th July, 2007*, Book of Abstracts OC1.2.11.

Europium-containing polymers as humidity-sensing materials.

Knall, A. C.; Pein, A.; Noormofidi, N.; Stelzer, F.; Slugovc, C. *American Chemical Society, 234th National Meeting & Exposition, Boston, USA, 19th - 23th Aug., 2007*, POLY-573.

Polymerisable Phosphorescent Transition Metal Complexes.

Noormofidi, N.; Pein, A.; Knall, A. C.; Slugovc, C. *10th Conference on Methods and Applications of Fluorescence, Salzburg, Sep. 9-11, 2007*, PRLS-6.

Optical humidity sensor materials based on europium.

Knall, A. C.; Pein, A.; Noormofidi, N.; Tscherner, M.; Konrad, C.; Ribitsch, V.; Uray, G.; Stelzer, F.; Slugovc, C. *10th Conference on Methods and Applications of Fluorescence, Salzburg, Sep. 9-11, 2007*, PRLS-7.

Synthesis of antimicrobial polymers optimized for blending with commodity materials.

Noormofidi, N.; Kreutzwiesner, E.; Slugovc, C.; Stelzer, F. *Innovative Science for Successful Business, 4th Partnering Day for Biomedical Research, Graz, Oct. 18, 2007*.

Phosphorescent Transition Metal Complexes as Building Blocks for Ring Opening Metathesis Polymerisation.

Noormofidi, N.; Pein, A.; Knall, A. C.; Slugovc, C. *3rd STIPOMAT Workshop, Les Diablerets, Switzerland, 14th - 17th Oct., 2007*.

ROM-polymerizable Europium complexes and their application in sensing layers.

Knall, A. C.; Pein, A.; Noormofidi, N.; Tscherner, M.; Stelzer, F.; Slugovc, C. *5. Workshop Anorganische Chemie in Österreich, Graz, March 17-18, 2008*, Book of Abstracts p. 23.

Preparation, Characterization and Applications of Europium-Containing Copolymers.

Knall, A. C.; Pein, A.; Noormofidi, N.; Tscherner, M.; Stelzer, F.; Slugovc, C. *1st Joint Austrian & Slovenian Polymer Meeting (ASPM 2008), Graz, March 26-28, 2008*, OPE2 OP1.

Antimicrobial Copolymers Compounded With Polyethylene.

Kreuzwiesner, E.; Noormofidi, N.; Kern, W.; Slugovc, C.; Stelzer, F. *1st Joint Austrian & Slovenian Polymer Meeting (ASPM 2008), Graz, March 26-28, 2008*, P8.

Antimicrobial ROM Polymers Optimized for Blending with Commodity Materials.

Noormofidi, N.; Kreuzwiesner, E.; Ramensteiner, K.; Slugovc, C.; Stelzer, F. *Zing, Polymer Synthesis, Cancun, Mexico, March 17-20, 2008*, P7.

Antimicrobial Copolymers Compounded with Polyethylene.

Kreuzwiesner, E.; Noormofidi, N.; Stelzer, F.; Kern, W.; Slugovc, C. *Zing, Polymer Synthesis, Cancun, Mexico, March 17-20, 2008*, Book of Abstracts, p12.

Luminescent Metal Complexes as Building Blocks for Ring Opening Metathesis Polymerisation.

Noormofidi, N.; Pein, A.; Knall, A.; Slugovc, C. *Organometallics at the Centre, Cancun, Mexico, March 13-16, 2008*, P23.

Usage of Ruthenium Based Catalysts to Synthesize Antimicrobial Polymers.

Kreuzwiesner, E.; Noormofidi, N.; Stelzer, F.; Kern, W.; Slugovc, C. *Zing, Organometallics at the Centre, Cancun, Mexico, March 13-16, 2008*, P16.

Lifetime-Based Optical Humidity Measurements Using Europium-Containing Materials.

Knall, A. C.; Pein, A.; Noormofidi, N.; Tscherner, M.; Konrad, C.; Ribitsch, V.; Uray, G.; Stelzer, F.; Slugovc, C. *Europtrode IX, Dublin, Ireland, March 30 – April 4, 2008*, Book of Abstracts p. 106.

Antimicrobial ROM Polymers as Additives for Commodity Materials.

Noormofidi, N.; Kreuzwiesner, E.; Slugovc, C.; Stelzer, F. *International Workshop on Biomacromolecules 2008, Stockholm, Sweden, June, 1-4, 2008*.

Phosphorescent Eu and Ru complexes made polymerizable by ROMP.

Noormofidi, N.; Knall, A. C.; Slugovc, C. *8th International Symposium on Functional pi-Electron Systems, Graz, Austria, June 21 – 25, 2008*, P-104.

ROM Polymers Incorporating Ruthenium Complexes and their Application as Humidity and Oxygen Sensor Material.

Tendl, M.; Noormofidi, N.; Slugovc, C. *European Polymer Congress 2009 (epf09), Graz, Austria, Jul. 12-17, 2009*. Book of Abstracts p. 176. Poster